

PREDICTION OF TURBULENT SWIRLING REACTING FLOW
WITH NONORTHOGONAL GRID SYSTEM

BY

SEONGDO HA

Bachelor of Engineering
Yonsei University
Seoul, Korea
1977

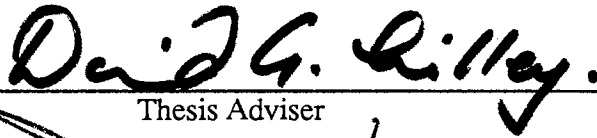
Master of Science
University of Texas at Austin
Austin, Texas
1983

Submitted to the Faculty of the
Graduate College of the
Oklahoma State University
in partial fulfillment of
the requirements for
the Degree of
DOCTOR of PHILOSOPHY
July, 1989

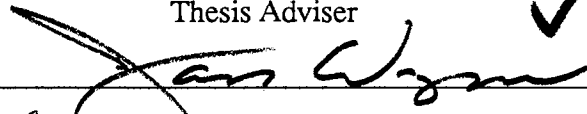
Thesis
1989D
H1115P
cop. 2

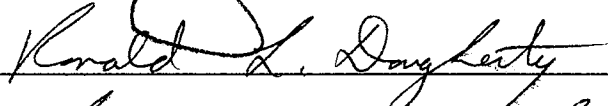
PREDICTION OF TURBULENT SWIRLING REACTING FLOW
WITH NONORTHOGONAL GRID SYSTEM

Thesis approved



Thesis Adviser









Dean of the Graduate College

ACKNOWLEDGMENTS

The author wishes to express his deepest appreciation to his major adviser, Dr. David G. Lilley for his valuable advice and guidance throughout this work. Further advice and criticism of the other committee members, Dr. Peter M. Moretti, Dr. Jan Wagner and Dr. Ronald L. Dougherty, is also greatly acknowledged.

Special gratitude and appreciation is expressed to the author's wife, Minjung, and pretty daughter, Juhyon. Their understanding, encouragement and countless sacrifices have been overwhelming. The author deeply appreciate the encouragement and financial support given his sister, Soonja, and his brother-in-law, Jaegi.

The author also express sincere gratitude to the Department of Mechanical and Aerospace Engineering for the financial support during the study.

TABLE OF CONTENTS

Chapter	Page
I. INTRODUCTION	1
1.1 Flowfield Prediction of Complex Flows	1
1.2 Computer Predictions of Axisymmetric Flows	2
1.3 Objectives of the Present Study	3
1.4 Outline of the Thesis	3
II. LITERATURE REVIEW	5
2.1 Experimental Work for Reacting Flows	5
2.2 Experimental Work for Nonreacting Flows	9
2.3 Theoretical Work	11
2.4 Irregular Boundary Treatment	14
III. MATHEMATICAL APPROACH	16
3.1 Governing Equations	16
3.2 Combustion Simulation	17
3.3 Solution Technique	19
3.4 Solution Procedure	20
IV. COMPUTER CODE DEVELOPMENTS	23
4.1 Background	23
4.2 New Code Developments	24
4.2.1 Multi-inlets	24
4.2.2 Exit Velocity Correction	25
4.2.3 Generalization of Stair-Step Boundary Approximation	25
4.2.4 Combustor Solver Code	26
4.2.5 Nonorthogonal Grid System	26
4.2.6 Treatment of Extra Terms Resulted from Nonorthogonal Grid	28
V. THE SAMPLE COMPUTATION	38
5.1 The Flow System Description	38
5.2 Input Data	38
5.3 Description of Outputs	40

Chapter	Page
VI. RESULTS AND DISCUSSION	42
6.1 Laminar Flow Prediction	43
6.2 Turbulent Flow Prediction	44
6.3 General Predictions of Flows in Model Combustors	46
6.4 Comparisons of Predictions of Standard STARPIC and New Code	47
6.5 Discretization of Flux Equations in Nonorthogonal Grid System	48
6.6 Accuracy of Predictions	50
VII. CLOSURE	51
6.1 Conclusions	51
6.2 Recommendations for further Work	52
REFERENCES	54
APPENDIXES	64
APPENDIX A TABLES	65
APPENDIX B FIGURES	84
APPENDIX C TYPICAL OUTPUTS	128

LIST OF TABLES

Table	Page
I. Selected Test Cases	66
II. Source Terms and Exchange Coefficients Used in the Governing Equation of the General Variable ϕ	67
III. The Form of the Components of the Linearized Source Terms	68
IV. Predicted Axial and Radial Velocities of Case 1	69
V. Predicted Axial and Radial Velocities of Case 2	70
VI. Predicted Axial and Radial Velocities of Case 3(a)	71
VII. Predicted Axial, Radial and Swirl Velocities of Case 3(b)	72
VIII. Predicted Axial and Radial Velocities, and Concentrations of Case 4	74
IX. Predicted Axial, Radial and Swirl Velocities, and Fuel Concentrations and Temperature of Case 5	76
X. Flat Inlet Velocities for Test Cases	79
XI. Newly Defined Input Parameters in the Code	80
XII. Newly Defined Variables in the Code	81

LIST OF FIGURES

Figure	Page
1. Schematic Illustration of the Flow Systems of Test Cases	85
2. Staggered Grid and Notation for the Rectangular Computational Mesh	87
3. The Three Control Volumes Associated with points of Three Grids	88
4. Flow Chart of Computational Scheme	89
5. Schematics of Multi-inlet System	90
6. Nonorthogonal Grids with 30 degrees Slope	91
7. Fortran Variables Related the Nonorthogonal Grids for C-Cells	92
8. Fortran Variables Related the Nonorthogonal Grids for U-Cells	93
9. Fortran Variables Related the Nonorthogonal Grids for V-Cells	94
10. Control Volumes at the Sloping Wall	95
11. Notations of C-Control Volume for the Grid Line Skewness	96
12. Notations of C-Control Volume for the Sloping Control Surfaces	97
13. Notations for Control Volumes of Nonorthogonal Grid	98
14. Notations of C-Control Volume for P Calculation at the Top Sloping Wall	99
15. Schematic of the Flow for the Sample Computation	100
16. Grid System of the Flow for the Sample Computation	101
17. Mean Axial Velocity Profiles of Case 1	102
18. Predicted Streamline Pattern of Case 1	103
19. Predicted Mean Axial Velocity Profiles of Case 1	104
20. Mean Axial Velocity Profiles of Case 2	105

Figure	Page
21. Predicted Streamline Pattern of Case 2	106
22. Predicted Mean Axial Velocity Profiles of Case 2	107
23. Mean Axial Velocity Profiles of Case 3 (without Swirl)	108
24. Predicted Streamline Pattern of Case 3 (without Swirl)	109
25. Predicted Mean Axial Velocity Profiles of Case 3 (without Swirl)	110
26. Mean Axial Velocity Profiles of Case 3 (Swirl No. 0.67)	111
27. Mean Swirl Velocity Profiles of Case 3 (Swirl No. 0.67)	112
28. Predicted Streamline Pattern of Case 3 (Swirl No. 0.67)	113
29. Predicted Mean Axial and Swirl Velocity Profiles of Case 3 (Swirl No. 0.67) . .	114
30. Mean Axial Velocity Profiles of Case 4	115
31. Inner Jet Mean Concentration Profiles of Case 4	116
32. Predicted Streamline Pattern of Case 4	117
33. Predicted Mean Axial Velocity and Concentration Profiles of Case 4	118
34. Mean Axial Velocity Profiles of Case 5	119
35. Mean Temperature Profiles of Case 5	120
36. Mean Concentration Profiles of Case 5	121
37. Predicted Streamline Pattern of Case 5	122
38. Predicted Mean Flowfield Property Profiles of Case 5	123
39. Mean Axial Velocity Profiles of Case 3(a) (without Swirl)	125
40. Mean Axial Velocity Profiles of Case 3(b) (Swirl No. 0.67)	126
41. Mean Swirl Velocity Profiles of Case 3(b) (Swirl No. 0.67)	127

NOMENCLATURE

a	Coupling coefficient, or linear interpolation coefficients
A	Area
b, c, d	Linear interpolation coefficients
C_{EBU}	Eddy-Breakup constant
C_{g_1} , C_{g_2}	Fuel fluctuating concentration constants
C_{μ}	Turbulent constant
C_p	Specific heat
D	Diameter
E	Eastern neighbor
E/R	Activation energy
f	Combined quantity
fu	Fuel
g	Mean square fluctuating component of fuel concentration
h	Stagnation enthalpy
H_{fu}	Heat of combustion
i	Stoichiometric ratio
k	Turbulence kinetic energy
m	Mass fraction
M	Molecular weight
N	Northern neighbor
ox	Oxygen
p	Pressure

P	Chemical kinetic reaction constant
pr	Product
r	Radial direction
R	Radius of outer wall
R_{fu}	Mean fuel reaction rate
S	Southern neighbor
S_p S_u	Components of linearized source term
S_ϕ	Source of ϕ variable
u	Axial velocity component
v	Radial velocity component
Vol	Volume of cell
V_T	Total resultant velocity
w	Swirl velocity component
W	Western neighbor

Greek Letters

ϕ	Turbulence dissipation rate
Γ	Turbulent exchange coefficient
μ	Effective viscosity
μ_1	Laminar viscosity
μ_2	Turbulent viscosity
ρ	Time-mean density
ϕ	General dependent variable
θ	Flow angle with regard to x-direction

θ_0 Slope angle with regard to x-direction

Subscripts

e, w, n, s Control surface of east, west, north and south

P Center point of cell

x, r x-and r-direction

p-x, p-r Projection to x- and r- direction

nb Neighbor nodes

sx Surface with regard to x- direction

in Flow in

out Flow out

Superscripts

' RMS values of fluctuating component (except p')

* Old value at the node point

CHAPTER I

INTRODUCTION

1.1 Flowfield Prediction of Complex Flows

Turbulent reacting flows have attracted increasing interest in recent years. The requirement of the increased combustion efficiency and the decreased pollutant emissions from a variety of devices, from power plants to jet engines, have led to the need for improved methods of prediction and calculation for turbulent swirling flows involving chemical reactions. In combustion system design situations, costly and lengthy experimental procedures must be supplemented with mathematical models. Economical design practices can be greatly facilitated by the understanding of prior predictions of the combustor flowfields obtained via the use of mathematical models. Mathematical models of steadily increasing realism and refinement are being developed, both in the dimensionality of the model (together with computational procedures) and in problems associated with the simulation of the physical processes occurring.

However, in chemically reacting flows, the flow characteristics are complicated by nonlinear interactions between chemical and fluid dynamic processes. The presence of liquid sprayed or solid particles which are subject to intimate interaction within a gaseous flowfield add another complexity in the calculation of flow properties. Practical combustion systems often have complex flowfields to enhance flame characteristics due to the introduction of swirling inlet flow, laterally induced jets, and contoured boundary geometry. The strong favorable effects of applying swirl are extensively used as aid to the flame stabilization and promotion of rapid mixing. The prediction of turbulent, swirling,

reacting flows found in furnaces and gas turbine combustors have received considerable attention in several recent textbooks (1-5).

This study is concerned with a theoretical prediction technique for swirling, reacting, turbulent flowfields in the practical combustors.

1.2 Computer Predictions of Axisymmetric Flows

Most practical flowfields are in cylindrical polar coordinates. An axisymmetric, two-dimensional flow has been of special interest in the prediction of flow properties because of its geometric simplicity and convenience in mathematical modeling and its practical application to many flow systems. There are text books to provide numerical methods to flow problems in detail (6, 7). The stream function-vorticity and primitive pressure-velocity approaches are two common ways for the calculation of flowfield. One of the latter approaches (Control Volume Approach) and its application are extensively described in the text book (8). A finite difference computer program, called STARPIC, can predict an axisymmetric, turbulent, swirling, recirculating flow under isothermal condition. This program was previously developed at OSU by Lilley & Rhode (9). The results of their predictions with the STARPIC code and complementary experimental work by other researchers at OSU were presented in the final NASA report (10).

The STARPIC program solves for a single species, isothermal flow in the rectangular grid system covering axisymmetric domains, including swirl and turbulence via a two-equation turbulence model. Important present day research needs include:

1. Variable density, multi-species (gaseous) mixing at constant or different temperature
2. Combustion of a gaseous fuel, either with premixed entry or separated fuel and air entries into the domain
3. More realistic simulation of confining outer boundary walls, such as the gradual expansion or the downstream exit nozzle

1.3 Objectives of the Present Study

A general computer program should be easy to run in order to obtain the effective prediction of a given flow system even for the persons with little background in turbulent reacting flow and computational methods. Other complexities should be able to be added by individual users without difficulties. As mentioned above, the standard STARPIC code has limitations of application to meet the present day research needs. To resolve these requirements the standard STARPIC computer program needs its prediction capabilities extended.

New code developments and modifications will be incorporated into the STARPIC code. The specific objectives of the present study are:

1. To permit the multi-inlet capability
2. To include the turbulent mixing of two or more different gases at equal or different temperature
3. To allow gaseous combustion simulation
4. To develop nonorthogonal grid system to cover irregular domain with generalized boundary location
5. To apply the resulting computer program to predict the flows being investigated experimentally by other researchers at OSU and elsewhere

1.4 Outline of the Thesis

The first chapter of this seven-chapter thesis is the introduction. The complexity of flowfield of turbulent swirling reacting flows are briefly described. This chapter also highlights some previous OSU works in the above flows and present day research needs. Finally, the present study objectives were stated in detail.

Chapter II reviewed both experimental and theoretical studies of other workers. The experimental study findings and the accuracy of the calculations of them are summarized.

The irregular boundary Treatments in numerical methods are reviewed, too.

The theoretical approach to the present flow problem is presented in Chapter III. The governing equations, combustion simulation, solution method and the procedure of computer code are described briefly.

Chapter IV provides the computer program developments. The limitations of the standard code are stated with its background. New developments are described in detail item by item. Construction of a nonorthogonal grid system is highlighted with the complete and lengthy presentation. The sample computation of the newly developed computer program is described in Chapter V. The brief descriptions of sample flow system, input data and typical outputs are included in this chapter.

The validation study is conducted in comparison with the present predicted values and the previous experimental data for the chosen test cases as given in Table I in Chapter VI. Five different flow systems are specially selected to perform the predictability of the new computer code. Laminar or turbulent and reacting or inert flow conditions and irregularity of the outer boundary wall are considered in choosing those test cases. These comparisons are described and discussed in details

Finally, Chapter VII is the closure of this work. The conclusions of the present investigation are summarized and the recommendations for further work are briefly stated.

CHAPTER II

LITERATURE REVIEW

The flowfield characteristics of turbulent reacting swirling flow has been important subject of various experimental and numerical investigations. Numerous previous studies about them currently exist and may be more in process. Some researchers have measured flow properties in furnace or combustor models while others have tried to predict them numerically. Since a given flow system is not always simple and regular, the irregularity of boundary has raised another obstacle to be resolved in order to predict a complex geometry flow with a computer.

2.1 Experimental Work in Reacting flow

Measurements of three velocity components and the corresponding correlations in nonswirling and swirling flow in a model furnace with and without combustion were obtained by Baker et al.(11). They employed swirl number of 0.52 to study the effect of swirl in an sudden expansion chamber. Their comparison revealed larger forward velocities in the combusting flow and correspondingly larger regions of recirculation. The swirl reduced the length of the flow and tended to increase the anisotropic region of the flow.

Spadaccini et al. (12) used an axisymmetric sudden expansion furnace with a central fuel injection and annular air. The air swirl number was 0.6 and the tangential momentum was imported to the flow with swirl vanes. Measurements of mean velocities, gas temperature and species concentrations were reported at various locations downstream, x/D

= 0.08, 0.82, 1.47, 2.86 and 4.25.

Measurements of mean axial velocity, and the corresponding normal stress was reported by Hutchinson et al. (13) for the flow of air and for a combusting mixture of natural gas in an axisymmetric furnace enclosure with a coaxial burner. The measurements were compared with the results of a calculation procedure incorporating a two-equation turbulence model and one step reaction model. Their comparison showed that the calculated results were in general agreement with measurements but that quantitative differences existed. The largest disagreement were in the wake and suggested that the two-equation turbulence model is inadequate in such a regions. The combustion model was considered another source of imprecision for the furnace calculation.

Smith et al. (14) investigated the flowfield of reactive recirculating jet mixing in a dump combustor. The ratio of the duct to inner nozzle diameter was 2.5. Radial distributions of mean axial and radial velocity and turbulent intensity, gas composition total pressure and static temperature were obtained for the axial stations $x/D = 0$ to 6 downstream. Their data indicate that mixing is slower in the chemically reacting flowfield than in the nonreactive one. The decay of concentration and velocity is less rapid for the reacting case. The large temporal temperature fluctuations indicate the requirement that any prediction technique must account for the huge fluctuations in temperature and concentration.

Velocity field characteristics of a swirling flow combustor were studied by Gouldin et al. (15) for reacting and nonreacting cases. The combustor consists of two confined, concentric swirling jets. The central jet flow is premixed methane-air; the annular jet flow is swirling. From the data, they concluded that turbulent transport is not the mechanism for swirl induced recirculation in the flow. It is interesting to note that the failure to accurately predict flow recirculation is most likely not the result of a pure turbulence model. Large anisotropic velocity fluctuations were observed in high shear regions and is the velocity of

the recirculation zone.

Brum and Samuelsen (16) have evaluated a dilute swirl combustor as a laboratory test bed for diagnostic tool development, model validation, and fuel effects studies in recirculating, turbulent flows. Measurements of simultaneously time-resolved temperature and velocity fluctuations were obtained by Larue et al. (17) to provide a qualitative and quantitative description of the flow with respect to the mixing processes and turbulent transport in a model laboratory, swirl-stabilized combustor. The mean temperature was shown nearly constant in the recirculation zone with instantaneous peak approximating the maximum adiabatic flame temperature. Axial heat fluxes in the central region were negative, reflecting a large population of high temperature, low velocity fluid from the recirculation region.

Owen (18) made both mean and turbulence measurements in the initial mixing of confined turbulent diffusion flame burner. Measurements showed that there were large differences in time averaged flowfields with and without inlet swirl. He noted that there were substantial large-scale contributions to the total RMS turbulent velocity field. These large-scale fluctuations result in significant deviations from isotropy over most initial mixing region. Such large-scale motions indicate that turbulence models based on local equilibrium principles, such as mixing lengths and others which utilized local mean gradients, will not adequately represent the physics of these combusting flows.

Velocity and temperature were measured in a cylindrical oil-fired furnace for a variety of swirl intensities (1.98, 1.247, 0.939 and 0.721) by Khalil et al. (19). Increasing the swirl intensity was found to increase the size and strength of the central recirculation zone. Their analytical study, based on the hypothesis of minimum kinetic energy gave quite good agreement with experimental results for the normal range of the swirl and outside the central recirculation zone.

Lewis and Smoot (20) made experimental measurements of fuel mixture fraction and species concentration in turbulent natural gas diffusion flames. They showed that a 350K

change in the wall temperature had a negligible effect on gas mixing rates, but did alter the local species distributions somewhat. More complete mixing was obtained at lower air temperatures. Lockwood et al. (21) also made measurements of mixture fraction in a small, cylindrical furnace, axially-fired with gaseous fuel for a variety of experimental conditions; Fuel/air ratio, swirl, burner geometry and the Reynolds number. The increased rate of decay of mixture fraction with axial distance resulted from increased swirl. They showed the effect of the Reynolds number was small, but not insignificant.

Temperature and concentration measurements in a gas-fired cylindrical furnace were reported by Hasson et al. (22). Data were obtained for two excess air levels and a swirl number 0.56. Bicen and Jones (23) reported mean and RMS values of axial and swirl velocity components in a nonaxisymmetric model can-type gas turbine combustor with dilution holes under isothermal and combusting flow conditions. They concluded that the influence of combustion on the velocity field was generally to increase the strength and decrease the width of primary recirculation, to accelerate the flow in the axial direction and to increase velocity fluctuations. The effect of air-fuel ratio was small on the primary zone flow but was more pronounced at downstream regions where the increased temperature and thus reduced densities associated with the lower air-fuel ratio values resulted in higher velocities at exit.

Temperature and species concentration measurements of a similar can-type turbine combustor has been made by Jones and Toral (24), and Heitor and Whitelaw (25). The data of the former researchers indicated that in general chemical equilibrium did not prevail, however in the downstream region the concentrations of CO₂ and O₂ and temperature are in close agreement with the calculated chemical equilibrium values. The latter researchers presented the influence of combustion on the velocity characteristics and the effect of air-fuel ratio in more details.

2.2 Experimental Work in Nonreacting Flows

Measurements of the velocity characteristics of turbulent, confined, coaxial-jet flows were made with swirl number, 0 and 0.23, by Habib and Whitelaw (26,27). Their results indicated as the swirl number increased from zero the central recirculation zone grows. Comparison between the measurements and calculation based on an effective viscosity hypotheses showed that the two-equation model, although able to represent the non-swirling flow is less appropriate to the swirling flow. They recommended an algebraic stress model or a stress transport model to allow non-isotropic viscosity and improve the calculations (26). The larger velocity ratio resulted in a larger region of recirculation, larger velocity gradients and larger turbulence intensities in the mixing region (27).

Rao et al (28) presented the experimental and theoretical investigation of axisymmetric enclosed swirling flows generated by vane swirlers, with 0 , 15 , 30 , 45 and 60 degrees. They concluded that a 45 degree swirler gave the largest size recirculation zone and a 60 degree vane angle swirler the smaller size one. Agreement between predicted values of velocity and kinetic energy and experimental values is fairly good, away from the swirler.

Extensive measurements of mean flow and turbulence characteristics were obtained by Yu and Gouldin (29) in a coaxial swirling jet model combustor. They showed that the outer swirl had a strong effect on the formation of a circulation zone and mixing characteristics in the interjet shear layer. High levels of turbulent fluctuations and large dissipation rates characterized the central flow region for both coswirl and counterswirl conditions, which the outer flow regions exhibited relatively low turbulence levels. More turbulence was generated in the interjet shear layer under counterswirl than for coswirl.

Owen (30) made the measurements in the initial mixing length region of free and confined coaxial air jets with recirculation to study the time averaged characteristics of the two flowfields. Measurements showed that there were large differences in the time-

averaged structure of the two flowfields, the size and recirculation mass flux being significantly larger in the confined flow than in the free expansion. The mean radial velocities measured in both initial mixing regions are the same order of magnitude as the mean axial velocities.

An experimental study of mixing downstream of swirling co-axial jets discharging into an expanded duct was conducted to obtain mean and fluctuating Roback (31, 32). From visualization techniques were also employed to determine qualitatively the time dependent characteristics of the flow and the scale of turbulence. They concluded that major mixing regions occurred at the interface between the near stream and the centerline recirculation zone, and at the interface between the inner jet and the annular jet streams. Mixing for swirling flow was completed in one-third the length required for nonswirling flow. Schetz et al. (33) also visualized and measured the swirling flow characteristics of ramjet combustor model under various conditions, swirl vane angle, confinement ratio, secondary injection rate, the length and diameter of the central hub.

Yoon and Lilley (34) employed a five-hole pitot probe to measure the mean velocity profiles in confined swirling flow in a sudden and gradual expansion. The swirl vane angles used were 0, 38, 45, 60 and 70 degrees. They showed that the presence of swirl shortens the corner recirculation zone and generates a central recirculation zone followed by a processing vortex core. The largest central recirculation zone occurred at the swirl vane angle 38 degrees. The strongest processing vortex core was observed at 38 degrees. The recirculation zone is shortened by the presence of a downstream contraction nozzle.

Measurements of turbulent, confined, swirling flows in a research combustor under co-and counterswirl conditions by Ramos and Somer (35). They showed that under both conditions a closed recirculation zone is created at the combustor centerline. This zone is characterized by the presence of a toroidal vortex, low tangential velocities, high turbulent intensities, and large dissipation rate of turbulent kinetic energy. Experimental Studies of sudden expansion flowfields were performed by other researchers (36-40) too.

2.3 Theoretical Studies

There are many publications to introduce theoretical approaches to solution of turbulent swirling flow under reacting or inert condition. First of all, text books about the swirling flow, combustion models, turbulence models, and general computational methods to flow problems are reviewed. A comprehensive and illustrated introduction to the phenomenon of swirl, its occurrence in the practical equipment and in the atmosphere, both with and without combustion is described in detail by Gupta et al. (1). Gupta & Lilley (2) have illustrated the solution techniques for complex turbulent reacting flow with emphasis on swirl flow combustion application. The several prediction methods used in the furnace and combustor flow modelling approaches are described and assessed in Khalil's book (3). The general theoretical basis for the study of turbulent reacting flows is well reviewed in Libby & Williams' text book (4). Various aspects of the theory, an overview and perspective of the field of such flows are also discussed in their book. Beer & Chigier (5) explained aerodynamic processes, which play important roles in diffusion flames, the type most generally used in industrial practice. Fundamental aspects and the basic understanding of various combustion phenomena are well handled in Kanury's (41) and Spalding's (42) books. Kuo's book (43) provides a comprehensive treatment of combustion with the emphasis on the theoretical modeling of combustion problems.

Launder & Spalding (44) have introduced several turbulence models and assessed in detail them, based on engineering calculation of turbulent flows. Turbulence analysis for the engineering purpose is well illustrated in Schetz's book (45). Bradshaw's book (46) gives an introduction to our state of knowledge of turbulence in most of the branches of science as a helpful guide for research workers. The nature and theories of turbulence are treated in detail more mathematically in Hinze's book (47). A wide variety of turbulent phenomena and the basic tools of turbulence theories are described by Tennekes & Lumley

(48). Numerical methods to flow problems are illustrated in other text books (6,7,49). The basic structure of SIMPLE algorithm and its application to heat transfer and fluid flow are extensively shown in Patankar's book (8).

From now on, the related papers are reviewed. Jones & Whitelaw (26,27) have described and appraised components of calculation methods of such flows. Recent problems and progress in the numerical simulation for combustor applications are surveyed by Lilley (28). He has reviewed the difficulties, developments and useful prediction methods already being made to aid designers of practical combustion equipment. Gupta & Lilley (29) have reported the present status and related combustion research needs in the area of modelling and nonintrusive physical diagnostics as applied to combustion systems.

Gosman et al. (54) predicted the flowfield in a gaseous-fired cylindrical combustion chamber. They concluded that the qualitative nature of predictions is good for all three diffusion, premixed, and oxygen-enriched flames.

The calculation of local flow properties in a furnace was performed by Khalil et al. (55) will k- ϵ turbulence model with three reaction models. The comparisons showed that the predicted values are in general agreement with measurements but differences still remain. Ramos (56) investigated numerically the flowfield in a swirl stabilized combustor with the two-step chemical reaction model. The calculations were in reasonable agreement with the available experimental data. Numerical simulation of combustor flowfield with k- ϵ turbulence and one-step chemical reaction model was presented by Novick et al. (57). Samples & Lilley (58) studied the similar flowfield with two-step chemical reaction model including a radiation heat transfer simulation. The flowfield in a widely-spaced co-axial jet diffusion flame combustor was investigated numerically by Sturgess & Syed (59). Mongia et al. (60) reported assessment of physical models of turbulent reacting and inert flows.

Calculation of field values in hydrogen/air diffusion flames via the probability density functions (PDF) to take account of the fluctuations in the mixture fraction was presented by Kent & Bilger (61). They found the form of the PDF has little effect on the velocity and

conserved scalar mean fields but the effect on mean temperatures and species concentrations is significant. When large number of species are involved in chemical reaction, only PDF transport equation formulation offers the possibility of reaction modeling (62). However, the complexity, run times, and multidimensionality of the approach require further investigation (52). Many other papers (63-68) related to the PDF were published.

Studies of the interaction between turbulence and combustion in practical combustion systems are discussed in details in references (69-72). Turbulence models in various flow conditions, inert or reacting, and swirling were studied and assessed in papers (73-79).

The spatial differencing of the convective terms of the conservation equations in an Eulerian coordinate system can result in numerical diffusion. The use of a higher order differencing scheme eliminates or significantly reduces this diffusion. However, the use of central-differencing method, for example, often produces oscillations in the solution that have no physical significance (6). The use of an upwind differencing technique eliminates the oscillations but introduces a diffusion-like term into the differential equation. The hybrid finite differencing scheme (combination of the upwind and central differencing schemes) which is currently used in TEACH-type code, although yielding physically realistic solutions in all circumstances, introduces excess numerical diffusion for many flows (80). Therefore, several improved finite differencing schemes (81-88) were developed to reduce the numerical diffusion. Some of them are assessed in references 88 through 90.

Among those improved schemes, the Bounded Skew Upwind Differencing Scheme has been recommended to reduce numerical diffusion for TEACH-type code to calculate complex flows in terms of accuracy and stability (87).

2.4 Irregular Boundary Treatment

There are three ways to handle the irregular boundary domains in numerical methods:

1. Boundary approximation with series of stair steps to fit the given grid system.
2. Coordinate transformation to change the irregular domain into a regular one on the transformed coordinate system.
3. Employment of a numerical method which is independent of the domain shapes, such as Finite Element Method.

The boundary approximation with series of stair steps is commonly used in numerical methods since its application is easy and does not need any other special knowledge. However, the application of boundary fitted grid system may produce more accurate results.

Finite Element Method has the advantages of fitting irregular boundaries with ease but has the disadvantage of complexities at the mathematical point of view comparing with the finite difference method. Solution of the Navier-Stokes equations have been presented for two-dimensional steady (91-92) as well as transient (93) incompressible flows. Turbulent boundary layers in supersonic compressible flows (94) have also been successfully calculated. Numerous developments and improvements have been carried out in this method. This method laid a firm foundation to a wide variety of solution methods and provided expanded possibilities of application (95).

Independent variable transformation techniques are thought to be the most accurate approach (96) for numerical representation of boundary conditions. These widely applicable methods map an irregular physical domain (e.g., x, y or x, r) into a transformed rectangular $\xi = \xi(x, y)$ and $\eta = \eta(x, y)$ which are either algebraically specified (analytical transformation) or effected by numerical solutions of differential or integral equations (numerical transformation).

Oberkampf (97) transformed general systems of first order and second order partial differential equations using generalized domain mapping functions. He discussed important features of the transformed equations as they relate to computational procedures. Barfield (98) used the complex Green's functions to map an irregular domain into unit circle and then into a rectangular polygon employing a Schwarz-Christoffel transformation. The coordinate generation methods for the two dimensional domain were developed by several researchers (99-102). Mastin & Thomson (103) and Miki & Takagi (104) have developed a general method for generating the three-dimensional coordinate systems. The applications of boundary fitting coordinate transformation to the flow problems were presented by many researchers. Some of the recent papers are appended (105-117).

Thacher (118) reported a brief review of techniques for generating irregular computational grids. Rhode & Lilley (119) surveyed extensively the methods for treating domains with irregular boundaries.

CHAPTER III

THE MATHEMATICAL APPROACH

3.1 The Governing Equations

In the modeling and prediction of combustor flowfields, the problem is simulated by simultaneous nonlinear partial differential equations. The turbulent Reynolds equations for conservation of mass, momentum, stagnation enthalpy, chemical species mass fractions, turbulent kinetic energy and turbulence dissipation rate, govern the two-dimensional, axisymmetric, swirling steady flow of the chemically reacting multi-component mixtures (2). Each of these equations contains similar terms for the convection, diffusion and source terms of a general flowfield variable ϕ . Introduction of turbulent exchange coefficients and the usual turbulent diffusion-flux laws provides a similarity in the form among all the governing partial differential equations. This similarity allows them to be put in the common form:

$$\frac{1}{r} \left[\frac{\partial}{\partial x} (\rho u r \phi) + \frac{\partial}{\partial r} (\rho v r \phi) - \frac{\partial}{\partial x} \left(r \Gamma_{\phi} \frac{\partial \phi}{\partial x} \right) - \frac{\partial}{\partial r} \left(r \Gamma_{\phi} \frac{\partial \phi}{\partial r} \right) \right] = S_{\phi} \quad (3.1)$$

where ϕ is one of the time-mean flowfield variables; $u, v, w, h, m_{f_u}, f, k$ and ϵ . Table II shows the source terms, S_{ϕ} , and the turbulent exchange coefficients, Γ_{ϕ} , for each variable.

The standard two-equation k - ϵ turbulent model is utilized to specify the turbulent viscosity where

$$\mu_t = C_{\mu} \rho k^2 / \epsilon \quad (3.2)$$

and

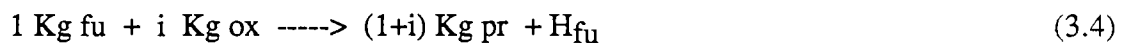
$$\mu = \mu_l + \mu_t \quad (3.3)$$

which is widely used for the turbulent flow prediction by computer programs because this model is moderate in complexity and is considered to be superior to other models having a similar degree of complexity (1-3).

3.2 Combustion Simulation

The conservation equations of stagnation enthalpy and chemical species mass fraction are not completely closed forms since the density and mass rate of creation or destruction of species are unknowns. Those values must be specified prior to the solution of the equations. Introduction of chemical reaction model and thermodynamic considerations provide the necessary extra informations to close the system.

In a multi-component system, simplifications can be introduced through the use of the concept of a simple chemically reacting system to reduce the number of chemical species equations to solve. This assumes that the fuel and oxidant react chemically in a unique proportion, combining with a stoichiometric oxidant/fuel ratio of i to form product plus release of energy by fuel burning (finite rate chemistry assumption). Furthermore, the effective diffusivities of all the chemical species are taken to be equal and the reaction is a single step with no intermediate compounds. This simple exothermic three-component chemical reaction model (2) follows



$$h = c_p T + H_{fu} m_{fu} + V_T^2 / 2 \quad (3.5)$$

$$m_{fu} + m_{ox} + m_{pr} = 1 \quad (3.6)$$

$$f = m_{ox} - i m_{fu} \quad (3.7)$$

This model is characterized by equations for h , m_{fu} and f . The combined concentration quantity, f , equation can be deduced by eliminating the source term from the fuel and oxidant differential equations. It is convenient to solve partial differential equations for m_{fu} and f (rather than m_{fu} and m_{ox}), from which m_{ox} can be deduced (2,3).

The influence of chemical kinetics is included. The fuel and oxidant may coexist at a

point at same time in the flow and the consumption rate of fuel (R_{fu}) is calculated depending on local species concentrations, temperature and turbulence levels. To calculate the consumption rate of fuel, one can use either the time-averaged Arrhenius model or Eddy-Breakup reaction model (2,3,42) :

$$(R_{fu}) = -P p^2 m_{fu} m_{ox} \exp(-E/RT) \quad (3.8)$$

$$(R_{fu}) = -C_{EBU} \rho g^{1/2} \epsilon/k \quad (3.9)$$

P , E/R and C_{EBU} are constants for turbulent flames of high temperature and high Reynolds numbers. The latter model tries to assert the effect of turbulence on the reaction, the time to heat up the premixed mixture by eddies of hot combustion product being related to the rate of dissipation of the concentration. Generally, the mean reaction rates are calculated from the minimum of the Arrhenius and the Eddy-Breakup models. The variable g (mean square fluctuating component of fuel concentration, $g = \overline{f^2}$) may be obtained from its governing equation or, with the assumption that generation equals dissipation, its reduced algebraic equation:

$$g = \frac{C_{g1} \mu k \left[\left(\frac{\partial m_{fu}}{\partial r} \right)^2 + \left(\frac{\partial m_{fu}}{\partial x} \right)^2 \right]}{C_{g2} \rho \epsilon} \quad (3.10)$$

where $C_{g1} = 2.8$ and $C_{g2} = 2.0$ are constants. R_{fu} works as the source term in the fuel mass fraction equation. All other properties, which will be used in calculation, at any point in the flowfield may be deduced successively using the following relations:

$$m_{ox} = f + i m_{fu} \quad (3.11)$$

$$m_{pr} = 1 - m_{ox} - m_{fu} \quad (3.12)$$

$$T = (h - H_{fu} m_{fu} - V_T^2/2)/c_p \quad (3.13)$$

$$\rho = pM/(RT), \quad \text{where } 1/M = \sum_j (m_j/M_j) \quad ((3.14)$$

When both the heat of combustion, H_{fu} , and the consumption rate of fuel, R_{fu} , are assigned the zero values, a turbulent mixing solution can be obtained on either the isothermal or nonisothermal flows with different temperature inlets.

3.3 Solution Technique

The governing partial differential equations described in the previous section are coupled and nonlinear. Since, at the present time, it is not possible to obtain analytical solutions to those equations. One of numerical techniques has to be used in order to solve them.

Solution of hydrodynamics may be via the stream function-vorticity or the primitive pressure-velocity approaches which are most common numerical methods in the field of computational fluid mechanics. The present solution technique is based on the SIMPLE (Semi-Implicit Method for Pressure Linked Equations) algorithm (8) which is one of the latter approaches.

The staggered grid system described in Figure 2 was used to formulate the governing differential equations into the finite difference equations. All variables except u- and v-velocities are stored at the central grid nodes (intersections of the solid lines), while the u- and v-velocities are stored at the points which are denoted by arrows (and labeled w and s respectively) located midway between the grid intersections. The bumerang-shape envelope encloses a triad of points with the reference location P at (I,J). The advantages of this staggered grid system are: first, it places the u- and v-velocities between the pressure nodes which drive them; and secondly, the velocities are directly available for the calculation of the convective fluxes across the boundaries of control volume surrounding the grid node. Figure 3 shows three types of the control volumes, C, U and V which are appropriate for the P, w and s locations respectively.

The finite difference equations for each ϕ are constructed by integrating Equation (3.1) over the appropriate control volume (centered about the location of ϕ) and expressing the result in terms of neighboring grid point values. The convection and diffusion terms become surface integrals of the convection and diffusion fluxes while the source term becomes the volume integral of source. Since the source depends upon the dependent

variable, we can express the dependence in a linear form. This is done because first the nominally linear frame work would allow only a formally linear dependence, and secondly the incorporation of linear dependence is better than treating the source as a constant (6,8).

The resulting equation is

$$\left[\rho u \phi - \Gamma_{\phi} \frac{\partial \phi}{\partial x} \right]_{e} A_e - \left[\rho u \phi - \Gamma_{\phi} \frac{\partial \phi}{\partial x} \right]_{w} A_w + \left[\rho v \phi - \Gamma_{\phi} \frac{\partial \phi}{\partial r} \right]_{n} A_n - \left[\rho v \phi - \Gamma_{\phi} \frac{\partial \phi}{\partial r} \right]_{s} A_s = [S_p^{\phi} \phi_p + S_u^{\phi}] \cdot \text{Vol} \quad (3.15)$$

where S_p^{ϕ} and S_u^{ϕ} are tabulated in Table III and subscript n, s, e and w refer to north, south, east and west control surfaces. Using the hybrid scheme which is a combination of the so-called central and upwind differences, Equation (3-15) is discretized completely. The details of the discretization procedure are given in the report (9). The following final form of finite difference equation is obtained:

$$a_p^{\phi} \phi_p = \sum_j a_j^{\phi} \phi_j + S_u^{\phi} \quad (3.16)$$

$$\text{where } a_p^{\phi} = \sum_j a_j^{\phi} - S_p^{\phi} \quad (3.17)$$

$$\sum_j = \text{sum over the N, S, E and W neighbors.}$$

3.4 Solution Procedure

The finite difference equations (3.16) result in a system of strongly coupled simultaneous algebraic equations. Although they appear linear they are not since the coefficients and source terms are themselves functions of the variables, and the velocity equations are strongly linked through the pressure. The solution of coupled nonlinear equations proceeds using an iterative scheme. The iteration technique greatly simplifies the construction of the numerical method and provides a way in which, in principle, one can handle any nonlinearity and interlinked. In general, an iteration method has two roles: (a) We cast nonlinear and interlinked equations into nominally linear form and calculate the

coefficients from the previous iteration values of the variables. (b) The nominally linear algebraic equations for one dependent variable at a time are solved by an iteration method (such as the line-by-line method) rather than a direct method since a direct solution method used for multidimensional problems usually results in a disproportionately large amount of work spent in the equation-solving activity (6,8).

✓ In the iteration solution of the algebraic equations or in the overall iterative scheme employed for handling nonlinearity, it is often desirable to speed up or to slow down the changes, from iteration to iteration, in the values of the dependent variable. This process is called overrelaxation or underrelaxation depending on whether the variable changes are accelerated or slowed down. Overrelaxation is often used in conjunction with the Gauss-Seidel Method, the resulting scheme being known as Successive Over-Relaxation (SOR). Underrelaxation is often employed to avoid divergence in the iteration solution of strongly nonlinear equations. The overrelaxation factor is a value between 1 and 2, the underrelaxation factor between 0 and 1. There are no general rules for choosing the best value of the factor f. The optimum value depends on upon a number of factors, such as the nature of the problem, the number of grid points, the grid spacing, and the iterative procedure used. Usually a suitable value of f can be found by experience and from exploratory computations for the given problem (6-8)

In the code, a certain degree of underrelaxation is used to enhance convergence. The underrelaxation factor f ($0 < f < 1$) is applied directly to the dependent variable ϕ_P^{n+1} via

$$\left(\frac{a_P^\phi}{f_\phi} \right) \phi_P^{n+1} = \sum_j a_j^\phi \phi_j^n + S_u^\phi + (1 - f_\phi) \frac{a_P^\phi}{f_\phi} \phi_P^n \quad (3.18)$$

In addition to the dependent variables, other quantities can be underrelaxed with advantage. the density ρ is often main link between the flow equations and the equations for temperature concentration. An underrelaxation of ρ would cause the velocity field to respond rather slowly to the changes in temperature and concentration. A diffusion coefficient Γ can be underrelaxed to restrain the influence of the turbulence quantities on

the velocity field. To enhance convergence the density and the diffusion coefficient are underrelaxed via

$$\rho = f_{\rho} \rho_{\text{new}} + (1 - f_{\rho}) \rho_{\text{old}} \quad (3.19)$$

$$\Gamma = f_{\Gamma} \Gamma_{\text{new}} + (1 - f_{\Gamma}) \Gamma_{\text{old}} \quad (3.20)$$

The well-known tridiagonal matrix algorithm (TDMA) is used to solve the algebraic equations for each dependent variable. Since TDMA can be applied along a grid line, in the two dimensional problem one applies the TDMA along each vertical grid line from left to right sequentially in the solution domain each iteration step (line by line method). The values at gridpoints along a vertical grid line are considered to be unknown (values at P, N, and S for each point P), and the most recent values at E and W neighbor points are considered known and included in the column vector C. The coefficients and source terms of Equations (3.16) are updated prior to each iteration because previous ones are only tentative.

The method of monitoring convergence is to examine how perfectly the discretization equations are satisfied by the current values of the dependent variables. For each grid point a residual R_p^{ϕ} is defined by

$$R_p^{\phi} = \sum_j a_j^{\phi} \phi_j + S_u^{\phi} - a_p^{\phi} \phi_p \quad (3.21)$$

When the summation of $|R^{\phi}|$ all over the flow domain becomes smaller than a predetermined value, the computed solution is considered converged. The layout and the flow chart of the computer program are shown briefly in Figure 4.

CHAPTER IV

COMPUTER CODE DEVELOPMENTS

4.1 Background

The computer code, STARPIC (acronym for Swirling Turbulent Axisymmetric Recirculating flow in Practical Isothermal Combustor geometry) was developed at OSU to predict the mean velocity fields and streamline patterns of various flow systems. The development of STARPIC began with the nonswirling TEACH (acronym for Teaching Elliptic Axisymmetric Characteristics Heuristically) computer program(75). The SIMPLE algorithm which focussed attention directly on the primitive pressure-velocity variable has been embodied into the TEACH program. In addition to the incorporation of swirl, some numerical special features were included into the STARPIC code, such as; (a) a generalized stair-step simulation of the sloping wall boundary, (b) an advanced nonuniform grid system, (c) the application of wall functions derived from a recent experiment, and (d) streamline calculation and plotting. The details of STARPIC are extensively described in the NASA report (9). However, the standard STARPIC code has limitations on application, such as isothermal flows with a single species only, constant density and rectangular grids. The code to be developed in this study will start with the STARPIC code. The new code will resolve the above limits of STARPIC and have more capability of wide application to complex flow systems. New development will be described in details in the following sections.

4.2 New Developments

4.2.1 Multi-inlets

To handle complex flow systems, the capability of treating multi-inlets must be ready in the code. Figure 5 showed the schematics of a flow system which has multi-inlets with grids and notations. Two side inlets, A and B, and one top inlet (circumferential inlet) can be specified with control parameters and input data. The number of inlets can be controlled by following parameters:

IGCS : side inlet control code 1 = one axisymmetric inlet

2 = two concentric inlets

IGCT : top inlet control code 0 = no top inlet

1 = one top inlet

At each inlet, inlet conditions can be specified with following variables:

Side inlet, A : UIN (u velocity, m/sec)

FUIN (mass fraction of fuel)

OXIN (mass fraction of oxygen)

TIN (inlet temperature, K)

Side inlet, B : UINB, FUINB, OXINB, TINB

Top inlet : UIN2, VIN2, WIN2 (swirl velocity), FUIN2, OXIN, TIN2

To calculate UIN2 and WIN2, Two angles are introduced, SUA (top inlet upstream angle of injection) for UIN2 and SSA (top inlet swirl angle) for WIN2. The locations of inlets can be assigned with the specification of gridline values:

Side inlet, A : JINAS (inlet south J)

JINAN (inlet north J)

Side inlet, B : JINBS (inlet south J)

JINBN (inlet north J)

Top inlet : IINW (inlet west I)

IINE (inlet east I)

4.2.2 Exit Velocity Correction

In the original STARPIC code, to obtain fast convergence they calculate UINC (u-velocity increment) by $(\dot{m}_{in} - \dot{m}_{out}) (\rho A)_{exit}$ and adjust the exit velocities by adding UINC to the exit velocity for all J location of exit at each iteration. However, for the variable density case, the following new UINC calculation will provide more consistency: First, DEUINC (ρu increment) can be computed by $(\dot{m}_{in} - \dot{m}_{out}) (\rho A)_{exit}$, and second, UINC(j) is found by $DEUINC/\rho_j$ at each J location of exit. UINC(j) will be added to the exit u-velocities at the corresponding J locations to adjust the exit velocities. This new development also works for the constant density flows automatically, since the two schemes for exit velocity adjustment are identical in the constant density case.

4.2.3 Generalization of Stair-Step Boundary Approximation

The standard STARPIC code has the capability of the stair-step boundary approximation for an irregular boundary wall which has only a positive slope angle. Therefore, the presence of a block, or a converging-diverging nozzle at the middle of the outer wall boundary or an exit block in the flow system will require several fundamental modifications of the computer program. A person who has not the details of the standard STARPIC code may meet difficulties in the code modifications. The new code has resolved this problem with the complete generalization of the stair-step boundary approximation. A new variable, KSLP(I), is included to define the kind of slope angle at every I location of outer wall boundary as following:

KSLP(I) = 1 : Positive or zero slope angle wall

= 2 : Negative slope angle wall

The values of KSLP(I) are not used in the nonorthogonal grid system code.

4.2.4 Combustion Solver Code

The combustion simulation described in details in Section 3.2 is added to the original STARPIC code. The new code includes three subroutines, such as CALCH for the stagnation enthalpy, CALCFU and CALCOF for the chemical species, and some other modifications which are involved on the combustion simulation.

4.2.5 Nonorthogonal Grid System

When an irregular boundary, like a sloping wall, occurs, that the boundary can be approximated with a series of stair-steps in the standard STARPIC code which requires the rectangular cell grid system. In the new code, the capability of a nonorthogonal grid system will be incorporated to treat the irregular boundary. The following steps will be added to the standard code :

- (a) Y-locations of boundary points, YB(I) , and the angle of slope at those points. The location of slope end, SX1, is also defined as shown in Figure 6. The angles of slopes at the outer wall boundary points, ANGS(I), are calculated within the code using YB(I).
- (b) Nonorthogonal grid generation : I-gridlines along the y-location are parallel each other and equally spaced along an I-gridline. However, J-gridlines along the x-direction are not parallel each other and may or may not be equally spaced. Figure 6 shows a nonorthogonal grid system.
- (c) Geometry of C, U and V-cells is illustrated in Figure 7, 8 and 9.
- (d) Each cell-volume can be calculated by area times depth. Since the face of cell-volume is combination of two trapezoids from Figure 7, the area of the face can be computed by adding the two trapezoid areas.

$$C : VOL = RCV(I,J)*(0.25*(SNSU(I,J)+SNS(I,J))*DXPW(I) \\ + 0.25*(SNSU(I+1,J)+SNS(I,J))*DXEP(I))$$

$$U : VOL = RCU(I,J)*(0.5*(SNS(I-1,J)+SNS(I,J))*SEWU(I))$$

$$V : VOL = RV(I,J)*(0.25*(DYPSU(I,J)+SNSV(I,J))*DXPW(I) \\ + 0.25*(DYPSU(I+1,J)+SNSV(I,J))*DXEP(I))$$

(e) Wall function for slope wall

When the normal direction to the wall is ξ as shown in Figure 10, the wall diffusion flux of ϕ is generally

$$\mu \frac{\partial \phi}{\partial \xi} A_{\text{wall}} \quad (4.1)$$

For u-cell, the wall diffusion flux of u is

$$\mu \frac{\partial u}{\partial \xi} A_{\text{wall}} = \mu \frac{\partial u}{\partial r} \frac{\partial r}{\partial \xi} \frac{\Delta x_w}{\cos \theta_0} \quad (4.2)$$

Since $\frac{\partial r}{\partial \xi} = \cos \theta_0$.

$$\mu \frac{\partial u}{\partial \xi} A_{\text{wall}} = \mu \frac{\partial u}{\partial r} \Delta x_w = \mu \frac{\partial u}{\partial r} A_{p-r} \quad (4.3)$$

where A_{p-r} is the projection area to the r-direction. This is the same expression of the wall diffusion flux of u from the north wall in the standard code. For v-cell, similarly, we have

$$\mu \frac{\partial v}{\partial \xi} A_{\text{wall}} = \mu \frac{\partial v}{\partial x} \frac{\partial x}{\partial \xi} \frac{\Delta y_w}{\sin \theta_0} = \mu \frac{\partial v}{\partial x} \Delta y_w = \mu \frac{\partial v}{\partial x} A_{p-x} \quad (4.4)$$

However, there is no direct contribution to v-control volume because the v-control volume including the wall is excluded in the calculation. For c-cell of w-momentum equation, there are two wall diffusion flux terms of w considering r- and x-directions :

$$r : \mu \frac{\partial w}{\partial \xi} A_{\text{wall}} = \mu \frac{\partial w}{\partial r} \frac{\partial r}{\partial \xi} \frac{\Delta x_w}{\cos \theta_0} = \mu \frac{\partial w}{\partial r} \Delta x_w = \mu \frac{\partial w}{\partial r} A_{p-r} \quad (4.5)$$

$$x : \mu \frac{\partial w}{\partial \xi} A_{\text{wall}} = \mu \frac{\partial w}{\partial x} \frac{\partial x}{\partial \xi} \frac{\Delta y_w}{\sin \theta_0} = \mu \frac{\partial w}{\partial x} \Delta y_w = \mu \frac{\partial w}{\partial x} A_{p-x} \quad (4.6)$$

where A_{p-x} is the projection area to the x-direction. For k-equation, the general

expression (9) of the generation source term, G , is

$$G = 2\mu \left[\left(\frac{\partial u}{\partial x} \right)^2 + \left(\frac{\partial v}{\partial r} \right)^2 + \left(\frac{v}{r} \right)^2 \right] + \frac{\tau_t^2}{\mu} \quad (4.7)$$

τ_t can be calculated by using the total resultant velocity, V_T , parallel to the wall (2,3,9):

$$\tau_t = -V_t k C_\mu^{0.25} C_D^{0.25} k_p^{0.5} \ln(EY_p^+) \quad (4.8)$$

where V_T can be found by following equation

$$V_T = \left[\left[\left(\frac{u_p + u_e}{2} \right)^2 + \left(\frac{v_p}{2} \right)^2 \right] \cos^2(\theta_0 - \theta) + w_p^2 \right]^{0.5} \quad (4.9)$$

with the flow angle $\theta = \tan^{-1} \left(\frac{v_s}{u_e + u_w} \right)$ and the slope wall angle θ_0 with regard to x -direction (3). Figure 10 illustrates the geometry of each cell for the wall functions.

4.2.6 Treatment of Extra Terms Resulted from Nonorthogonal Grid

There are extra terms introduced in the discretization of the governing equations since the control surfaces are not orthogonal the discretizing coordinate system. Special considerations must be required in order to complete the discretization. As shown the control volumes in Figure 11, the top and bottom control surfaces are not parallel to the x -coordinate and this results in extra terms on the integration of the governing equations over the control volume.

(1) Continuity Equations: The continuity equation for a steady state, axisymmetric flow is given as

$$\frac{\partial(\rho u)}{\partial x} + \frac{\partial(\rho v)}{\partial r} = 0 \quad (4.10)$$

Integration of this equation over the control volume (see Figure 11) results

$$(\rho u A)_e - (\rho u A)_w - (\rho u A_x)_n + (\rho u A_x)_s + (\rho v A)_n - (\rho v A)_s = 0 \quad (4.11)$$

where A is the projection area of the control surface (top or bottom) to the x -direction.

$(\rho u A_x)_n$ and $(\rho u A_x)_s$ are introduced as the extra mass flow due to u -velocity through the top and bottom control surfaces.

(2) The Governing Discretization Equation : Integration the governing equation given

in the common form (3.1) over the control volumes (centered about the location ϕ as shown in Figure 11) produces

$$\begin{aligned} & \left[\rho u \phi - \Gamma_{\phi} \frac{\partial \phi}{\partial x} \right]_{e} A_e - \left[\rho u \phi - \Gamma_{\phi} \frac{\partial \phi}{\partial x} \right]_{w} A_w - \left[\rho u \phi - \Gamma_{\phi} \frac{\partial \phi}{\partial x} \right]_{n} A_{nx} + \left[\rho u \phi - \Gamma_{\phi} \frac{\partial \phi}{\partial x} \right]_{s} A_{sx} \\ & + \left[\rho v \phi - \Gamma_{\phi} \frac{\partial \phi}{\partial r} \right]_{n} A_n - \left[\rho v \phi - \Gamma_{\phi} \frac{\partial \phi}{\partial r} \right]_{s} A_s = [S_P \phi_{\phi} + S_u] \cdot \text{Vol} \end{aligned} \quad (4.12)$$

The convection and diffusion terms becomes surface integrals of the convection and diffusion fluxes while the source term is linearized as mentioned before. The extra terms which are not included in the standard derivation are

$$\left[\rho u \phi - \Gamma_{\phi} \frac{\partial \phi}{\partial x} \right]_{n} A_{nx}, \quad \left[\rho u \phi - \Gamma_{\phi} \frac{\partial \phi}{\partial x} \right]_{s} A_{sx} \quad (4.13)$$

Again, A_{nx} and A_{sx} are the projection areas of the north and south control surfaces, A_n and A_s , to the x-direction, respectively. All the terms in Equation (4.12) must be discretized along the parallel to the given axes. In this nonorthogonal grid system, x-grid lines are to the r-axis, but r-grid lines may or may not parallel to the x-axis. Therefore, two extra terms which are not included in the standard derivation (9) are introduced to be considered due to the grid nonorthogonality:

$$\left[\rho u \phi - \Gamma_{\phi} \frac{\partial \phi}{\partial x} \right]_{e} A_e, \quad \left[\rho u \phi - \Gamma_{\phi} \frac{\partial \phi}{\partial x} \right]_{w} A_w \quad (4.14)$$

Where the skewness of the r-grid lines as shown in Figure 11 is large, the necessity of skewness consideration becomes inevitable in the discretization. Equation (4.14) should be discretized along the line P'E' and the line W'P'', respectively, with respect to the east and west control surfaces as shown in Figure 11.

The final discretization equation of orthogonal grid system was

$$AP\phi_P = AE\phi_E + AW\phi_W + AN\phi_N + AS\phi_S \quad (4.15)$$

Where $AP = AE + AW + AN + AS$. AP , AE , AW , AN and AS are the coefficients resulted from the discretization of the governing equation, using the hybrid scheme.

However, in this nonorthogonal grid system, the governing equation is discretized into the following form (see Figure 11)

$$\begin{aligned}
AE\phi_P + AW\phi_{P''} + AN\phi_P + AS\phi_P = AE\phi_E + AW\phi_W \\
+ AN\phi_N + AS\phi_S
\end{aligned} \tag{4.16}$$

Since ϕ_P , $\phi_{P''}$, ϕ_E and ϕ_W are not the nodal point values, these values need to be approximated using the neighbor nodal points. In this study, the following estimations are taken

$$\phi_E = (\phi_E - \phi_{SE}) b^+ + \phi_{SE} \tag{4.17a}$$

$$\phi_{P'} = (\phi_P - \phi_S) a^+ + \phi_S \tag{4.17b}$$

$$\phi_W = (\phi_W - \phi_{SW}) a + \phi_{SW} \tag{4.17c}$$

$$\phi_{P''} = (\phi_P - \phi_S) b + \phi_S \tag{4.17d}$$

Where a, b, a+, and b+ are the interpolation coefficients using the locations of the corresponding points (see Figure 7, 8 and 11) like

$$a = CA(i,j) = [RU(i,j) - R(i-1,j-1)] / DYPS(i-1,j) \tag{4.18a}$$

$$b = CB(i,j) = [RU(i,j) - R(i,j-1)] / DYPS(i,j) \tag{4.18b}$$

$$a^+ = CA(i+1,j) \tag{4.18c}$$

$$b^+ = CB(i+1,j) \tag{4.18d}$$

In the computer program, more variables are introduced to express the coefficients of the linear interpolation for the other control volumes, UA and UB for u-volume, and VA and VB for v-volume. These coefficients are calculated in the similar way. Introduction of Equation (4.17) into Equation (4.16) and Rearrangement of the resulting equation produces

$$AP'\phi_P = AE'\phi_E + AW'\phi_W + AN'\phi_N + AS'\phi_S + ASE'\phi_{SE} + ASW\phi_{SW} \tag{4.19}$$

$$\text{Where } AP' = AW \cdot b + AE \cdot a^+ + AN + AS \tag{4.20a}$$

$$AE' = AE \cdot b^+ \tag{4.20b}$$

$$AW' = AW \cdot a \tag{4.20c}$$

$$AN' = AN \tag{4.20d}$$

$$AS' = AS - AW(1 - b) - AE(1 - a^+) \tag{4.20e}$$

$$ASE = AE(1 - b^+) \tag{4.20f}$$

$$ASW = AW(1 - a) \quad (4.20g)$$

Here, AE, AW, AN and AS are the coefficients given in Equation (4.14). Two more nodal points are added comparing with the standard form.

When the skewness of nonorthogonal grid due to the sloping boundary is not much steep and so the contributions of the extra terms may not be big. However, to make a general computer program, the discretization of those extra terms must be considered carefully in details in the code. As shown in Figure 12, there is not a standard way in discretizing the extra terms for the sloping control surfaces, north and south, considering x-direction discretization. In this study, the extra terms are discretized using ϕ_A and ϕ_B for the south sloping surface, and ϕ_C and ϕ_D for the north one. Since ϕ_A , ϕ_B , ϕ_C and ϕ_D are not nodal point values, using the neighbor nodal point values, these values can be approximated with the linear interpolation

$$\phi_A = (\phi_w - \phi_{sw}) c + \phi_{sw} \quad (4.21a)$$

$$\phi_B = (\phi_e - \phi_{se}) d + \phi_{se} \quad (4.21b)$$

$$\phi_C = (\phi_{nw} - \phi_w) c^+ + \phi_w \quad (4.21c)$$

$$\phi_D = (\phi_{ne} - \phi_e) d^+ + \phi_e \quad (4.21d)$$

Where c , d , c^+ and d^+ are the coefficients of the linear interpolation using the locations of the corresponding points (see Figures 7, 8 and 12)

$$c = CC(I,j) = [(RUS(i,j) + RUS(i+1,j))/2 - RU(i,j-1)]/DYPSU(i,j) \quad (4.22a)$$

$$d = CD(i,j) = [(RUS(i,j) + RUS(i+1,j))/2 - RU(i+1,j-1)]/DYPSU(i+1,j) \quad (4.22b)$$

$$c^+ = CC(i,j+1) \quad (4.22c)$$

$$d^+ = CD(i,j+1) \quad (4.22d)$$

In the computer code, more variables, UC and UD for the u-volume, and VC and VD for the v-volume, are defined to represent the coefficients of the linear interpolation for each control volume. However, ϕ_w , ϕ_{sw} , ϕ_{nw} , ϕ_e , ϕ_{se} and ϕ_{ne} are not nodal point values, either. These values are approximated as following;

$$\phi_w = 0.5 \times (\phi_p + \phi_w) \quad (4.23a)$$

$$\phi_{sw} = 0.5 \times (\phi_S + \phi_{SW}) \quad (4.23b)$$

$$\phi_{TW} = 0.5 \times (\phi_N + \phi_{NW}) \quad (4.23c)$$

$$\phi_e = 0.5 \times (\phi_P + \phi_E) \quad (4.23d)$$

$$\phi_{TE} = 0.5 \times (\phi_N + \phi_{NE}) \quad (4.23e)$$

$$\phi_{SE} = 0.5 \times (\phi_S + \phi_{SE}) \quad (4.23f)$$

After applying the hybrid scheme to the extra terms using ϕ_A , ϕ_B , ϕ_C , and ϕ_D , we can obtain a discretized form of the extra terms

$$ASX \phi_A + ANX \phi_D = ASX \phi_B + ANX \phi_C \quad (4.24)$$

where ASX and ANX are the coefficients resulted from the discretization. Introduction of Equations (4.21) and (4.23) into Equation (4.24) results in a final form of the discretized equation with only the nodal point values;

$$APT \phi_P = AET \phi_E + AWT \phi_W + ANT \phi_N + AST \phi_S + ANE \phi_{NE} + ANW \phi_{NW} \\ + ASE \phi_{SE} + ASW \phi_{SW} \quad (4.25)$$

$$\text{where } APT = 0.5 \cdot [ANX(c^+ - d^+) + ASX(c - d)] \quad (4.26a)$$

$$AET = -0.5 \cdot [ANX(1 - d^+) - ASX \cdot d] \quad (4.26b)$$

$$AWT = -0.5 \cdot [ASX \cdot c - ANX(1 - c^+)] \quad (4.26c)$$

$$ANT = 0.5 \cdot [ANX(c^+ - d^+)] \quad (4.26d)$$

$$AST = 0.5 \cdot [ASX(c - d)] \quad (4.26e)$$

$$ANE = -0.5 \cdot ANX \cdot d^+ \quad (4.26f)$$

$$ANW = 0.5 \cdot ANX \cdot c^+ \quad (4.26g)$$

$$ASE = 0.5 \cdot ASX(1 - d) \quad (4.26h)$$

$$ASW = 0.5 \cdot ASX(1 - c) \quad (4.26i)$$

From Equation (4.18), four more nodal points, ϕ_{NE} , ϕ_{NW} , ϕ_{SE} and ϕ_{SW} are included due to the extra terms. The extra coefficients corresponding to these nodal points denote ANE, ANW, ASE and ASW, respectively, in the computer code. These coefficients are also incorporated in the residual source calculation for the convergence check and the

column vector $C(I)$ calculation in the subroutine LISOLV.

(3) The Pressure and Velocity Corrections : The discretization of Equation (4.12)

with $\phi = u_w$ and u_e for the u -control volume (see Figure 13(a)) can be written as

$$a_w u_w = \sum a_{nb} u_{nb} + b + P_w A_w - P_p A_p + P_{n,w} A_{nx,w} - P_{s,w} A_{sx,w} \quad (4.27)$$

$$a_e u_e = \sum a_{nb} u_{nb} + b + P_p A_p - P_e A_e + P_{n,e} A_{nx,e} - P_{s,e} A_{sx,e} \quad (4.28)$$

With $\phi = v_s$ and v_n for the v -control volume (see Figure 13(c)), we have

$$a_s v_s = \sum a_{nb} v_{nb} + b + (P_s - P_p) A_s \quad (4.29)$$

$$a_n v_n = \sum a_{nb} v_{nb} + b + (P_p - P_n) A_n \quad (4.30)$$

These momentum equations can be solved only when the pressure field is known or somehow estimated. Unless the correct pressure field is employed, the resulting velocity field will not satisfy the continuity equation. Such an imperfect velocity field based on a guessed pressure field P will be denoted by u^* and v^* . The starred velocity field will result from the solution of the following equations :

$$a_w u_w^* = \sum a_{nb} u_{nb}^* + b + P_w^* A_w - P_p^* A_p + P_{n,w}^* A_{nx,w} - P_{s,w}^* A_{sx,w} \quad (4.31)$$

$$a_e u_e^* = \sum a_{nb} u_{nb}^* + b + P_p^* A_p - P_e^* A_e + P_{n,e}^* A_{nx,e} - P_{s,e}^* A_{sx,e} \quad (4.32)$$

$$a_s v_s^* = \sum a_{nb} v_{nb}^* + b + (P_s^* - P_p^*) A_s \quad (4.33)$$

$$a_n v_n^* = \sum a_{nb} v_{nb}^* + b + (P_p^* - P_n^*) A_n \quad (4.34)$$

Let us propose that the correct pressure P is obtained from

$$P = P^* + P' \quad (4.35)$$

Where P' is the pressure correction. The corresponding velocity corrections, u' and v' can be introduced in a similar way :

$$u = u^* + u' \quad (4.36)$$

$$v = v^* + v' \quad (4.37)$$

If we subtract Equation (4.31) from Equation (4.27), we obtain

$$\begin{aligned} a_w (u_w - u_w^*) = & \sum a_{nb} (u_{nb} - u_{nb}^*) + (P_w - P_w^*) A_w - (P_p - P_p^*) A_p \\ & + (P_{n,w} - P_{n,w}^*) A_{nx,w} - (P_{s,w} - P_{s,w}^*) A_{sx,w} \end{aligned} \quad (4.38)$$

By using P' and u' , this equation becomes

$$a_w u_w' = \sum a_{nb} u_{nb}' + P_w' A_w - P_p' A_p + P_{n,w}' A_{nx,w} - P_{s,w}' A_{sx,w} \quad (4.39)$$

For simplicity, $\sum a_{nb} u_{nb}'$ term will be neglected. The result is

$$a_w u_w' = P_w' A_w - P_p' A_p + P_{n,w}' A_{nx,w} - P_{s,w}' A_{sx,w} \quad (4.40)$$

or

$$u_w' = \frac{A_w P_w'}{a_w} - \frac{A_p P_p'}{a_w} + \frac{A_{nx,w} P_{n,w}'}{a_w} - \frac{A_{sx,w} P_{s,w}'}{a_w} \quad (4.41)$$

Now, the velocity correction formula for u_w can be written as

$$u_w' = u_w^* + \frac{A_w P_w'}{a_w} - \frac{A_p P_p'}{a_w} + \frac{A_{nx,w} P_{n,w}'}{a_w} - \frac{A_{sx,w} P_{s,w}'}{a_w} \quad (4.42)$$

The correction formulas for other velocities can be derived in the similar manner :

$$u_e' = u_e^* + \frac{A_p P_p'}{a_e} - \frac{A_e P_e'}{a_e} + \frac{A_{nx,e} P_{n,e}'}{a_e} - \frac{A_{sx,e} P_{s,e}'}{a_e} \quad (4.43)$$

$$v_s' = v_s^* + \frac{A_s}{a_s} (P_s' - P_p') \quad (4.44)$$

$$v_n' = v_n^* + \frac{A_n}{a_n} (P_p' - P_n') \quad (4.45)$$

(4) The Pressure Correction Equation. In the discretized continuity equation (4.11), we need u and u values which are not given since these locates differently from the regular u location (see Figure 13(a)). Those values can be estimated approximately by

$$u_n = 0.25 \times (u_{nw} + u_w + u_{ne} + u_e) \quad (4.46)$$

$$u_s = 0.25 \times (u_{sw} + u_w + u_{se} + u_e) \quad (4.47)$$

Then, Equation (4.11) becomes

$$\begin{aligned} (\rho u A)_e - (\rho u A)_w - \frac{(\rho A_x)_n}{4} (u_{nw} + u_w + u_{ne} + u_e) \\ + \frac{(\rho A_x)_s}{4} (u_{sw} + u_w + u_{se} + u_e) + (\rho v A)_n - (\rho v A)_s = 0 \end{aligned} \quad (4.48)$$

Now, we need to substitute for the velocity components in this equation with the velocity correction formulas, Equations (4.42) through (4.45), in order to obtain the pressure correction equation. However, prior to this step, another several approximations are required for the undetermined values such as $P_{n,w}'$, $P_{s,w}'$, $P_{n,e}'$ and $P_{s,e}'$ in the velocity correction formulas. Those values can be approximated using the surrounding node values

$$P'_{n,w} = 0.25 \times (P'_{NW} + P'_W + P'_P + P'_N) \quad (4.49a)$$

$$P'_{s,w} = 0.25 \times (P'_{SW} + P'_W + P'_P + P'_S) \quad (4.49b)$$

$$P'_{n,e} = 0.25 \times (P'_{NE} + P'_E + P'_P + P'_N) \quad (4.49c)$$

$$P'_{s,e} = 0.25 \times (P'_{SE} + P'_E + P'_P + P'_S) \quad (4.49d)$$

The complete velocity correction formulas for u_{nw} , u_{ne} , u_{sw} and u_{se} can be written as following

$$u_{nw} = u_{nw}^* + \frac{A_{NW}}{a_{nw}} P'_{NW} - \frac{A_{NP}}{a_{nw}} P'_N + \frac{A_{nx,nw}}{a_{nw}} P'_{n,nw} - \frac{A_{sx,nw}}{a_{nw}} P'_{s,nw} \quad (4.50)$$

$$u_{ne} = u_{ne}^* + \frac{A_{NP}}{a_{ne}} P'_N - \frac{A_{NE}}{a_{ne}} P'_N + \frac{A_{nx,ne}}{a_{ne}} P'_{n,ne} - \frac{A_{sx,ne}}{a_{ne}} P'_{s,ne} \quad (4.51)$$

$$u_{sw} = u_{sw}^* + \frac{A_{sW}}{a_{sw}} P'_{SW} - \frac{A_{SP}}{a_{sw}} P'_S + \frac{A_{nx,sw}}{a_{sw}} P'_{n,sw} - \frac{A_{sx,sw}}{a_{sw}} P'_{s,sw} \quad (5.52)$$

$$u_{se} = u_{se}^* + \frac{A_{SP}}{a_{se}} P'_S - \frac{A_{SE}}{a_{se}} P'_{SE} + \frac{A_{nx,se}}{a_{se}} P'_{n,se} - \frac{A_{sx,se}}{a_{se}} P'_{s,se} \quad (4.53)$$

However, to avoid the complexity due to these terms, we will take the following simple expressions for u_n and u_s by neglecting all other terms except the first one on the right hand side in Equations (4.50) through (4.53) :

$$u_n = 0.25 \times (u_{nw}^* + u_w^* + u_{ne}^* + u_e^*) \quad (4.54)$$

$$u_s = 0.25 \times (u_{sw}^* + u_w^* + u_{se}^* + u_e^*) \quad (4.55)$$

By introducing Equations, (4.41) through (4.45) and (4.49) through (4.55) into Equation (4.48) and rearranging the resulting equation, we obtain the final discretized form of the pressure correction equation ;

$$a_p P'_p = a_E P'_E + a_W P'_W + a_N P'_N + a_S P'_S + a_{NE} P'_{NE} + a_{SE} P'_{SE} + a_{NW} P'_{NW} + a_{SW} P'_{SW} + b \quad (4.56)$$

where

$$a_p = (\rho A)_e \left[\frac{A_p}{a_e} + \frac{A_{nx,e}}{4 a_e} - \frac{A_{sx,e}}{4 a_e} \right] + (\rho A)_w \left[\frac{A_p}{a_w} - \frac{A_{nx,w}}{4 a_w} + \frac{A_{sx,w}}{4 a_w} \right] + (\rho A)_n \frac{A_N}{a_n} + (\rho A)_s \frac{A_S}{a_s} \quad (4.57a)$$

$$a_E = (\rho A)_e \left[\frac{A_E}{a_e} - \frac{A_{nx,e}}{4 a_e} + \frac{A_{sx,e}}{4 a_e} \right] \quad (4.57b)$$

$$a_w = (\rho A)_w \left[\frac{A_w}{a_w} + \frac{A_{nx,w}}{4 a_w} - \frac{A_{sx,w}}{4 a_w} \right] \quad (4.57c)$$

$$a_n = (\rho A)_n \frac{A_n}{a_n} - (\rho A)_e \frac{A_{nx,e}}{4 a_e} + (\rho A)_w \frac{A_{nx,w}}{4 a_w} \quad (4.57d)$$

$$a_s = (\rho A)_s \frac{A_s}{a_s} + (\rho A)_e \frac{A_{sx,e}}{4 a_e} - (\rho A)_w \frac{A_{sx,w}}{4 a_w} \quad (4.57e)$$

$$a_{NE} = -(\rho A)_e \frac{A_{nx,e}}{4 a_e} \quad (4.57f)$$

$$a_{SE} = (\rho A)_e \frac{A_{sx,e}}{4 a_e} \quad (4.57g)$$

$$a_{NW} = (\rho A)_w \frac{A_{nx,w}}{4 a_w} \quad (4.57h)$$

$$a_{SW} = -(\rho A)_w \frac{A_{sx,w}}{4 a_w} \quad (4.57i)$$

$$b = (\rho u^* A)_w - (\rho u^* A)_e + \frac{(\rho A_x)_n}{4} (u_{nw}^* + u_w^* + u_{ne}^* + u_e^*) \\ - \frac{(\rho A_x)_s}{4} (u_{sw}^* + u_w^* + u_{se}^* + u_e^*) + (\rho v^* A)_s - (\rho v^* A)_n \quad (4.57j)$$

From Equation (4.56), we note $a_p \neq \sum a_{nb}$. For the north boundary cell ($J = NJM1$), $P'_{n,w}$ and $P'_{n,e}$ can not be estimated appropriately because P' is not known at the wall boundary.

In this study, $P'_{n,w}$ is approximated using the linear interpolation with P'_1 and P'_1 , and $P'_{n,e}$ with P'_2 and P'_e as shown in Figure 13. P'_1 , P'_w , P'_2 and P'_e also calculated approximately;

$$P'_1 = 0.25 \times (P'_w + P'_p + P'_{sw} + P'_s) \quad (4.58)$$

$$P'_w = 0.5 \times (P'_w + P'_p) \quad (4.59)$$

$$P'_2 = 0.25 \times (P'_e + P'_p + P'_{se} + P'_s) \quad (4.60)$$

$$P'_e = 0.5 \times (P'_e + P'_p) \quad (4.61)$$

Then, $P'_{n,w}$ and $P'_{n,e}$ can be found as following

$$P'_{n,w} = (P'_w - P'_1) AI + P'_1 \quad (4.62)$$

$$P'_{n,e} = (P'_e - P'_2) BI + P'_2 \quad (4.63)$$

where AI and BI are the coefficients of the linear interpolation using the locations of the

corresponding points (see Figure 8 and 14).

$$AI = SNSU(i,NJM1)/(RU(i,j) - RUS(i,j)) \quad (4.64a)$$

$$BI = SNSU(i+1,NJM1)/(RU(i+1,NJM1) - RUS(i+1,NJM1)) \quad (4.64b)$$

With these expressions, we obtain a slightly different discretized equation for P' about the north boundary cells :

$$a_P P'_P = a_E P'_E + a_W P'_W + a_N P'_N + a_S P'_S + a_{SE} P'_{SE} + a_{SW} P'_{SW} + b \quad (4.65)$$

where

$$a_P = (\rho A)_e \left[\frac{A_P}{a_e} + \frac{A_{nx,e}}{4 a_e} (b + 1) - \frac{A_{sx,e}}{4 a_e} \right] + (\rho A)_w \left[\frac{A_P}{a_w} - \frac{A_{nx,w}}{4 a_w} (a + 1) + \frac{A_{sx,w}}{4 a_w} \right] + (\rho A)_n \frac{A_N}{a_n} + (\rho A)_s \frac{A_S}{a_s} \quad (4.66a)$$

$$a_E = (\rho A)_e \left[\frac{A_E}{a_e} - \frac{A_{nx,e}}{4 a_e} (b + 1) + \frac{A_{sx,e}}{4 a_e} \right] \quad (4.66b)$$

$$a_W = (\rho A)_w \left[\frac{A_W}{a_w} + \frac{A_{nx,w}}{4 a_w} (a + 1) - \frac{A_{sx,w}}{4 a_w} \right] \quad (4.66c)$$

$$a_N = (\rho A)_n \frac{A_N}{a_n} \quad (4.66d)$$

$$a_S = (\rho A)_s \frac{A_S}{a_s} + (\rho A)_e \left[-\frac{A_{nx,e}}{4 a_e} (1 - b) + \frac{A_{sx,e}}{4 a_e} \right] + (\rho A)_w \left[\frac{A_{nx,w}}{4 a_w} (1 - a) - \frac{A_{sx,w}}{4 a_w} \right] \quad (4.66e)$$

$$a_{NE} = 0 \quad (4.66f)$$

$$a_{NW} = 0 \quad (4.66g)$$

$$a_{SE} = (\rho A)_e \left[-\frac{A_{nx,e}}{4 a_e} (1 - b) + \frac{A_{sx,e}}{4 a_e} \right] \quad (4.66h)$$

$$a_{SW} = (\rho A)_w \left[\frac{A_{nx,w}}{4 a_w} (1 - a) - \frac{A_{sx,w}}{4 a_w} \right] \quad (4.66i)$$

$$b = (\rho u^* A)_w - (\rho u^* A)_e - \frac{(\rho A_x)_s}{4} (u_{sw}^* + u_w^* + u_{se}^* + u_e^*) + (\rho v^* A)_e s - (\rho v^* A)_n \quad (4.66j)$$

CHAPTER V

THE SAMPLE COMPUTATION

5.1 The Flow System Description

The sample computer code outputs given in Appendix C are concerned with the turbulent reacting swirling flow in an idealized combustion chamber as shown in Figure 15. The sample flow system has two concentric inlets and one circumferential inlet, a gradual expansion wall (30 degrees slope angle) at left side. The diameter of outer wall is 0.36 m and the length of combustion chamber 0.7 m. An air at 300 K enters through the annular inlet ($R_2 = 0.1$ m, $R_3 = 0.14$ m) and the circumferential inlet (0.02 m gap). Those velocities are 20 m/sec and 5 m/sec, respectively. A fuel gas (methane) enters through the central pipe inlet ($R_1 = 0.08$ m) with the velocity 2.857 m/sec at 300 K. The air-fuel ratio is 15 % excess air on a mass basis. An ignition pilot is employed near the annular wall of the inlet to start combustion. In the computer program, six hot spots are located at nodal points near the annular wall.

5.2 Input Data

The flow domain is covered by a 23×9 mesh system ($N_I = 23$ for the x-direction, $N_J = 9$ for the r-direction). The details of grid system are shown in Figure 16. The computer code has the capability of automatic grid generation in both uniform and expansion grids. However, it is more convenient to define a grid system in case of multi-inlet. The wall between two concentric inlets and the circumferential inlet cause a little difficulties in the automatic grid generation. In this sample computation, the user has assigned the grid

system as given in Figure 16, $NI = 23$, $NJ = 9$, $X(I)$, $RLARGE = 0.18$, $RSMALL = 0.14$
AND $SX1 = 0.06282$. The outer boundary location $YB(I)$ are defined as follows,

$$YB(1) = RSMALL$$

$$YB(I) = YB(1) + X(I) \times \tan \theta \quad \text{for } X(I) \leq SX1$$

$$YB(I) = RLARGE \quad \text{for } X(I) \geq SX1$$

where θ is the slope angle.

$Y(I,J)$ are calculated using the $YB(I)$ in the code.

Next, we need to define the geometry control parameters,

$$INOG = 1 \text{ (nonorthogonal grid system)}$$

$$IAEW = 1 \text{ (linear interpolation with lower two points)}$$

$$IGCT = 1 \text{ (1 top inlet)}$$

$$IGCS = 2 \text{ (2 side concentric inlets)}$$

The sizes of inlets are assigned as follows,

$$JINAS = 2 \text{ (south node point of central pipe inlet)}$$

$$JINAN = 5 \text{ (north node point of central pipe inlet)}$$

$$JINBS = 7 \text{ (south node point of annular inlet)}$$

$$JINBN = 8 \text{ (north node point of annular inlet)}$$

$$IINW = 6 \text{ (west node point of top inlet)}$$

$$IINE = 6 \text{ (east node point of top inlet)}$$

The inlet conditions need to be given next for each inlet. For the central pipe inlet,

$$UIN = 2.857$$

$$FUIN = 1.$$

$$OXIN = 0.$$

$$TIN = 300.$$

For the annular inlet,

$$UINB = 20.$$

$$FUINB = 0.$$

$$OXINB = 0.232$$

$$TINB = 300.$$

For the circumferential (top) inlet,

$$VIN2 = 5.$$

$$FUIN2 = 0.$$

$$OXIN2 = 0.232$$

$$TIN2 = 300.$$

The fluid properties are assigned as follows,

$$WFU = 16. \text{ (molecular weight of methane)}$$

$$WOX = 32. \text{ (molecular weight of oxygen)}$$

$$HFU = 4.7E7 \text{ (heat of combustion)}$$

$$OXDFU = 4. \text{ (oxygen fuel ratio)}$$

$$TWALL = 300. \text{ (wall temperature)}$$

Another parameter frequently requiring different values is swirl strength. The program is set up via LFS and LFSMAX to sequentially calculate through a range of the given swirl vane angles or the given swirl numbers. These angles and swirl numbers are specified in DATA statements for the array VANB and SWNB respectively. VANB is activated if the control parameter NSBR = 0 and SWNB if NSBR = 1. The weak swirl solution was used as the initial conditions for the strong swirl computation to prevent divergence of solution in the strong swirl calculation with arbitrary given initial conditions. For this sample flow, swirl number is 0.4.

5.3 Description of Outputs

The typical computer outputs are printouts of values for the flowfield properties (u, v, w, h, m_{fu} , m_{ox} , m_{pr} , T, k, and ϵ etc.) u-velocity decay profiles and fuel mass fraction profiles

at the preassigned downstream locations (IPB(I)) and the plot of streamline pattern. These are included in Appendix C.

The u-velocity field values show that combustion increases the u-velocities up to 58.6 m/sec at the exit by comparing the averaged isothermal u-velocity, 7.6 m/sec. The negative u-velocities happen near the wall region next to the top inlet as shown in the u-field values and the u-velocity decay profiles. From the stream function values and the plot of streamline pattern, the wall streamline is detached and moves down due to the top inlet velocity (VIN2). A small recirculation zone occurs in the region just downstream of the top inlet. For this flow system, combustion is still in progress at the exit since a large amount of fuel is remained at the exit by considering the fuel fluxes 0.0473 kg/sec at inlet and 0.0351 kg/sec at the exit.

0.0473 kg/s
0.0351 kg/s

CHAPTER VI

RESULTS AND DISCUSSION

A new computer code has been developed to solve axisymmetric flows with a boundary-fitted nonorthogonal grid system technique. The code also has the capability of generalized stair-step boundary approximation for irregular domain with the orthogonal grid system. Once a new code has been developed, the verification of the code predictability needs to be investigated for various flow cases; laminar or turbulent, and nonreacting or reacting flows. Five selected test cases are outlined in Table I. The schematics of the five flow systems are described in Figure 1. These are specially chosen to demonstrate the predictive capability of the new code for different flow systems by comparing the results with available experimental data.

The computational grid sizes are (30×9) for Case 1 to 3 and (26×16) for Case 4 and 5. Flat inlet profiles are assumed for all cases as shown in Table X. Comparisons and flowfields are illustrated in Figure 17 through 38. Each figure shows a radial profile of a chosen mean flowfield property such as u-velocity, w-velocity species concentration, and temperature at a given axial station. Velocities are nondimensionalized using a fixed quantity, averaged inlet velocity, U_{in} , and the radial locations are normalized with the radius of the outer boundary wall at the given axial locations, R. Axial locations are denoted by their nondimensional distances, x/D . Predicted streamline patterns are expressed in an artistic plot based on the line printer plot and computer outputs. Tables IV through IX provide the predicted mean flowfield properties at the downstream locations.

6.1 Laminar Flow Prediction

The experimental data for laminar flows in the irregular domains are very rare.

Forrester & Young (120), Young & Tsai (121) and Bentz (122) presented the flow characteristics in a steady laminar flow through an axisymmetric converging-diverging tube. The new code is employed to predict a steady laminar flow in the irregular boundary wall pipe, which was studied experimentally by Bentz (122), for Test Case 1. He obtained velocity profiles in a pipe flow which has a bell-shaped constriction (as shown in Figure 1-(a) using a laser Doppler velocimeter. The range of Reynolds number was 2 through 168. He compared the experimental data with the theoretical values obtained by Lee and Fung (123) for the flow in exactly the same exponentially shaped contour. The results showed that both curves have similar shapes, however, the maximum experimental velocity was larger than the maximum theoretical value.

Figure 17 shows comparisons of the experimental data with the results at the two axial stations, $x/D = 0.325$, and 1.5 . The predictions are in agreement with experimental values. However, the computed center line velocity at the downstream location $x/D = 0.325$ is less than the experimental value similar to the Lee and Fung's results. From the predicted streamline pattern as shown in Figure 18, a recirculation zone occurs in the corner. The separation point is $x/D = 0.25$ and the reattachment point $x/D = 1.4$. These values are smaller than their experimental ones, 0.3 and 2.1 , respectively. Macagno and Hung (128) investigated the relations between the reattachment point and the Reynolds number of the laminar flow in a sudden expansion pipe (diameter ratio D/d of 2) using dye. The Reynolds numbers are up to 200, and they found that the reattachment length linearly increases with the Reynolds numbers. From these relations, the reattachment point for the Bentz flow ($Re = 57$) would be $x/D = 2.4$ on the basis of a sudden expansion assumption. But the Bentz experiment has a gradual exponential expansion, and they found $x/D = 2.1$

which is slightly shorter. Figure 19 shows the predicted mean axial velocity profiles at three downstream locations, $x/D = 1.5, 3$ and 4 .

6.2 Turbulent Flow Predictions

A turbulent flow within an irregular domain is used to show the predictability of the new code for Test Case 2. Deshpande and Giddens (124) performed detailed measurements of turbulent flow through a constricted tube with a cosine curve contour as shown in Figure 1-(b) using a laser Doppler anemometer. Rastogi (125) predicted this flow numerically with body-fitted orthogonal curvilinear coordinates. Comparisons of his computed values with the experimental data revealed that the calculated centerline velocities are smaller than those measured downstream of the constriction throat.

Figure 20 compares the measured values with the predicted ones at the downstream locations, $x/D = 1$, and 2 . The calculations are in reasonable agreement with the experimental data. As shown in Figure 21, the flow separates at $x/D = 0.3$ and reattaches at $x/D = 2.3$. Comparisons of the separation and reattachment points are not possible since the measured data is not available. Mean axial velocity profiles are plotted at the downstream locations, $x/D = 1, 2, 3$, and 4 in Figure 22.

For Test Case 3, a gradual expanding swirling flow experimentally investigated by Yoon and Lilley (34) is employed to demonstrate the prediction capability of the present code for another irregular domain boundary flow. They conducted mean velocity measurements at the downstream distances $x/D = 0.5$ and 1 with several swirl vane angles ($0, 38, 45, 60$ and 70 degrees) under an isothermal flow condition.

Figure 23 illustrates the current computed values and the experimental data. The predicted velocity profiles without swirl are similar in shape to the experimental ones. The predicted reattachment point is $x/D = 2$ as shown in Figure 24, however, the measured one is $x/D = 2.3$. Chaturvedi (129) measured the reattachment point for turbulent flows in four abrupt expansions (diameter ratio D/d of 2) with half angles of $15, 30, 45$, and 90 degrees.

The reattachment lengths for $Re = 2 \times 10^5$ are $x/D = 1.7, 2.1, 2.2,$ and $2.3,$ respectively. Moon and Rudinger (130) studied experimentally the reattachment point for the turbulent flow in a sudden expansion circular duct with an expansion ratio D/d of 1.43. The reattachment length for $Re = 2.8 \times 10^5$ is found to be $x/D = 1.3.$ They showed that the reattachment length is practically independent of Reynolds number, over the range of 10^3 to $10^6.$ This length for turbulent flows is between six and nine step heights. The predicted reattachment lengths for turbulent flows (Cases 2 and 3) shows the independence of Reynolds number. These lengths are in good agreement with the measured values. The features of the radial profiles of mean axial velocities are illustrated in Figure 25.

The presence of swirl (swirl No. 0.67) results in disagreement between the computed values and the measured ones near the inlet region as shown in Figures 26 and 27, the mean axial and swirl velocity profiles, respectively. The peak of the predicted mean axial velocity profile is at $r/R = 0.5,$ however, the measurements give a peak near the wall. The calculated profile of mean axial velocity at the downstream distance, $x/D = 1,$ is close to the measured one but is lower than it near the wall. From Figure 26-(a), the predicted mean swirl velocities are larger than the experimental values at $x/D = 0.5$ downstream location. The computed values are in agreement with the measured data, except the peak locations are slightly different. A central recirculation zone occurs in the swirling flow. This zone is extended to $x/D = 1.64$ which is much longer than the measured value, $x/D = 0.5.$ The corner recirculation zone appears smaller due to the swirl. Figure 29 shows the radial profiles of mean axial velocities at the different downstream locations. Rhode (126) made flowfield predictions in the same flow system with the standard STARPIC and performed comparisons with his measurements. His comparisons are similar to the present ones. He showed that poor agreement results at $x/D = 0.5,$ although there was good agreement for the further downstream locations, $x/D \geq 1.5.$

6.3 General Predictions of Flows in Model Combustor

The prediction abilities of the present code for a turbulent mixing nonreacting flow and a turbulent swirling reacting flow are confirmed with Test Case 4 and 5. Johnson and Bennett (127) measured the mean and fluctuating velocity and species concentration distribution and their correlations for the sudden expansion flow system as shown in Figure 1-(d). Their experimental method employed a laser velocimetry to obtain velocity data and a laser induced fluorescence technique to obtain species concentration data.

The present numerical results of Test Case 4 are plotted in Figure 30 for velocity and figure 31 for species concentration with comparisons of experimental data (127) at the two downstream locations, $x/D = 1.67$ and 5. The computed profiles of velocity and concentrations are in excellent agreement with the measured ones. The streamline pattern in Figure 32 shows the corner recirculation zone and the reattachment point, $x/D = 1.9$. The flow stream converges slightly a short distance downstream from the annular inlet. This streamline convergence towards the axis of symmetry is encouraged by the thick annular wall separator between between the two concentric inlets. Further downstream, the converging streamline diverges back to the full pipe diameter at the reattachment point. The point of smallest flow cross section is termed the vena contracta; this corresponds to the point of lowest pressure (131,132). Figure 33 gives the features of radial profiles of mean axial velocities and concentrations at different axial locations. The mixing looks almost complete at $x/D = 2.5$ as shown in Figure 33-(b).

The calculation of a turbulent reacting flow using the present code is conducted with the flow of Spadaccini et al. (12) for Test Case 5. They reported measurements of mean velocities, gas temperature and species concentrations at various locations downstream of the burner exit. Since inlet profiles were not measured, flat inlet profiles were employed for the current computation.

Calculated and measured profiles of mean axial velocity and gas temperature at the two axial locations ($x/D = 0.49$, and 1.99) are compared in Figures 34 and 35. Fuel and oxygen concentration profiles are compared at $x/D = 1.47$ in Figure 36. From the comparisons, the predicted velocities at $x/D = 0.49$ are lower than measured data, especially near the center line. At the further downstream location ($x/D = 1.99$), the profile of the calculated velocity is close to the experimental one except at the central region. Species concentration calculations are in agreement with the measured values. However, predicted maximum temperature is a little higher than the measured temperature. A small recirculation appears near the location, $x/D = 0.5$ and $r/R = 0.4$ as shown Figure 37-(a). For this flow, the swirl (swirl No. 0.52) is not strong enough to create a central recirculation zone. Figure 38 illustrates mean axial velocity, temperature and fuel concentration profiles at different downstream locations.

6.4 Comparisons of Predictions of Standard STARPIC and New Code

Yoon and Lilley's flow system (34) is employed to compare the two predictions obtained using the standard STARPIC code which has an orthogonal grid scheme and the newly developed code which has a nonorthogonal grid scheme. Two runs of the STARPIC code, coarse grid (20×8) and fine grid (33×16), are performed. Figure 39 shows the comparisons of the two different computer code predictions at two downstream locations, $x/D = 0.5$ and 1 . Both codes result in similar predictions which are in agreement with the experimental data. Similar results are produced with both coarse and fine grid computations of STARPIC code. The 45 degree gradual expansion wall causes divergence of the solution in the fine grid calculation of this new code. The discretizing approximation due to the grid nonorthogonality may be a reason of divergence in the solution procedure. With a fine grid system, the stair-step boundary approximation would be a more appropriate approach than the nonorthogonal grid approach for an irregular outer boundary wall which has steep slope angles. The approximated stair-step boundary is close to the

real boundary in a fine grid system.

The comparisons of these two different code predictions for swirling flow (Case 3(b)) are shown in Figures 40 and 41, which are mean axial and swirl velocity profiles, respectively, at two downstream locations, $x/D = 0.5$ and 1. For the mean axial velocity, both code predictions are in relatively poor agreement with the experimental data at $x/D = 0.5$ which is near inlet region as shown in Figure 40. However, at $x/D = 1$ location, the new code with nonorthogonal grid system predicts slightly closer to the experimental values than the old STARPIC code prediction. Figure 41 shows that the STARPIC code gives a better quality prediction than the new code for the swirl velocity. Considering the computer run time, the new code has taken 69 seconds but the other code 51 seconds. The extra flux term calculations of nonorthogonal grid scheme cause more computing time in the new code than the orthogonal grid scheme in the STARPIC code.

For the 45 degree expansion problem considered, it appears that the orthogonal grid system is a more efficient method than the nonorthogonal grid system. However the latter has an advantage of easy implementation for a generalized irregular outer boundary wall location. This special feature is particularly important in practical applications.

6.5 Discretization of Flux Equations in Nonorthogonal Grid System

Beginning with the standard STARPIC computer program, three major intermediate steps (Methods 1, 2 and 3) were carried out with a 45 degree gradual expansion flow (Test Case 3(a)) and the results of each approach were investigated thoroughly to develop the new code. These three steps and findings are discussed briefly in this section.

As the first step (Method 1), the nonorthogonal grid is incorporated into the STARPIC code. However, fluxes over the vertical east and west surfaces are simply computed from the usual grid point values. That is, values at E' and W' are taken to be the same as at E and W in calculating these fluxes, see Figure 13. The north and south sloping

surfaces has only vertical r-direction fluxes passing over them: no consideration is given to additional x-direction fluxes. The iterative solution of this simplified code diverged, since the 45 degree slope may be too steep to neglect these effects. This lead to the desire to include additional terms in the representation of the equations in the nonorthogonal grid system.

In the second step of Method 2, the fluxes on the north and south sloping control surfaces are included in the discretization of equations as described in detail in Chapter IV. However, E' and W' values are again taken to be the values at E and W as in Method 1. The code of Method 2 resulted in a converged solution. But the results are coarse and of poorer quality than those of Method 3.

In Method 3, in addition to the changes of Method 2, the gridline nonorthogonality at the east and west control surfaces is considered in the flux equation discretization at these surfaces. Values of E' and W' are inferred from linear interpolation using values of SE and E, and SW and W, respectively. The detailed description is given in Chapter IV. Comparisons are made among the experimental data and the results of Methods 2 and 3 as follows:

Results at $x/D = 0.5$

	Method 2	Method 3	Experiment
Maximum axial velocity (m/sec)	18.3	14.8	14.2
Centerline velocity (m/sec)	11.2	14.8	14.2
Maximum axial reverse velocity (m/sec)	-5.16	-4.04	-3.9

Results at $x/D = 1.0$

	Method 2	Method 3	Experiment
Maximum axial velocity (m/sec)	16.1	13.5	13.2
Centerline velocity (m/sec)	11.3	13.5	13.2
Maximum axial reverse velocity (m/sec)	-4.21	-2.28	-1.6

The reattachment lengths are $x/D = 2.3$ for Method 2, 2 for Method 3, and 2.3 for the experiment. Method 3 shows that the flow diverges more rapidly than Method 2. A shorter corner recirculation zone length is found in Method 3. For Method 3 and the experiment have the maximum values of mean axial velocity at the centerline but Method 2 has that value at $r/R = 0.36$ for both downstream locations. Method 3 results smaller values of reverse axial velocity near wall and centerline velocity, which are close to the measured values, than Method 2. From these comparisons of predictions of Test Case 3(a), the Method 3 produces more accurate predictions than the earlier Methods 1 and 2.

6.6 Accuracy of Predictions

The overall accuracy of the nonorthogonal grid code predictions can be described with the differences between the predicted values and the measured data. Considering the calculated values at the location, $x/D = 1$, for the irregular boundary domain flows of Cases 1, 2 and 3, the averaged difference between predicted mean axial velocities and the measured ones without swirl is within 5 %. However, the presence of swirl increases this difference to 8 % and a mean swirl velocity difference of about 6 % is seen. The differences of reattachment lengths are approximately 33 % and 9 % in laminar and turbulent flows, respectively, for Cases 1, 2 and 3.

Now, the accuracy of predictions for the regular boundary domain flows of Cases 4 and 5 is discussed. For an isothermal flow of Case 4, the predicted values of mean axial velocity and species concentration are very close to the experimental data within 2 % differences. In case of a combusting flow of Case 5, the averaged differences are found 8 % for mean axial velocity, 2 % for fuel mass fraction, and 10 % for mean temperature.

CHAPTER VII

CLOSURE

7.1 Conclusions

Upon the completion of the development of a nonorthogonal grid system technique for an irregular outer boundary wall and the incorporation of a combustion simulation, with confirmatory comparisons using available experimental data, the follow conclusions are obtained:

1. The computer program using a nonorthogonal grid system can solve axisymmetric flows in irregular outer wall domains. However, there is a limitation in the radial direction grid. A fine grid of the radial coordinate for a large slope angle outer boundary wall is not acceptable to this nonorthogonal grid technique since the approximation of grid nonorthogonality causes divergence.

2. Flat inlet profile assumptions such as uniform axial and swirl velocity may produce poor predictions near the inlet region. These assumptions do not influence critically the flowfield calculation at further downstream locations.

3. Employment of the k- ϵ two-equation turbulence model results in good predictions for the nonswirling flows. However, the k- ϵ two-equation turbulence model may not be adequate enough to calculate flowfield of the swirling flow with a sloping outer boundary wall.

4. The simple one-step, three component combustion model produces qualitatively reasonable predictions for gaseous turbulent combustion flows. This combustion simulation is not enough to obtain a quantitatively reasonable temperature field for

combusting flows. All components involved in combustion need to be considered in combustion model.

5. Turbulent mixing is performed well when the high shear layer region occurs with large differences between the two concentric inlet velocities. Better mixing enhances more efficient combustion.

6. Inclusion of density into the exit velocity correction calculation gives better convergence for the variable density flow computation. The exit velocity correction is not a critical procedure to obtain a convergent solution, but this improves the convergence rate during the iteration process.

7. The boundary approximations may not cause any problems in the solution procedure even if they result in a different flowfield prediction comparing the real flowfield with the exact boundary. The approximated discretization of the governing differential equation for a nonorthogonal grid system may cause divergence in some flow cases, like a steep slope outer boundary wall flow.

7.2 Recommendations for Further Study

Further fundamental research should be extended in several areas to develop a more powerful and accurate calculation method. First, the discretization method of the flux equation on the sloping control surfaces and on the skewed grid lines will require more detailed investigations for the grid skewness to improve the accuracy of prediction and to remove the limitation of fine grid application for a steep slope outer boundary wall. Many computer experiments will be needed for each investigation with various flow systems. Second, the hybrid scheme currently being used may be replaced with other schemes (the quadratic upwind difference scheme or the skew-upwind difference scheme) to reduce numerical diffusion in case of streamline skewness with respect to the grid lines. Third, more than one-step chemical reaction model with dissociation needs to be incorporated into

the code to produce better solutions for combusting flows. Fourth, the capability of particle-laden flows should be incorporated into the code to improve flowfield predictions of liquid fuel droplet or coal particle laden gaseous flows. Fifth, The analytical or numerical coordinate transformation method can be employed to resolve the complex flow domains instead of the boundary approximation or a nonorthogonal grid approximation.

REFERENCES

- (1) Gupta, A. K., Lilley, D. G., and Syred, N., Swirl Flows. Abacus Press, Tunbridge Wells, England, 1985.
- ✓ (2) Gupta, A. K., and Lilley, D. G., Flowfield Modeling and Diagnostics. Abacus Press, Tunbridge Wells, England, 1985.
- (3) Khalil, E. E., Modeling of Furnaces and Combustors. Abacus Press, Tunbridge Wells, England, 1982.
- (4) Libby, P. A., and Williams, F. A., Turbulent reacting Flows. Springer-Verlag, Berlin, Heidelberg, 1980.
- ✓ (5) Beer, J. M., and Chigier, N. A., Combustion and Aerodynamics. Applied Science, London and Halsted-Wiley, New York, 1972.
- (6) Roache, P. J., Computational Fluid Dynamics. Hermosa Publishers, Albuquerque, New Mexico, 1972.
- ⑦ (7) Anderson, D. A., Tannehill, J. C., and Pletcher, R. H. Computational Fluid Mechanics and Heat Transfer. Hemisphere Publishing Co. and McGraw Hill Book Co. New York, 1984.
- (8) Patankar, S. V., Numerical Heat Transfer and Fluid Flow. Hemisphere Publishing Corporation, London, 1980.
- (9) Lilley, D. G., and Rhode, D. L., "STARPIC : A Computer Code for Swirling Turbulent Axisymmetric Recirculating Flows in Practical Isothermal Combustor Geometries." NASA-CR-3442, June, 1981.
- ⑩ (10) Lilley, D. G., "Investigations of Flowfields Found in Typical Combustor Geometries." Final Report on Grant NAG3-74, NASA CR-3869, February, 1985.
- (11) Baker, R. J., Hutchinson, P., Khalil, E. E., and Whitelaw, J. H., "Measurements of Three Velocity Components in a Model Furnace with and without Combustion." Proceedings 15th Symposium on Combustion. 1974, pp. 553-559.
- (12) Spadaccini, L. J., Owen, F. K., and Bowman, C. T., "Influence of Aerodynamic Phenomena on Pollutant Formation in Combustion." Environmental Protection Agency Report. EPA 600/2-76-2470. 1976.
- (13) Hutchinson, P., Khalil, E. E., Whitelaw, J. H., and Wigly, G., "The Calculation of Furnace-Flow Properties and Their Experimental Verification." Journal of Heat

Transfer, May 1976, pp. 276-283.

- (14) Smith, G. D., Giel, T. V., and Catalano, C. G., "Measurements of Reactive Recirculating Jet Mixing in a Combustor." AIAA Journal, Vol. 21, No. 2 1983, pp. 270-276.
- (15) Gouldin, F. C., Depsky, J. S., and Lee, S. L., "Velocity Field Characteristics of a Swirling Flow Combustor." AIAA 21st Aerospace Science Meeting, AIAA-83-0314, January 10 -13, 1983, Reno, Nevada.
- (16) Brum, R. D., and Samuelsen, G. S., "Assessment of a Dilute Swirl Combustor as a Bench Scale, Complex Flow Test Bed for Modeling, Diagnostics, and Fuel Effects Studies." AIAA/SAE/ASME 18th Joint Propulsion Conference. AIAA-82-1263. June 21-23, 1982, Cleveland, Ohio.
- (17) Larue, J. C., Samuelsen, G. S., and Seiler, E. T., "Momentum and Heat Flux in a Swirl-Stabilized Combustor." 20th Symposium (International) on Combustion / The Combustion Institute, 1984, pp. 277-285.
- (18) Owen, F. K., "Laser Velocity Measurements of a Confined Turbulent Diffusion Flame Burner." AIAA 14th Aerospace Science Meeting. AIAA-76-33. January 26-28, 1976, Washington, D.C.
- (19) Khalil, K. H. El-Mahallawy, F. M., and Moneib, H. A., "Effect of Combustion Air Swirl on the Flow Pattern In a Cylindrical Oil Fired Furnace." Sixteenth Symposium (International) on Combustion / The Combustion Institute, 1978, pp. 135-143.
- (20) Lewis, M. H., and Smoot, L. D., "Turbulent Gaseous Combustion Part I : Local Species Concentration Measurements." Combustion and Flame, Vol. 42, 1981, pp. 183-196.
- (22) Smith, P. J., and Smoot, L. D., "Turbulent Gaseous Combustion Part II : Theory and Evaluation for Local Properties." Combustion and Flame, Vol. 42, 1981, pp. 277-285.
- (21) Lockwood, F. C., El-Mahallawy, F. M., and Spalding, D. B., "An Experimental and Theoretical Investigation Turbulent Mixing in a Cylindrical Furnace." Combustion and Flame, Vol. 23, 1974, pp. 283-293.
- (22) Hassan, M. M., Lockwood, F. C., and Moneib, H. A., "Measurements in a Gas-Fired Cylindrical Furnace." Combustion and Flame, Vol. 51, 1983, pp. 249-261.
- (23) Bicen, A. F., and Jones, W. P., "Velocity Characteristics of Isothermal and Combusting Flows in a Model Combustor." Combustion and Flame, Vol. 49, 1986, pp. 1-15.
- (24) Jones, W. P., and Toral, H., "Temperature and Composition Measurements in a Research Gas Turbine Combustor." Combustion Science and Technology, Vol. 31, 1983, pp. 249-275.
- (25) Heitor, M. V., and Whitelaw, J. H., "Velocity, Temperature and Species

- Characteristics of the Flow in a Gas-Turbine Combustor." Combustion and Flame, Vol. 62, 1986, pp. 1-32.
- (26) Habib, M A., and Whitelaw, J. H., "Velocity Characteristics of Confined Coaxial Jets with and Without Swirl." Journal of Fluids Engineering, Vol. 102, March 1980, pp. 47-53.
- (27) Habib, M, A.,and Whitelaw, J. H., "Velocity Characteristics of a Confined Coaxial Jet." Journal of Fluids Engineering, Vol. 102, December 1979, pp. 521-529.
- (28) Rao, A. N., Ganesan, V., Gopalakrishnan, J. V., and Natarajan, R., "Experimental and Theoretical Investigations of Vane Generated Swirling Flows in a Circular Chamber." Journal of the Institute of Energy, September 1983, pp. 137-144.
- (29) Yu, B. T., and Gouldin, F. C., "Flow Measurements in a Model Swirl Combustor." AIAA Journal, Vol. 20, No. 5, May 1982, pp. 642-651.
- (30) Owen, F. K., "Measurements and Observations of Turbulent Recirculation Jet Flows." AIAA Journal, Vol. 14, No. 11, November 1976, pp. 1556-1562.
- (31) Johnson, B. V., and Roback, R., "Mass and Momentum Turbulent Transport Experiments with Confined Swirling Coaxial Jets Part I." AIAA/SAE/ASME 20th Joint Propulsion Conference. AIAA-84-1380 June 11-13, 1984, Cincinnati, Ohio.
- (32) Roback, R., and Johnson, B. V., "Mass and Momentum Turbulent Transport Experiments with Swirling Confined Coaxial Jets - Part 2." AIAA/ASME/SAE/ASEE 22nd Joint Propulsion Conference, AIAA-86-1665, June 16-18, 1986, Huntsville, Alabama.
- (33) Schetz, J. A., Hewitt, P. W., and Thomas, R., "Swirl Combustor Flow Visualization Studies in a Water Tunnel." AIAA/SAE/ASME 18th Joint Propulsion Conference, AIAA-82-1238, June 21-23, 1982, Cleveland, Ohio.
- (34) Yoon, H. K., and Lilley, D. G., "Five-Hole Pitot Probe Time Mean Velocity Measurements in Confined Swirling Flows." AIAA Paper 83-0313, January 1983.
- (35) Ramos, J. I., and Somer, H. T., "Swirling Flow in a Research Combustor." AIAA Journal, Vol. 23, No. 2, February 1985, pp. 241-248.
- (36) Altgeld, H., Jones, W.P., and Wilhaelmi, J., "Velocity Measurements in a Confirmed Swirl Driven Recirculating Flow." Experiments in Fluids, 1, 1983, pp. 73-78.
- (37) Drewry, J. E., "Fluid Dynamic Characterization of Sudden-Expansion Ramjet Combustor Flowfields." AIAA Journal, Vol 16, No. 4, April 1978, pp. 313-319.
- (38) Yang, B. T., and Yu, M. H., "The Flowfield in a Suddenly Enlarged Combustion Chamber." AIAA Journal, Vol 21, No 1, Jan., 1983, pp. 92-97.

- (39) Sampath, S. and Ganeson, V., "Experimental Theoretical Investigation of Flow behind Bluff Bodies." Journal of the Institute of Energy, Dec., 1981, pp. 213-224.
- (40) Somer H. T., "Swirling Flow in a Research Chamber." AIAA 21st Aerospace Sciences Meeting, AAA-83-0313, Jan. 10-13, 1987, Reno, Nevada.
- (41) Kanury, A. M., Introduction to Combustion Phenomena. Gordon and Breach, Science Publishers, Inc., New York, 1975.
- (42) Spalding, B. B., Combustion and Mass Transfer. Pergaman Press, New York, 1979.
- (43) Kuo, K. K., Principles of Combustion. John Wiley & Sons. Inc., New York, 1986.
- (44) Launder, B. E., and Spalding, D. B., Mathematical Models of Turbulence. Academic Press, New York, 1972.
- (45) Schetz, J. A., Foundations of Boundary Layer Theory for Momentum, Heat, and Mass, for Transfer. Prentice-Hall, Inc., Englewood Cliffs, New Jersey, 1984.
- (46) Bradshaw, P., Topics in Applied Physics: Turbulence. Vol. 12, Springer-Verla Berlin Heidelberg, 1976.
- (47) Hinze, J. O., Turbulence. McGraw-Hill, New York, 1959.
- (48) Tennekes, H. and Lumley, J. L., A First Course in Turbulence, Prentice-Hall International, 1972.
- (49) Chow, C. Y., An Introduction to Computational Fluid Mechanics. John Wiley & Sons, Inc., New York, 1979.
- (50) Jones, W. P., and Whitelaw, J. H., "Calculation Methods for Reacting Turbulent Flows : A Review." Combustion and Flame, Vol. 48, 1982, pp. 1-26.
- (51) Jones, W. P., and Whitelaw, J. H., "Modelling and Measurements in Turbulent Combustion." 20th Symposium (International) on Combustion / The Combustion Institute, 1984, pp. 233-249.
- (52) Lilley, D. G., "Computer Solution of Reacting Flowfield." Proceedings of ASME Computers in Engineering Conference, August 12-15, 1984, Las Vegas, Nevada.
- (53) Gupta, A. K., and Lilley, D. G., "The Gray Areas in Combustion Research." AIAA/ASME/SAE/ASEE 22nd Joint Propulsion Conference, AIAA-86-1663, June 16-18, 1986, Huntsville, Alabama.
- (54) Gosman, A. D., Lockwood, F. C., and Salooja, A. P., "The Prediction of Cylindrical Furnaces Gaseous Fueled with Premixed and Diffusion Burners." 17th Symposium (International) on Combustion / the Combustion Institute, 1978, pp. 747-760.

- (55) Khalil, E. E., Spalding, D. B., and Whitelaw, J. H., "The Calculation of Local Flow Properties in Two-Dimensional Furnaces." International Journal for Heat and Mass Transfer, Vol. 17, 1975, pp. 775-791.
- (56) Ramos, J. I., "A Numerical Study of a Swirl Stabilized Combustor." Journal of Non-Equilibrium Thermodynamics, Vol. 10, 1985, pp. 263-286.
- (57) Novick, A. S., and Miles, G. A., "Numerical Simulation of Combustor Flow Fields." AIAA/SAE 14th Joint Propulsion Conference, AIAA-78-949, July 25-27, 1978, Las Vegas, Nevada.
- (58) Samples, J. W., and Lilley, D. G., "Chemically Reacting Axisymmetric Flowfield Prediction." AIAA 22nd Aerospace Sciences Meeting, AIAA-84-0364, January 9-12, 1984, Reno, Nevada.
- (59) Sturgess, G. J., and Syed, S. A., "Dynamic Behavior of Turbulent Flow in a Widely-Spaced Coaxial Jet Diffusion Flame Combustor." AIAA 21st Aerospace Sciences Meeting, AIAA-83-0575, January 10-13, 1984, Reno, Nevada.
- (60) Mongia, H.C., Reynolds, R.S., and Srinivasan, R., "Multidimensional Gas Turbine Combustion Modeling: Applications and Limitations." AIAA Journal, Vol. 24, No. 6, June 1986, pp. 890-904.
- (61) Kent, J. H., and Bilger, R. W., "The Prediction of Turbulent Diffusion Flame Fields and Nitric Oxide Formation." 16th Symposium (international) on Combustion / The Combustion Institute, 1978, pp. 1643-1656.
- (62) Pope, S.B., "The Probability Approach to the Modeling of Turbulent Reacting Flows." Combustion and Flame 27, 1976, pp. 299-312.
- (63) Borgi, R., and Escudie, D., "Assessment of a Theoretical Model of Turbulent Combustion by Comparison with a Simple Experiment." Combustion and Flame, Vol. 56, pp. 149-164.
- (64) Anand, M. S., and Pope, S. B., "Calculation of Premixed Turbulent Flames by PDF Methods." Combustion and Flame, Vol. 67, pp. 127-142.
- (65) Nikjooy, M., So, R. M. C., Peck, R. E., "Modelling of Jet- and Swirl-Stabilized Reacting Flows in Axisymmetric Combustors." Combustion Sciences and Technology. Vol. 58, 1988, pp. 135-153.
- (66) Smith, P. J., and Smoot, D., "Turbulent Gaseous Combustion Part II Theory and Evaluation for Local Properties." Combustion and Flame, Vol. 42, 1981, pp. 277-285.
- (67) Shyy, W., Correa, S. M., and Braaten, M. E., "Computation of Flow in a Gas Turbine Combustor." Combustion Science and Technology, Vol. 58, 1988, pp. 97-117.
- (68) Picart, A., Borghi, R., and Chollet, J. P., "Numerical Simulation of Turbulent Reactive Flows." Computers and Fluids, Vol. 16, No. 4, 1988, pp. 475-484.
- (69) Bray, K. N. C., "The Interaction between Turbulence and Combustion." 17th

- Symposium (International) on Combustion / The Combustion Institute, 1979, pp. 223-233.
- (70) Ballal, D. R., and Chent, T. H., "Turbulence-Combustion Interaction in Practical Combustion Systems." AIAA/ASME/SAE/ASEE 22nd Joint Propulsion Conference, AIAA-86-1607, June 16-18, 1986, Huntsville, Alabama.
- (71) Ballal, D. R., "Studies of Turbulent Flow-Flame Interaction." AIAA Journal, Vol. 24, No. 7, 1986, pp. 1148-1154.
- (72) Chomiak, J., "Dissipation Fluctuations and the Structure and Propagation of Turbulent Flames Premixed Gases at High Reynolds Numbers." 16th Symposium (International) on Combustion / The Combustion Institute, 1978, pp. 1665-1673.
- (73) Launder, B. E., and Spalding, D. B., "The Numerical Computation of Turbulent Flows." Computer Methods in Applied Mechanics and Engineering, Vol. 3, 1974, pp. 269-289.
- (74) Peck, R. E. and Samuelsen, G. S., "Eddy Viscosity Modeling in the Prediction of Turbulent, Backmixed Combustion Performance." Sixteenth Symposium (International) on Combustion/The Combustion Institute, 1978, pp. 1675-1687.
- (75) Abujela, M. T. and Lilley, D. G., "Limitations and Empirical Extensions of the k-e Model as Applied to Turbulent Confined Swirling Flows." AIAA 22nd Aerospace Sciences Meeting, AIAA-84-0441, January 9-12, 1984, Reno, Nevada.
- (76) Abujela, M. T., Jackson, T. W., and Lilley, D. G., "Swirl Flow Turbulence Modeling." AIAA/SAE/ASME 20th Joint Propulsion Conference, AIAA-84-1376, June 11-13, 1984, Cincinnati, Ohio.
- (77) Rhode, D. L. and Stowers, S. T., "Turbulence Model Assessment for the Confined Mixing of Co-Swirling Concentric Jets." AIAA/ASE/ASME/ASEE 21st Joint Propulsion Conference, AIAA-85-1269, July 8-10, 1985, Monterey, California.
- (78) Amano, R. S., "Development of a Turbulence Near-Wall Model and Its Application to Separated and Reattached Flows." Numerical Heat Transfer, Vol. 7., 1984, pp. 59-75.
- (79) Jennings, M. J. and Morel, T., "Observations on the Application of the k-e Model to Internal Combustion Engine Flows." Combustion Science and Technology, Vol. 58. 1988, pp. 177-193.
- (80) Sturgess, G. J., "Aerothermal Modeling , Phase I - Final Report," NASA Report CR-168202, May 27, 1983.
- (81) Agarwal, R. K., "A Third-Order-Accurate Upwind Scheme for Navier-Stokes Solutions at High Reynolds Numbers." Paper No. AIAA-81-0112, AIAA 19th Aerospace Sciences Meeting, St. Louis, Missouri, January 12-15, 1981.
- (82) Leonard, B. P., "A Stable and Accurate Convective Modeling Procedure Based on Quadratic Upstream Interpolation," Computer Methods in Applied Mechanics and

Engineering, Vol. 19, 1979, pp. 59-98.

- (83) Raithby, G. D., "Skew - Upstream Differencing Scheme for Problems Involving Fluid Flow," Computer Methods in Applied Mechanics and Engineering, Vol. 9, 1976.
- (84) Rubin, S. G. and Graves Jr., R. A., "Viscous Flow Solutions with a Cubic Spline Approximation," Computers and Fluids, Vol. 3, 1975, pp. 1-36.
- (85) Glas, J. and Rodi, W., "A Higher Order Numerical Scheme for Scalar Transport," Computer Methods in Applied Mechanics and Engineering, Vol. 31, 1982, pp. 337-358.
- (86) Boris, J. P. and Book, D. L., "Flux-Corrected Transport I: Shasta - A Fluid Transport Algorithm that Works," Journal of Computational Physics, Vol. 11, 1973.
- (87) Syed, S. A., Pratt & Whitney, and Chiappetta, L., "Finite Difference Methods for Reducing Numerical Diffusion in TEACH-type Calculations," Paper No. AIAA-85-0057, AIAA 23rd Aerospace Sciences Meeting, January 14-17, 1985, Reno, Nevada.
- (88) Syed, S. A., Chiappetta, L. M., and Gosman, A. D., "Error REduction Program, Final Report," NASA CR 174776, Jan., 1985.
- (89) Syed, S. A., Pratt & Whitney, Gosman, A. D., and Peric, M., "Assessment of Discretization Schemes to Reduce Numerical Diffusion in the Calculation of Complex Flows," Paper No. AIAA-85-0441, AIAA 23rd Aerospace Sciences Meeting, Reno, Nevada, Jan. 14-17., 1985.
- (90) Sharif, M. A. R. and Busnaina, A. A., "Assessment of Finite Difference Approximations for the Advection Terms in the Simulation of Practical Flow Problems," Department of Mechanical and Industrial Engineering Report, No. MIE-148, Clarkson University, Potsdam, New York, June 1987.
- (91) Baker, A. J., "Numerical Solution to the Dynamics of Viscous Fluid Flow Using a Finite Element Idealization," Proceedings of IASS Pacific Symposium on Hydrodynamically Loaded Shells, Oct., 1971.
- (92) Cheng, R. T., "Numerical Solution of the Navier-Stokes Equations by the Finite Element Method," Physics of Fluids, Vol. 15, Dec., 1982, pp. 2098-2105.
- (93) Baker, A. J., "Finite Element Solution Algorithm for Viscous Incompressible Fluid Dynamics," International Journal for Numerical Methods in Engineering, Vol. 6, 1973, pp. 89-101.
- (94) Baker, A. J. and Zelanzny, S. W., "A Theoretical Study of Mixing Downstream of Transverse Injection into a Supersonic Boundary Layer," CR-112254, Dec., 1972, NASE.
- (95) Gallagher, R. H., Oden, J. T., Taylor, C., and Zienkiewicz, O. C., Finite Elements in Fluids, Vol. 1, Viscous Flow and Hydrodynamics, John Wiley & Sons Ltd., New York, 1975

- (96) Roache, P. J., "Semi-indirect Method for Internal Flows in Flush Inlets," AIAA Third Computer Dynamics Conference, Albuquerque, New Mexico, June 27-28, 1977, pp. 149-155.
- (97) Oberkampf, W. L., "Domain Mapping for the Numerical Solution of Partial Differential Equations." International Journal for Numerical Methods in Engineering, Vol. 10, 1976, pp. 211-223.
- (98) Barfield, W. D., "Numerical Methods for Generating Orthogonal Curvilinear Meshes." Journal of Computational Physics, Vol. 5, 1970, pp. 23-33.
- (99) Thompson, J. F., Thames, F. C., and Mastin, C. W., "Automatic Numerical Generation of Body-Fitted Curvilinear Coordinate System for Field Containing Any Number of Arbitrary Two-Dimensional Bodies," Journal of Computational Physics, Vol. 15, pp. 299-319.
- (100) Barfield, W. D., "Numerical Method for Generating Orthogonal Curvilinear Grids." Journal of Computational Physics, Vol. 5, 1970, pp. 23-33..
- (101) Amsden, A. A., and Hirt, C. W., "A Simple Scheme for Generating General Curvilinear Grids," Journal of Computational Physics, Vol. 11, 1973, pp. 348-359.
- (102) Floryan, J. M., "Conformal-Mapping-Based Coordinate Generation Method for Flows in Periodic Configurations". Journal of Computational Physics, Vol. 62, 1986, pp. 221-247.
- (103) Mastin, C. W., and Thomson, J. F., "Three-Dimensional Body-Fitted Coordinate Systems for Numerical Solutions of the Navier-Stokes Equations." Presented at AIAA 11th Fluid and Plasma Dynamics Conference, July 10-12, 1978, Seattle, Washington.
- (104) Miki, K. and Takagi, T., "A Domain Decomposition and Overlapping Method for the Generation of Three-Dimensional Boundary-Fitted Coordinate Systems." Journal of Computational Physics, Vol. 53, 1984, pp. 319-330.
- (105) Aubert, X., and Deville, M. "Steady Viscous Flows by Compact Differences in Boundary-Fitted Coordinates." Journal of Computational Physics, Vol. 49, 1983, pp. 490-522.
- (106) Dvinsky, A. S., and Popel, A. S., "Numerical Solution of Two-Dimensional Stokes Equations for Flow with Particles in a Channel of Arbitrary Shapes Using Boundary-Conforming Coordinates." Journal of Computational Physics, Vol. 67, 1986, pp. 73-90.
- (107) Reggio, M., and Camarero, R., "Numerical Solution Procedure for Viscous Incompressible Flows." Numerical Heat Transfer, Vol. 10, 1986, pp. 131-146.
- (108) Pope, S. B. "The Calculation of Turbulent Recirculating Flows, in General Orthogonal Coordinates." Journal of Computational Physics, Vol. 27, 1976, pp. 192-217.

- (109) Raithby, G. D., Galpin, P. F., and Doormaal, J. P. "Prediction of Heat and Fluid Flow in Complex Geometries Using General Orthogonal Coordinates." Numerical Heat Transfer, Vol. 12, 1986, pp. 125-142.
- (110) Grag, V. K., and Maji, P. K. "Flow through a Converging-Diverging Tube with Constant Wall Enthalpy." Numerical Heat Transfer, Vol. 12, 1987, pp. 285-305.
- (111) Rangwalla, A. A., and Munson, B. R. "Numerical Solution for Viscous flow for Two-dimensional domains Using Orthogonal Coordinate Systems." Journal of Computational Physics, Vol. 70, 1987, pp. 373-393.
- (112) Faghri, M., Sparrow, E. M., and Prata, A. T. "Finite-Difference Solutions of Convection-Diffusion Problems in Irregular Domains, Using a Nonorthogonal Coordinate Transformation." Numerical Heat Transfer, Vol. 7, 1984, pp. 183-209.
- (113) Shyy, W., Tong, S. S., and Correa, S. M. "Numerical Recirculating Flow Calculation Using a Body-fitted Coordinate System." Numerical Heat Transfer, Vol. 8, 1985, pp. 99-113.
- (114) Braaten, M., and Shyy, W. "A Study of Recirculating Flow Computation Using Body-Fitted Coordinates : Consistency Aspects and Mesh Skewness." Numerical Heat Transfer, Vol. 9, 1986, pp. 556-574.
- (115) Coulter, J. P., and Guceri S. I. "Laminar and Turbulent Natural Convection within Irregularly Shaped Enclosures." Numerical Heat Transfer, Vol. 12, 1987, pp. 211-227.
- (116) Dvinsky, A. S., and Popel, A. S., "Numerical Solution of Two-Dimensional Stroke Equations for Flow with Particles in a Channel of Arbitrary Shapes Using Boundary-Conforming Coordinates." Journal of Computational Physics, Vol. 67, 1986, pp. 73-90.
- (117) Reggio, M., and Camarero, R., "Numerical Solution Procedure for Viscous Incompressible Flows." Numerical Heat Transfer, Vol. 10, 1986, pp. 131-146.
- (118) Tacker, W. C. "A Brief Review of Techniques for Generating Irregular Computation Grids." International Journal for Numerical Methods in Engineering, Vol. 15, 1980, pp. 1335-1341.
- (119) Rhode, D. L., and Lilley, D. G., "Selection of Irregular Boundary Transformation Method for Gas turbine flowfield Simulation." Report to School of Mechanical and Aerospace Engineering, Oklahoma State University, 1980.
- (120) Forrester, J. H., and Young, D. F., "Flow through a Converging-Diverging Tube and its Implications in Occlusive Vascular Disease-II." Journal of Biomechanics, Vol. 3, 1970, pp. 307-316
- (121) Young, D. F., and Tsai, F. Y., "Flow Characteristics in Models of Arterial Stenoses-I. Steady Flow." Journal of Biomechanics, Vol. 6, 1973, pp. 395-410
- (122) Bentz, J. C., "Hemodynamic Flow in the Region of a Simulated Stenosis." Ph.D. Thesis, University of Pennsylvania, Pennsylvania, 1974.

- (123) Lee, J. S., and Fung, Y. C., "Flow in Locally Constricted Tubes at Low Reynolds Numbers." Journal of Applied Mechanics, Vol. 37, Transactions of the American Society of Mechanical Engineers, Series E, March, 1970, pp. 9-16.
- (124) Peshpande, M. D., and Giddens, D. P., "Turbulent Measurements in a Constricted Tube." Journal of Fluid Mechanics, Vol. 97, Part 1, 1980, pp. 65-89.
- (125) Rastogi, A. K., "Hydrodynamics in Tubes Perturbed by Curvilinear Obstructions." Journal of Fluid Engineering, Transactions of the ASME, Vol. 106, September, 1984, pp. 262-269.
- (126) Rhode, D. L. "Predictions and Measurements of Isothermal Flowfields in Axisymmetric Combustor Geometries." Ph. D. Thesis, Oklahoma State University, Stillwater, OK, December 1981.
- (127) Johnson, B. V., and Bennett, J. C. "Velocity and Concentration Characteristics and Their Cross Correlation for Coaxial Jets in a Confined Sudden Expansion - Part I: Experiments." Symposium on the Fluid Mechanics of Combustion Systems, 1981 Spring Conference of ASME Fluid Engineering Divisions, June 22-24, 1981, Boulder, Colorado.
- (128) Macagno, E. O., and Hung, T. K., "Computational and Experimental Study of a Captive annular Eddy." Journal of Fluid Mechanics, Vol. 28, No. 7, 1967, pp. 43-64.
- (129) Chaturvedi, M. C., "Flow Characteristics of Axisymmetric Expansions." Journal of the Hydraulics Division, Proceedings of the ASCE, Vol. 89, No. HY3, 1963, pp. 61-92.
- (130) Moon, L. F., and Rudinger, G., "Velocity Distribution in an Abruptly Expanding Circular Duct." Journal of Fluids Engineering, March, 1977, pp. 226-230.
- (131) Baumeister, T., Avallone, E. A., and Baumeister III, T., Marks' Standard Handbook for Mechanical Engineers, 8th Edition, McGraw-Hill Book Company, 1978.
- (132) Streeter, V. L., Handbook of Fluid Dynamics, 1st Edition, McGraw-Hill Book Company, New York, 1961.

APPENDIXES

APPENDIX A
TABLES

TABLE I
SELECTED TEST CASES

Case No.	Authors	Fluid	Flow Type	Properties Measured	Swirl No.
1	Bentz (122)	Water	Laminar	u	
2	Deshpande & Giddens(124)	Water	Turbulent	u, u', w'	
3	Yoon & Lilley (34)	Air	Turbulent	u, v, w	0.67
4	Johnson & Bennett(127)	Water	Turbulent	u, f, u', f', k	
5	Spadaccini et al. (12)	Air/CH ₄	Turbulent	u, v, w, T, f	0.52

TABLE II
SOURCE TERMS AND EXCHANGE COEFFICIENTS USED IN THE
GENERAL EQUATION OF ϕ

ϕ	Γ_ϕ	S_ϕ
1	0	0
u	μ	$-\frac{\partial p}{\partial x} + S^u$
v	μ	$-\frac{\partial p}{\partial r} + \frac{\rho w^2}{r} - \frac{2v}{r^2} + S^v$
w	μ	$-\frac{\rho v w}{r} - \frac{w}{r^2} \frac{\partial}{\partial r} (r\mu) + S^w$
h	μ/σ_h	S_h
m_{fu}	μ/σ_m	R_{fu}
$m_{ox} - im_{fu}$	μ/σ_f	0
k	μ/σ_k	$G - C_d \rho \epsilon$
ϵ	μ/σ_e	$(C_1 \epsilon G - C_2 \rho \epsilon^2)/k$

In this table certain quantities are defined as follows:

$$S^u = \frac{\partial}{\partial x} \left(\mu \frac{\partial u}{\partial x} \right) + \frac{1}{r} \frac{\partial}{\partial r} \left(r\mu \frac{\partial v}{\partial x} \right)$$

$$S^v = \frac{\partial}{\partial x} \left(\mu \frac{\partial u}{\partial r} \right) + \frac{1}{r} \frac{\partial}{\partial r} \left(r\mu \frac{\partial v}{\partial r} \right)$$

$$S^w = 0$$

$$G = \mu \left[2 \left\{ \left(\frac{\partial u}{\partial x} \right)^2 + \left(\frac{\partial v}{\partial r} \right)^2 + \left(\frac{v}{r} \right)^2 \right\} + \left(\frac{\partial u}{\partial r} + \frac{\partial v}{\partial x} \right)^2 + \left\{ r \frac{\partial}{\partial r} \left(\frac{w}{r} \right) \right\}^2 + \right.$$

$$\left. \left(\frac{\partial w}{\partial x} \right)^2 \right]$$

TABLE III
THE FORM OF THE COMPONENTS OF THE LINEARIZED SOURCE TERM*

ϕ	Γ_ϕ	S_p^ϕ	S_u^ϕ/V
γ	0	0	0
u	μ	0	$S^u - \frac{\partial p}{\partial x}$
v	μ	$-2 \frac{\mu}{r^2}$	$S^v + \frac{\rho w^2}{r} - \frac{\partial p}{\partial r}$
w	μ	0	$-\frac{\rho v w}{r} - \frac{w}{r^2} \frac{\partial}{\partial r} (r\mu)$
h	μ/σ_h	0	
m_{fu}	μ/σ_m	$-R_{fu}/m_{fu}$	0
$m_{ox} - im_{fu}$	μ/σ_f	0	0
k	μ/σ_k	$-C_\mu C_D \rho^2 K/\mu$	G
ϵ	μ/σ_ϵ	$-C_2 \rho \epsilon/K$	$C_1 C_\mu G \rho K/\mu$

S^u , S^v , and G are as in TABLE II

TABLE IV
 PREDICTED AXIAL AND RADIAL VELOCITIES OF CASE 1

r/R	x/D					
	0.000	0.325	0.900	1.500	3.000	6.000
0.937	0.619	-0.117	-0.033	0.008	0.048	0.062
0.812	0.925	0.044	-0.001	0.068	0.142	0.171
0.687	1.231	0.346	0.131	0.177	0.238	0.266
0.563	1.231	0.669	0.361	0.337	0.337	0.346
0.438	1.231	0.889	0.622	0.525	0.438	0.412
0.313	1.231	1.024	0.821	0.694	0.532	0.463
0.188	1.231	1.085	0.932	0.807	0.606	0.498
0.063	1.231	1.097	0.971	0.859	0.646	0.516

u/U_{in}

r/R	x/D					
	0.000	0.325	0.900	1.500	3.000	6.000
0.875	0.000	4.239	0.428	0.342	0.087	0.007
0.750	0.000	5.079	1.483	0.995	0.278	0.021
0.625	0.000	4.237	2.705	1.624	0.498	0.040
0.500	0.000	3.040	2.862	1.896	0.663	0.055
0.375	0.000	2.161	2.236	1.671	0.698	0.060
0.250	0.000	1.443	1.384	1.141	0.575	0.052
0.125	0.000	0.742	0.611	0.550	0.321	0.030
0.000	0.000	0.000	0.000	0.000	0.000	0.000

v/U_{in} * 100

TABLE V
PREDICTED AXIAL AND RADIAL VELOCITIES OF CASE 2

r/R	x/D					
	0.000	1.000	2.000	3.000	4.000	5.000
0.929	1.000	-0.156	-0.061	0.105	0.197	0.226
0.786	1.000	-0.036	0.070	0.170	0.229	0.247
0.643	1.000	0.138	0.220	0.242	0.259	0.260
0.500	1.000	0.654	0.456	0.346	0.297	0.272
0.357	1.000	0.914	0.705	0.465	0.338	0.283
0.214	1.000	0.884	0.779	0.568	0.372	0.291
0.071	1.000	0.874	0.783	0.620	0.389	0.296

u/U_{in}

r/R	x/D					
	0.000	1.000	2.000	3.000	4.000	5.000
0.857	0.000	-6.510	1.418	0.777	0.486	0.107
0.714	0.000	-8.774	2.669	1.464	0.896	0.206
0.571	0.000	-3.715	3.444	1.961	1.192	0.273
0.429	0.000	-2.527	2.912	2.064	1.269	0.286
0.286	0.000	-1.391	1.177	1.653	1.066	0.236
0.143	0.000	-0.652	0.386	0.890	0.602	0.133
0.000	0.000	0.000	0.000	0.000	0.000	0.000

v/U_{in} * 100

TABLE VI
 PREDICTED AXIAL AND RADIAL VELOCITIES OF CASE 3

r/R	X/D					
	0.000	0.286	0.500	1.000	2.000	3.000
0.920	1.000	-0.373	-0.279	-0.156	0.000	0.131
0.773	1.000	-0.012	-0.066	0.005	0.109	0.188
0.627	1.000	0.474	0.355	0.222	0.230	0.245
0.480	1.000	0.770	0.730	0.647	0.412	0.321
0.333	1.000	0.918	0.895	0.828	0.613	0.407
0.200	1.000	0.974	0.955	0.891	0.749	0.485
0.067	1.000	0.981	0.962	0.899	0.789	0.528
u/U _{in}						
r/R	X/D					
	0.000	0.286	0.500	1.000	2.000	3.000
0.847	0.000	-4.583	1.691	1.484	1.248	0.774
0.700	0.000	-1.831	3.357	2.631	2.239	1.413
0.553	0.000	-1.066	1.854	2.286	2.890	1.889
0.407	0.000	-0.083	1.269	1.264	2.698	2.044
0.267	0.000	0.263	0.806	0.839	1.540	1.765
0.133	0.000	0.236	0.396	0.419	0.471	1.015
0.000	0.000	0.000	0.000	0.000	0.000	0.000
v/U _{in} * 100						

TABLE VII
 PREDICTED AXIAL, RADIAL AND SWIRL VELOCITIES OF CASE 3

r/R	x/D					
	0.000	0.286	0.500	1.000	2.000	3.000
0.920	1.000	-0.370	0.083	0.394	0.315	0.248
0.773	1.000	0.238	0.290	0.392	0.269	0.240
0.627	1.000	0.597	0.485	0.297	0.226	0.231
0.480	1.000	0.813	0.514	0.095	0.178	0.222
0.333	1.000	0.816	0.174	-0.085	0.133	0.213
0.200	0.000	-0.134	-0.404	-0.224	0.099	0.207
0.067	0.000	-0.315	-0.521	-0.296	0.082	0.204

u/U_{in}

r/R	x/D					
	0.000	0.286	0.500	1.000	2.000	3.000
0.847	0.000	7.467	12.389	1.522	-1.053	-0.204
0.700	0.000	20.330	19.494	1.266	-1.776	-0.321
0.553	0.000	25.798	21.654	-0.996	-2.167	-0.380
0.407	0.000	28.677	17.865	-2.523	-2.131	-0.368
0.267	0.000	22.588	-1.477	-2.258	-1.682	-0.288
0.133	0.000	6.502	-1.259	-1.215	-0.921	-0.157
0.000	0.000	0.000	0.000	0.000	0.000	0.000

v/U_{in} * 100

TABLE VII (Continued)

r/R	x/D					
	0.000	0.286	0.500	1.000	2.000	3.000
0.920	1.000	0.340	0.210	0.075	0.027	0.007
0.773	1.000	0.634	0.567	0.485	0.118	0.037
0.627	1.000	0.778	0.629	0.528	0.136	0.042
0.480	1.000	0.818	0.656	0.486	0.131	0.040
0.333	1.000	0.979	0.667	0.374	0.107	0.033
0.200	0.000	0.238	0.382	0.234	0.070	0.021
0.067	0.000	0.078	0.127	0.078	0.023	0.007
			w/U _{in}			

TABLE VIII
 PREDICTED AXIAL AND RADIAL VELOCITIES, AND CONCENTRATIONS
 OF CASE 4

r/R	x/D					
	0.000	0.250	0.840	2.500	4.840	7.300
0.951	0.000	-0.114	-0.164	0.074	0.143	0.152
0.820	0.000	-0.068	-0.070	0.114	0.174	0.178
0.623	0.000	0.083	0.182	0.192	0.194	0.193
0.443	1.000	0.848	0.643	0.285	0.208	0.201
0.328	1.000	0.985	0.909	0.340	0.215	0.205
0.228	0.000	0.647	0.709	0.377	0.221	0.207
0.115	0.313	0.236	0.415	0.401	0.225	0.208
0.016	0.313	0.206	0.304	0.407	0.226	0.209

u/U_{in}

r/R	x/D					
	0.000	0.250	0.840	2.500	4.840	7.300
0.918	0.000	-1.304	0.216	0.422	0.026	0.004
0.770	0.000	-3.131	0.820	1.137	0.072	0.010
0.574	0.000	-1.681	1.993	1.741	0.127	0.013
0.414	0.000	-1.705	1.836	1.665	0.135	0.011
0.301	0.000	-2.887	0.285	1.303	0.118	0.008
0.205	0.000	-2.618	-0.580	0.865	0.089	0.006
0.090	0.000	-0.054	-0.408	0.345	0.042	0.003
0.000	0.000	0.000	0.000	0.000	0.000	0.000

v/U_{in} * 100

TABLE VIII (Continued)

r/R	X/D					
	0.000	0.250	0.840	2.500	4.840	7.300
0.951	0.000	0.002	0.003	0.035	0.022	0.008
0.820	0.000	0.002	0.002	0.038	0.018	0.005
0.623	0.000	0.001	0.001	0.048	0.015	0.003
0.443	0.000	0.000	0.001	0.065	0.010	0.002
0.328	0.000	0.000	0.006	0.084	0.008	0.001
0.228	0.000	0.208	0.190	0.106	0.006	0.001
0.115	1.000	0.898	0.542	0.132	0.006	0.000
0.016	1.000	0.991	0.697	0.144	0.005	0.000

f

TABLE IX
 PREDICTED AXIAL, RADIAL AND SWIRL VELOCITIES, AND
 FUEL CONCENTRATIONS AND TEMPERATURE OF CASE 5

r/R	X/D					
	0.000	0.490	1.480	2.950	5.250	7.500
0.951	0.000	0.342	0.445	0.521	0.597	0.662
0.820	0.000	0.565	0.546	0.584	0.641	0.710
0.639	1.000	0.786	0.640	0.611	0.636	0.699
0.492	0.045	0.252	0.529	0.597	0.620	0.690
0.328	0.045	0.017	0.390	0.545	0.595	0.682
0.197	0.045	0.066	0.303	0.499	0.576	0.677
0.066	0.045	0.150	0.252	0.470	0.566	0.675

u/U_{in}

r/R	X/D					
	0.000	0.490	1.480	2.950	5.250	7.500
0.926	0.000	1.446	0.199	0.004	0.025	0.005
0.770	0.000	2.449	0.084	-0.350	-0.147	-0.120
0.598	0.000	-1.710	-2.085	-0.837	-0.300	-0.199
0.451	0.000	-5.796	-2.151	-0.935	-0.355	-0.215
0.295	0.000	-3.221	-1.412	-0.614	-0.309	-0.189
0.164	0.000	-1.473	-0.723	-0.365	-0.196	-0.123
0.041	0.000	-0.230	-0.188	-0.091	-0.052	-0.035

v/U_{in} * 100

TABLE IX (Continued)

r/R	X/D					
	0.000	0.490	1.480	2.950	5.250	7.500
0.951	0.000	0.564	0.583	0.601	0.620	0.615
0.820	0.000	0.535	0.547	0.593	0.627	0.636
0.639	0.665	0.535	0.564	0.558	0.535	0.523
0.492	0.000	0.466	0.609	0.514	0.444	0.420
0.328	0.000	0.414	0.538	0.406	0.319	0.293
0.197	0.000	0.274	0.372	0.267	0.199	0.180
0.066	0.000	0.093	0.135	0.095	0.069	0.062

w/U_{in}

r/R	X/D					
	0.000	0.490	1.480	2.950	5.250	7.500
0.951	0.000	0.012	0.012	0.012	0.012	0.010
0.820	0.000	0.014	0.015	0.015	0.014	0.010
0.639	0.000	0.050	0.027	0.020	0.015	0.010
0.492	1.000	0.182	0.047	0.025	0.016	0.009
0.328	1.000	0.195	0.066	0.031	0.016	0.008
0.197	1.000	0.247	0.075	0.035	0.016	0.007
0.066	1.000	0.322	0.079	0.037	0.016	0.006

m_{fu}

TABLE IX (Continued)

r/R	X/D					
	0.000	0.490	1.480	2.950	5.250	7.500
0.951	0.000	0.210	0.200	0.187	0.168	0.155
0.820	0.000	0.209	0.191	0.167	0.141	0.122
0.639	0.232	0.173	0.133	0.130	0.121	0.106
0.492	0.000	0.013	0.036	0.088	0.101	0.092
0.328	0.000	0.000	0.000	0.042	0.081	0.078
0.197	0.000	0.000	0.000	0.017	0.069	0.068
0.066	0.000	0.000	0.000	0.007	0.062	0.062
m _{ox}						
r/R	X/D					
	0.000	0.490	1.980	3.360	5.250	7.500
0.951	0.000	0.319	0.369	0.400	0.455	0.459
0.820	0.000	0.364	0.458	0.529	0.639	0.712
0.639	1.000	0.480	0.672	0.666	0.737	0.790
0.492	0.400	0.941	0.932	0.809	0.823	0.856
0.328	0.400	1.000	1.000	0.964	0.911	0.922
0.197	0.400	1.000	1.000	1.000	0.964	0.967
0.066	0.400	1.000	1.000	1.000	0.995	0.995
T/T _m						

TABLE X

FLAT INLET VELOCITIES FOR TEST CASES

Case	Inlet velocities (m/sec)		
1	UIN = 0.0134	VIN = 0	WIN = 0
2	UIN = 1.0144	VIN = 0	WIN = 0
3(a)	UIN = 15.5	VIN = 0	WIN = 0
3(b)	UIN = 14.9	VIN = 0	WIN = 14.9
4	UIN = 0.52 UINB = 1.66	VIN = 0 VIN = 0	WIN = 0 WINB = 0
5	UIN = 3.44 UINB = 75.6	VIN = 0 VIN = 0	WIN = 0 WINB = 5.02

TABLE XI

NEWLY DEFINED INPUT PARAMETERS IN THE CODE

Input Parameters	Definition
INOG	0 = Orthogonal Grid System 1 = Nonorthogonal Grid System
IGCS	1 = One Axisymmetric Inlet 2 = Two Concentric Inlets
IGCT	0 = No Top Inlet 1 = One Top Inlet
KSLP	1 = Positive or Zero Slope Angle 2 = Negative Slope Angle
IAEW	1 = Linear Interpolation with lower two Points 2 = Linear Interpolation with nearest two Points 3 = Three Point Lagrangian Interpolation

TABLE XII
NEWLY DEFINED VARIABLES IN THE CODE

Variables	Definition
ANE(I,J)	Extra coefficient of combined convective/diffusive fluxes at NE point.
ANT(I,J)	Extra coefficient of combined convective/diffusive fluxes at N point.
ANX	Projection area of north surface to x-direction
ANW(I,J)	Extra coefficient of combined convective/diffusive fluxes at NW point.
APT(I,J)	Extra sum of coefficients of combined convective/diffusive fluxes at P point
ASE(I,J)	Extra coefficient of combined convective/diffusive fluxes at SE point.
ASX	Projection area of south surface to x-direction
ASW(I,J)	Extra coefficient of combined convective/diffusive fluxes at SW point.
CFU	Specific heat of fuel
CMIX	Specific heat of mixture
COX	Specific heat of oxygen
CPR	Specific heat of product
DUE(I,J)	East coefficient of velocity-correlation term for u-velocity
DUN(I,J)	North coefficient of velocity-correlation term for u-velocity
DUS(I,J)	South coefficient of velocity-correlation term for u-velocity
DUW(I,J)	West coefficient of velocity-correlation term for u-velocity
FU(I,J)	Mass fraction of fuel

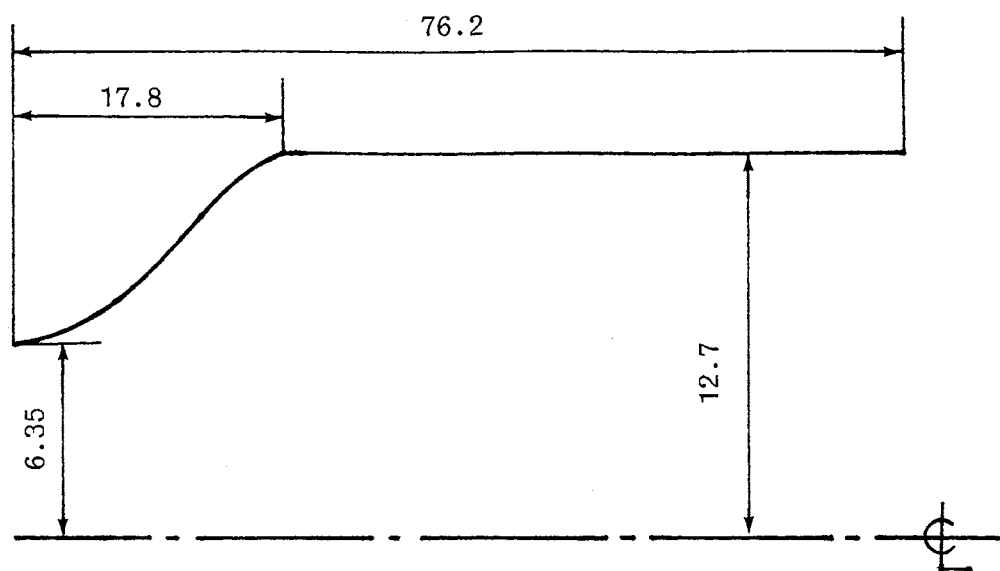
TABLE XII (Continued)

Variables	Definition
H(I,J)	Stagnation enthalpy
HFU	Heat of combustion
INCALF	Logical parameter for solution of fuel mass fraction equation
INCALH	Logical parameter for solution of stagnation enthalpy
INCALO	Logical parameter for solution of combined quantity
INPRO	Logical parameter for calculation of properties
IINE	East grid number of annular inlet
IINW	West grid number of annular inlet
JINAN	North grid number of central pipe inlet
JINAS	South grid number of central pipe inlet
JINBN	North grid number of annular inlet
JINBS	South grid number of annular inlet
OF(I,J)	Combined quantity of species calculation
OXDFU	Oxygen fuel ratio
PCA	Primary contraction angle
PR(I,J)	Mass fraction of product
PSA	Primary swirl angle
RCU	Radius of U-cell center
RCV	Radius of C-cell center
RU(I,J)	Radius of u-velocity location
RUS(I,J)	Radius of middle point of north and south u-velocity locations
RV(I,J)	Radius of v-velocity location

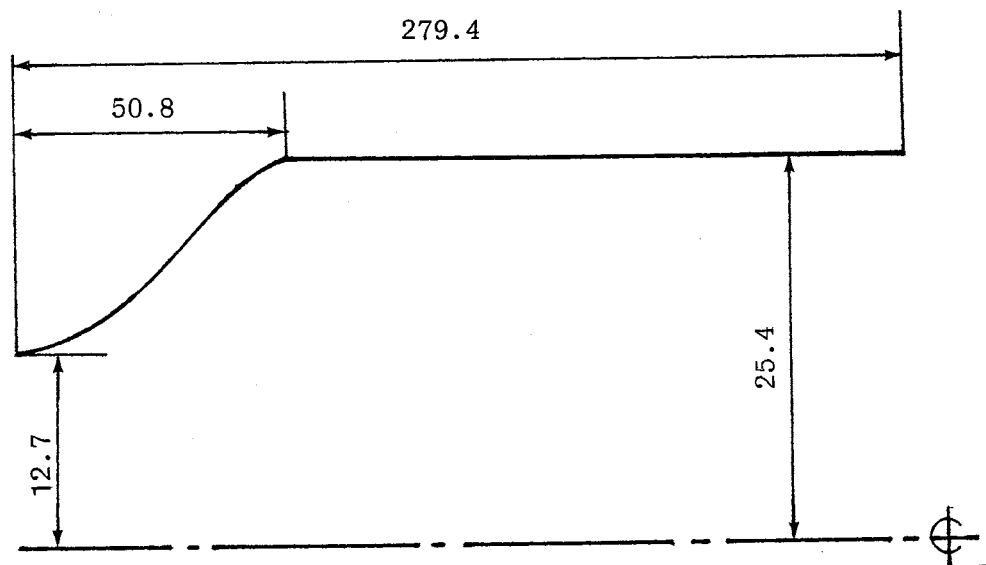
TABLE XII (Continued)

Variables	Definition
SSA	Secondary upstream angle
SUA	Secondary swirl angle
SX1	Length of slopping wall
TWALL	Wall temperature
URFF	Underrelaxation factor for fuel mass fraction
URFH	Underrelaxation factor for stagnation enthalpy
URFO	Underrelaxation factor for combined quantity
WFU	Molecular weight of fuel
YB(I)	Outer boundary location

APPENDIX B
FIGURES

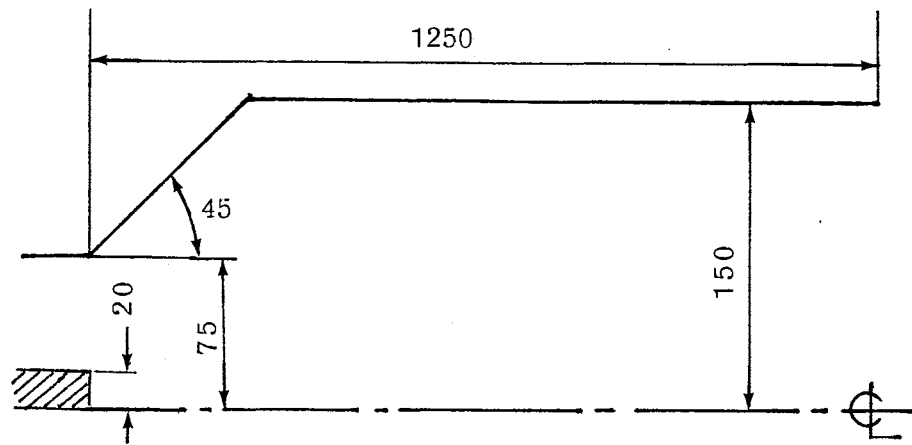


(a) Test Case 1

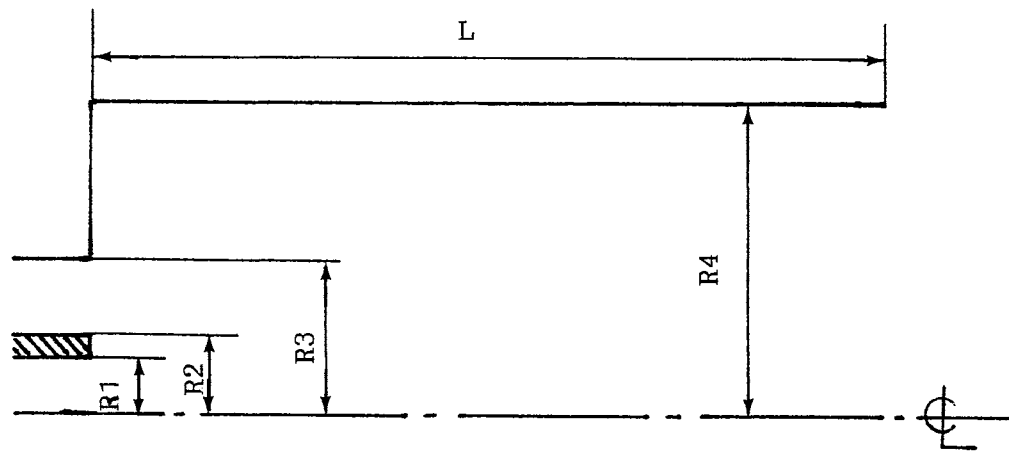


(b) Test Case 2

Figure 1. Schematic Illustration of the Flow Systems of Test Cases; Units mm



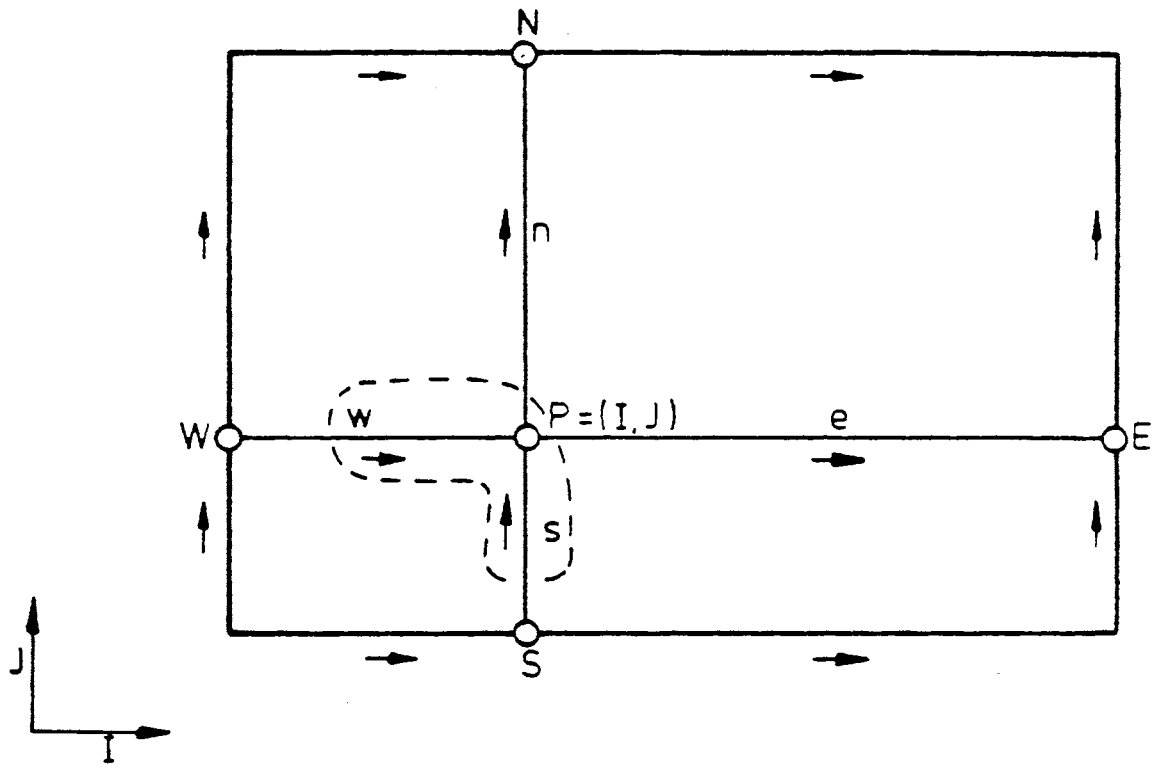
(c) Test Case 3



Case	R1	R2	R3	R4	L
4	12.5	15.3	29.5	61	1000
5	31.5	31.9	46.9	61	1000

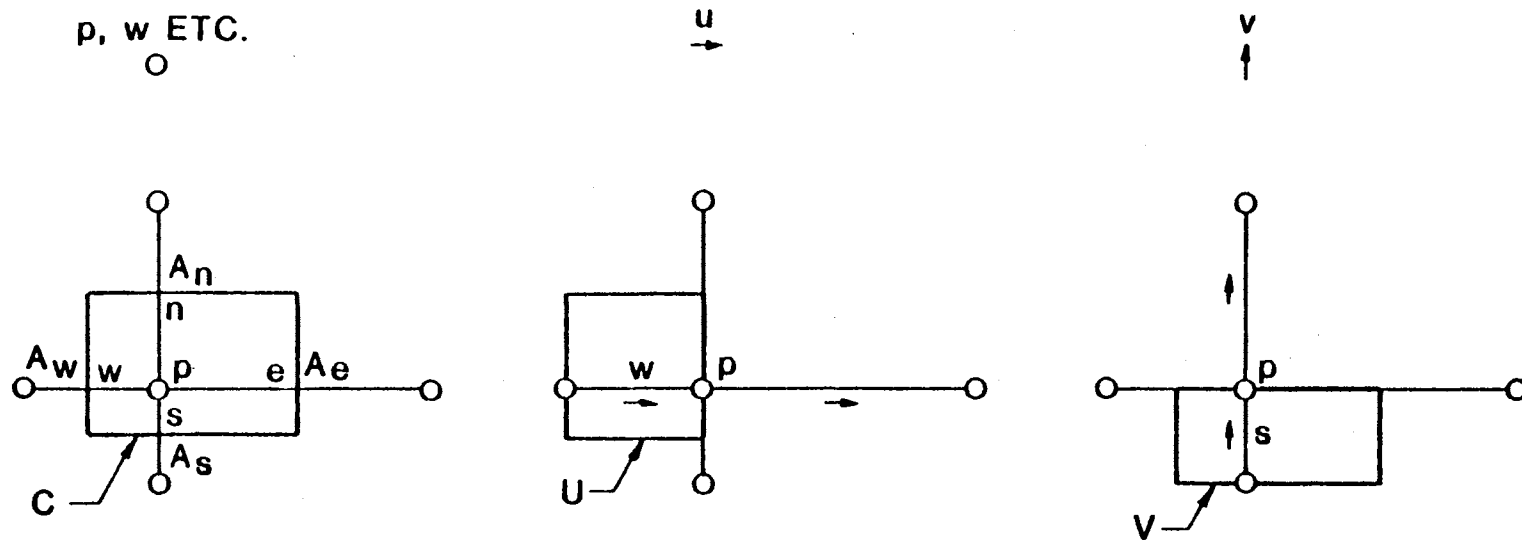
(d) Test Case 4 and 5

Figure 1. (Continued)



THREE GRIDS : FOR p, w ETC. - AT POSITION MARKED (O)
 FOR u VELOCITY - AT POSITION MARKED (\rightarrow)
 FOR v VELOCITY - AT POSITION MARKED (\uparrow)

Figure 2. Staggered Grid and Notation for the Rectangular Computational Mesh



**CONTROL VOLUMES C, U, V FACE
AREAS A_n, A_s, A_e AND A_w FOR C, SIMILAR FOR U AND V**

Figure 3. The Three Control Volumes Associated with points of Three Grids

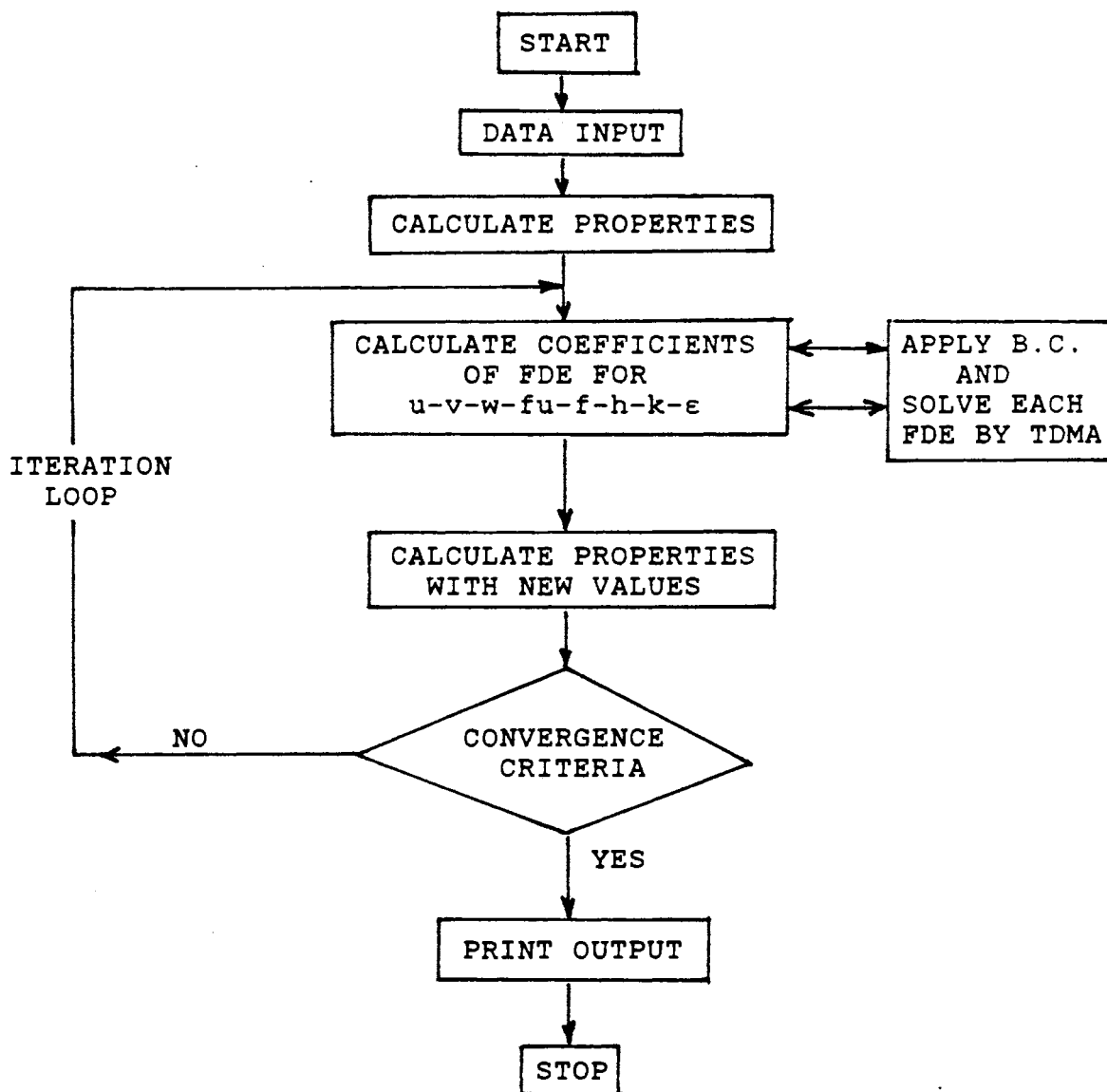


Figure 4. Flow Chart of Computational Scheme

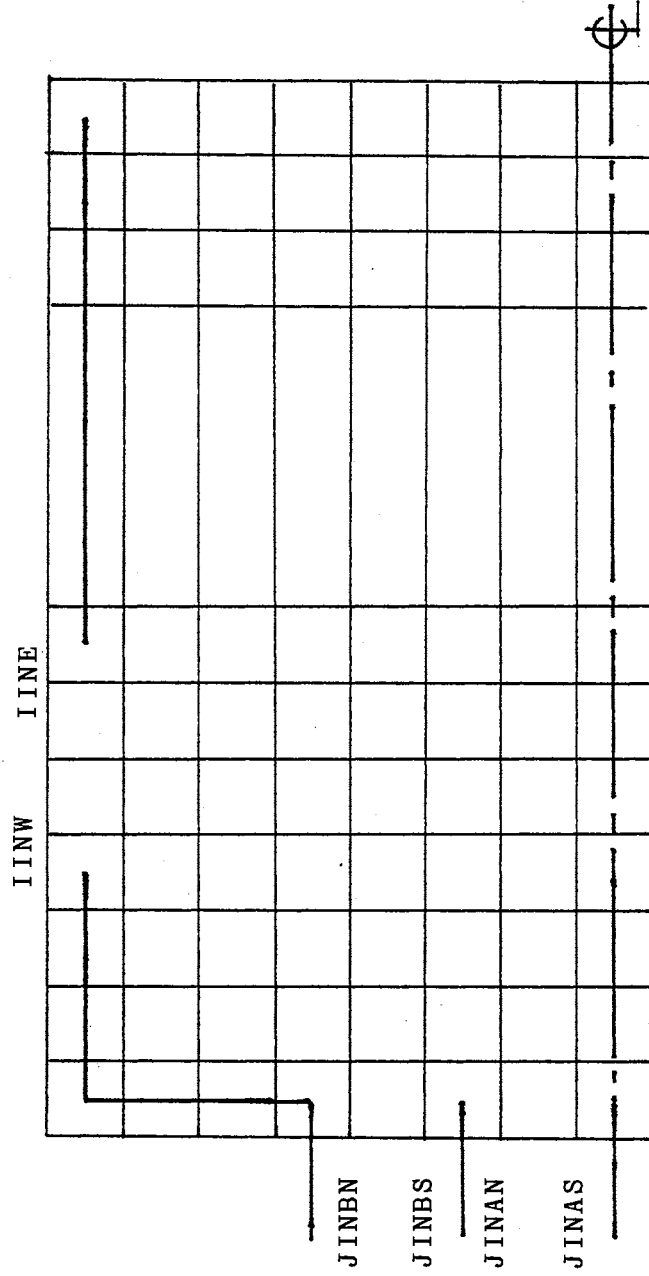


Figure 5. Schematics of Multi-inlet System

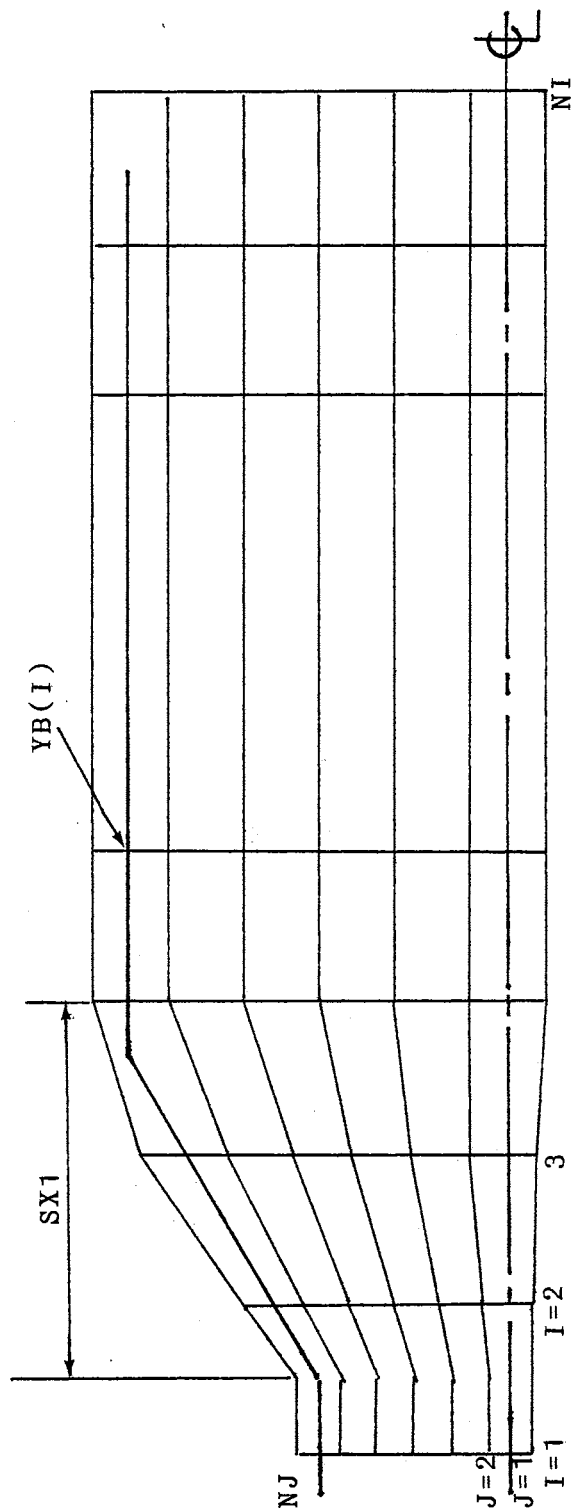


Figure 6. Nonorthogonal Grids with 30 degrees Slope

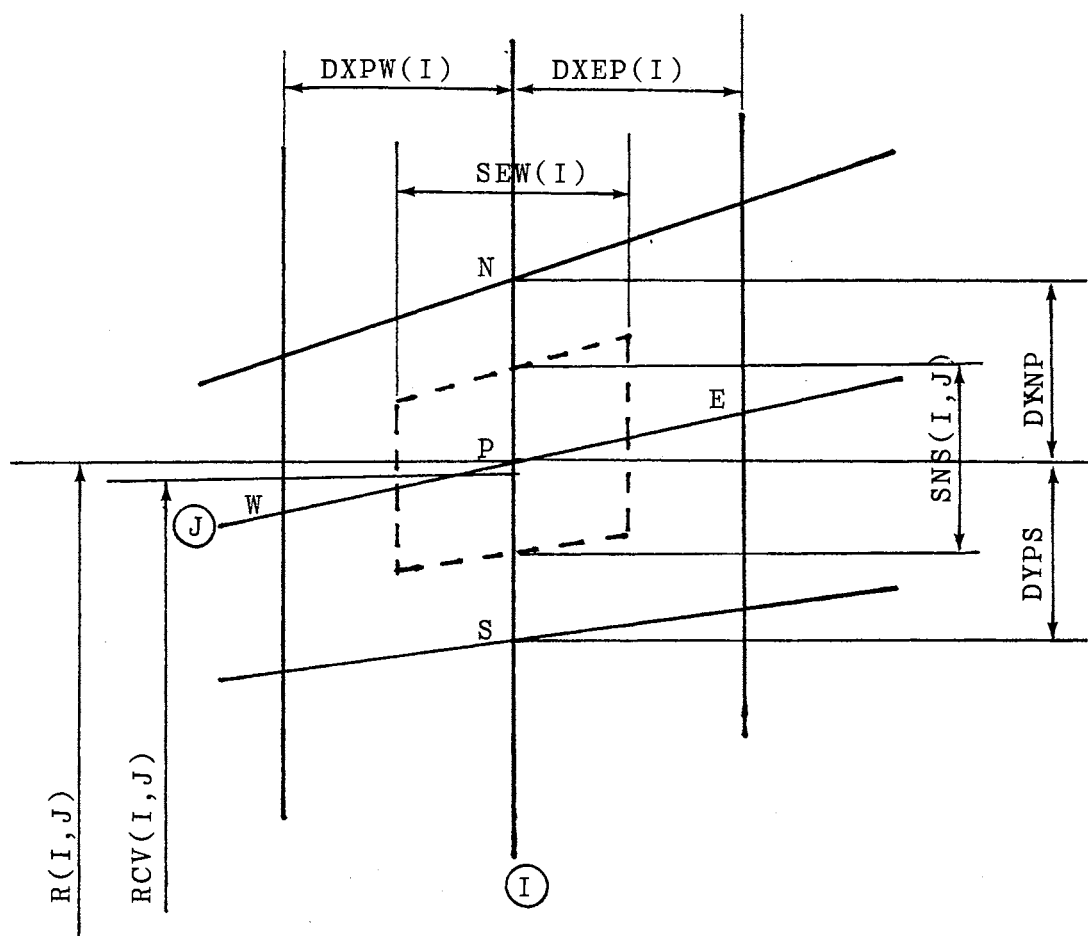


Figure 7. Fortran Variables Related the Nonorthogonal Grids for C-Cells

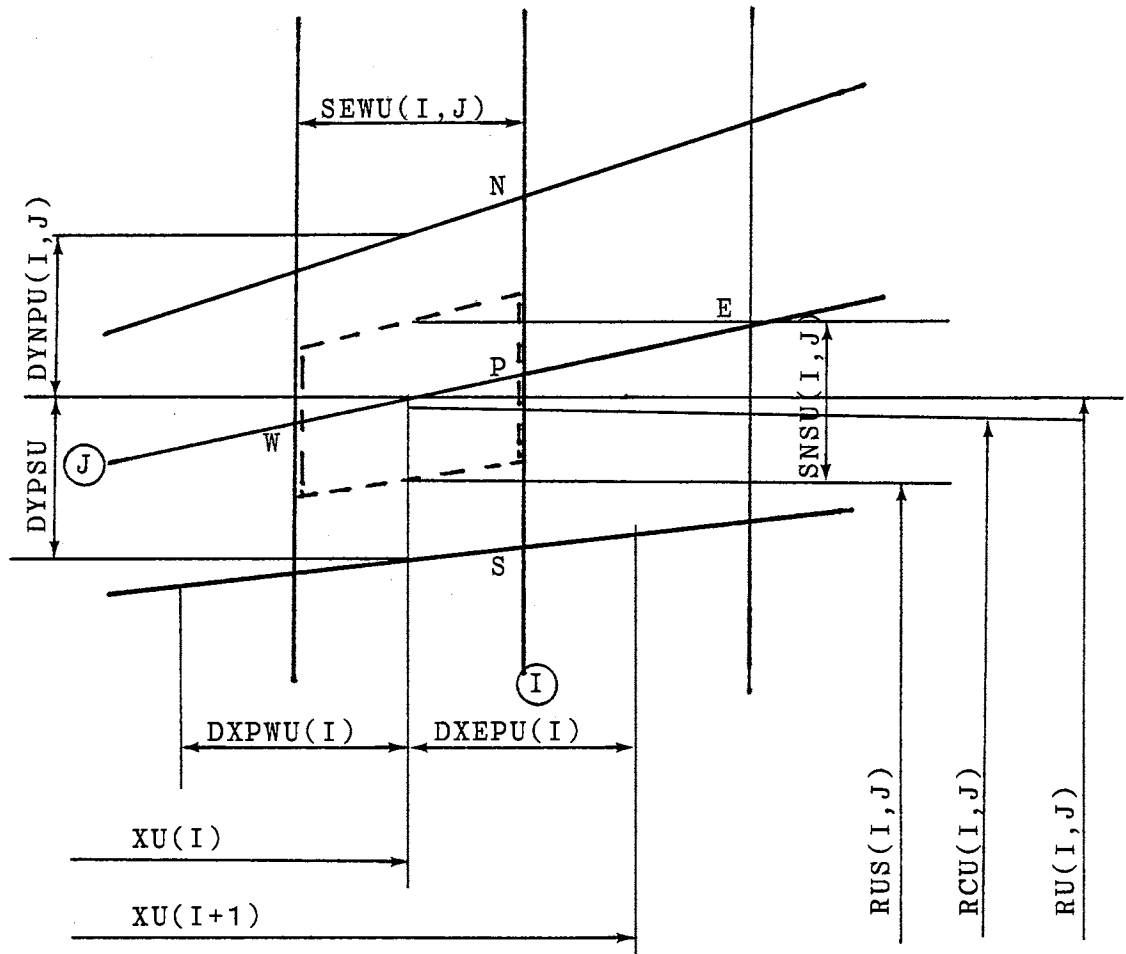


Figure 8. Fortran Variables Related the Nonorthogonal Grids for U-Cells

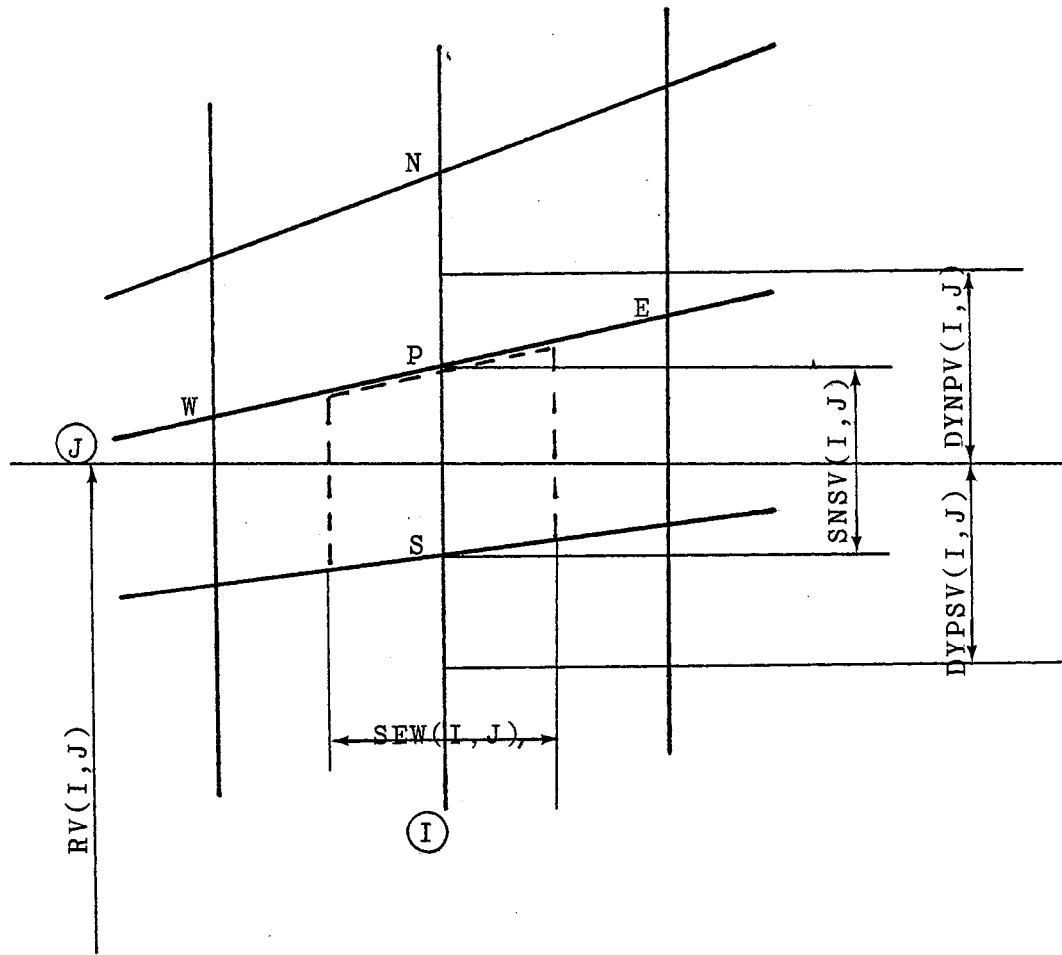


Figure 9. Fortran Variables Related the Nonorthogonal Grids for V-Cells

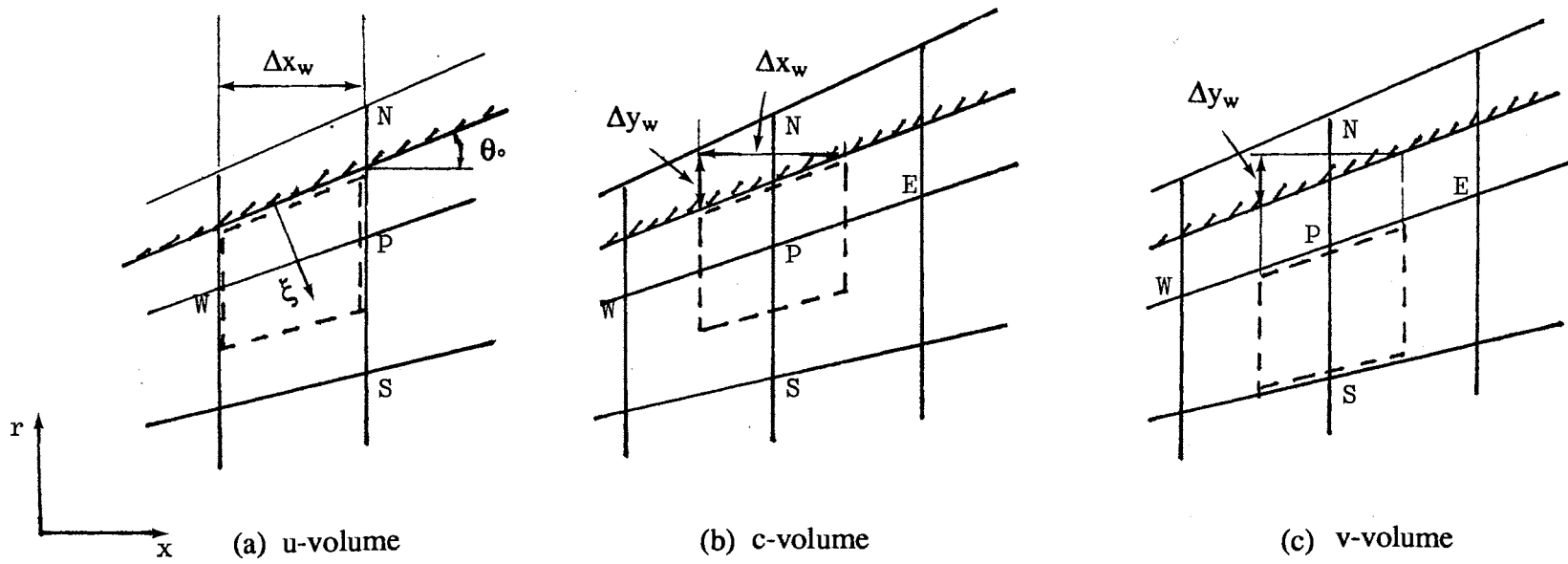


Figure 10. Control Volumes at the Sloping Wall

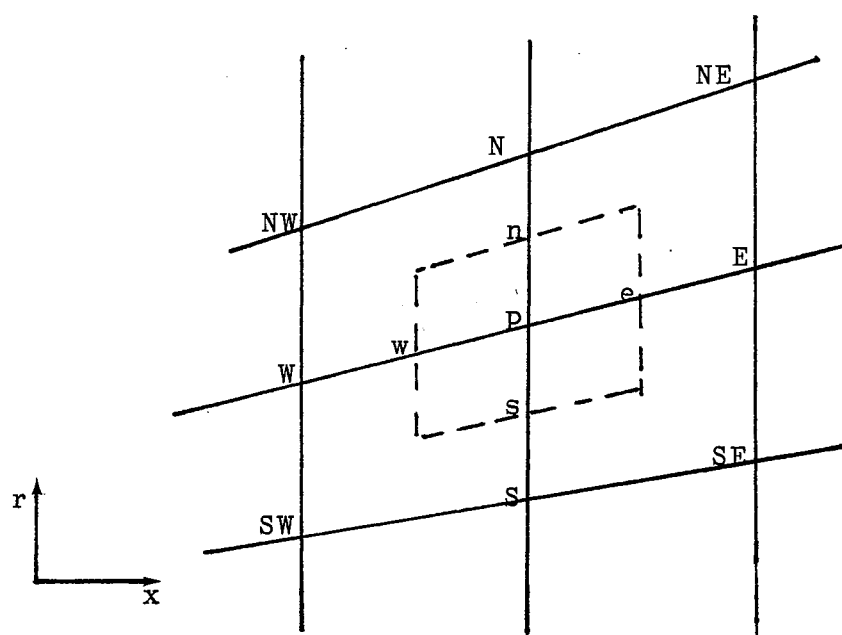


Figure 11. Notations of C-Control Volume for the Grid Line Skewness

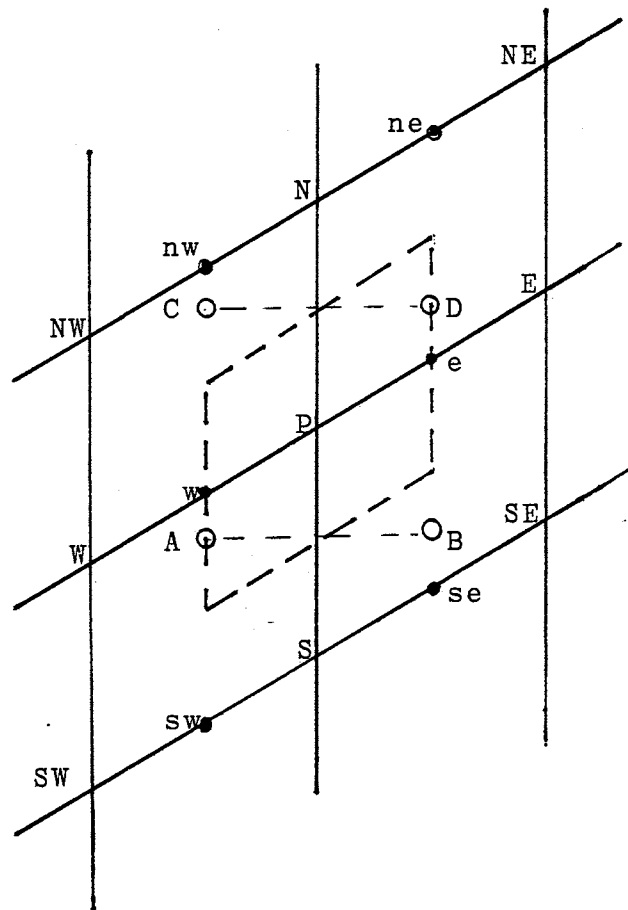


Figure 12. Notations of C-Control Volume for the Sloping Control Surfaces

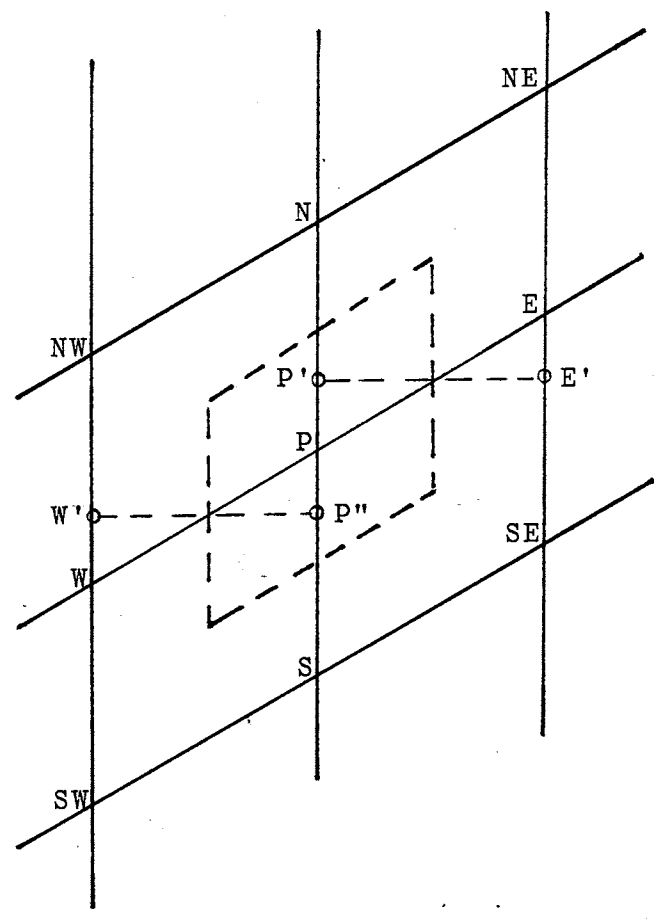


Figure 13. Notations for Control Volumes of Nonorthogonal Grid

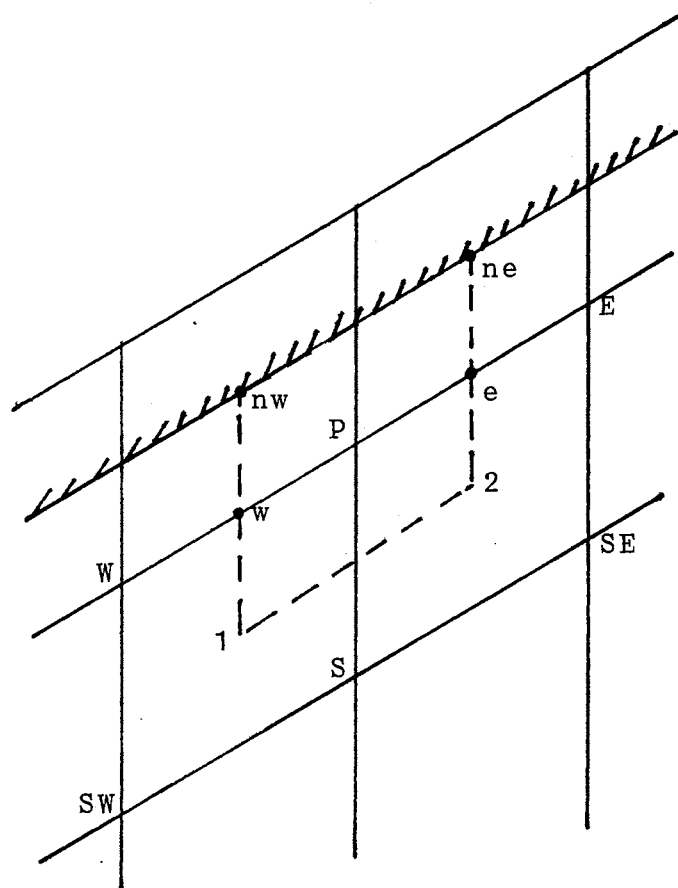
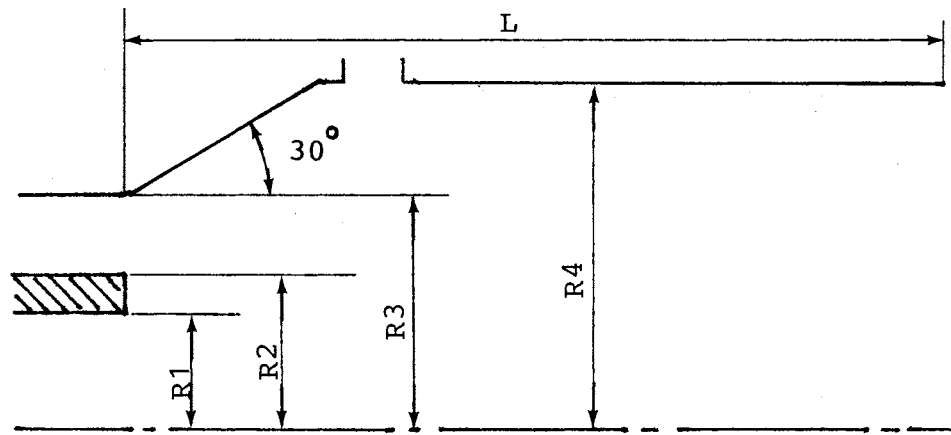


Figure 14. Notations of C-Control Volume for P Calculation at the Top Sloping Wall



$R1=0.08, R2=0.1, R3=0.14, R4=0.18$ unit meter

Figure 15. Schematic of the Flow for the Sample Computation

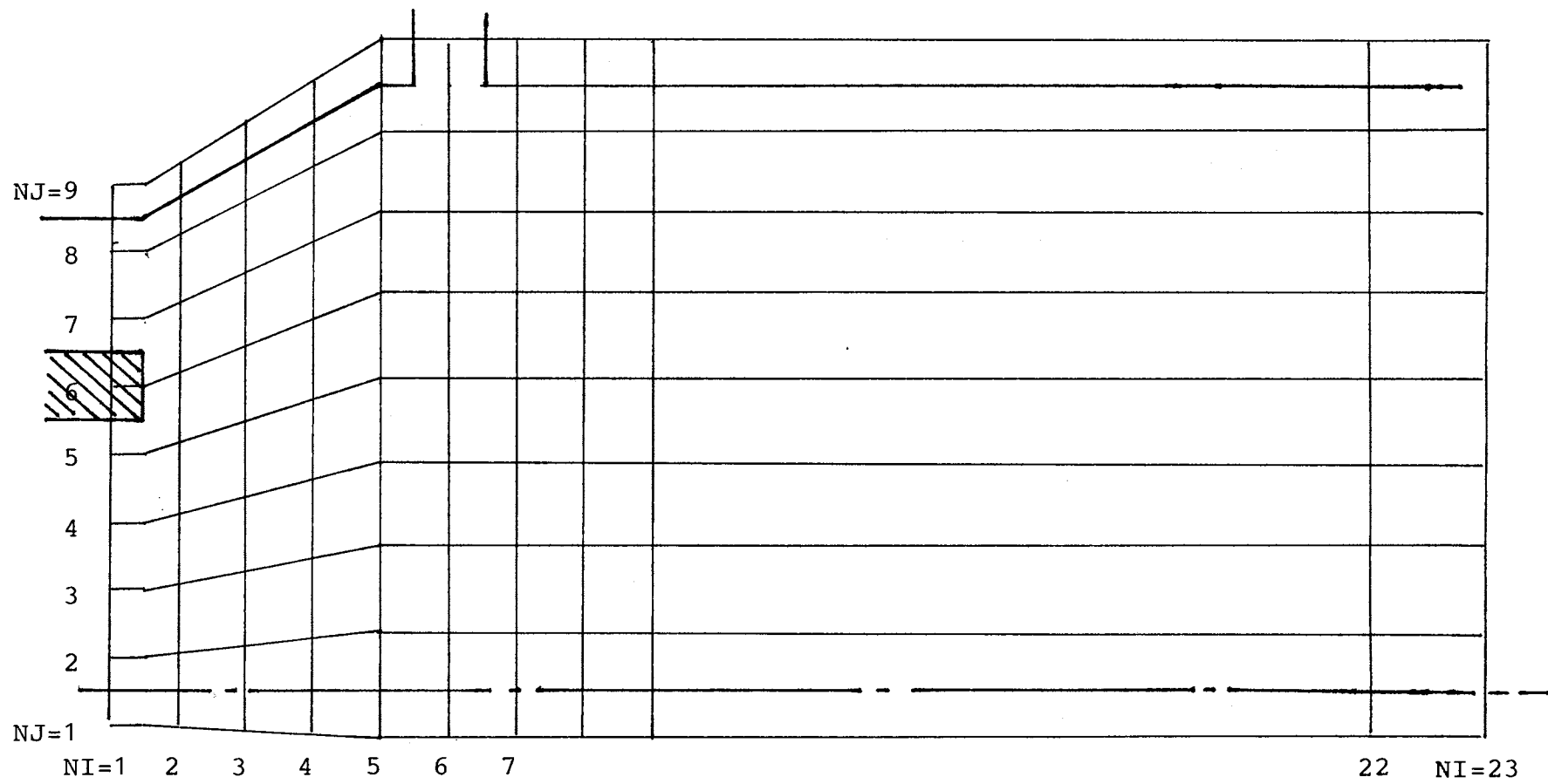


Figure 16. Grid System of the Flow for the Sample Computation

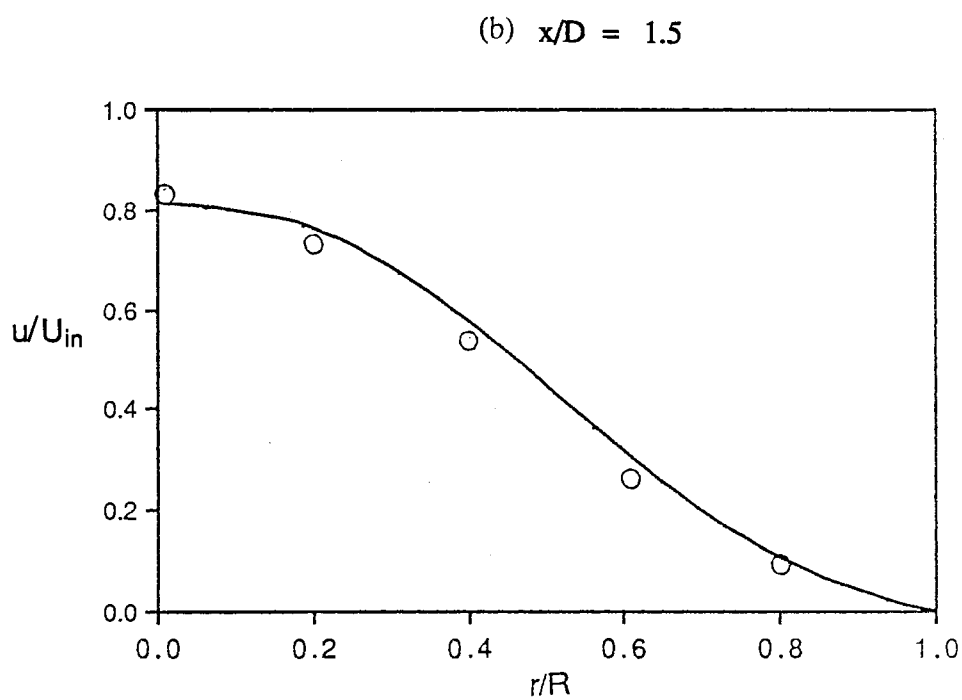
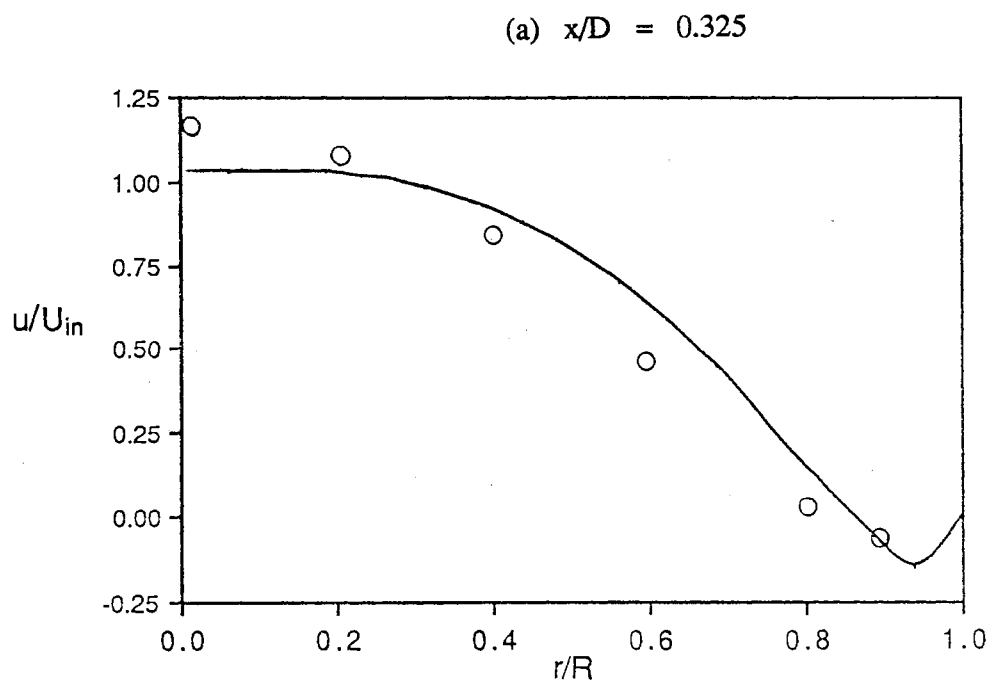


Figure 17. Mean Axial Velocity Profiles of Case 1
[O ; Experiment Ref. (122)]

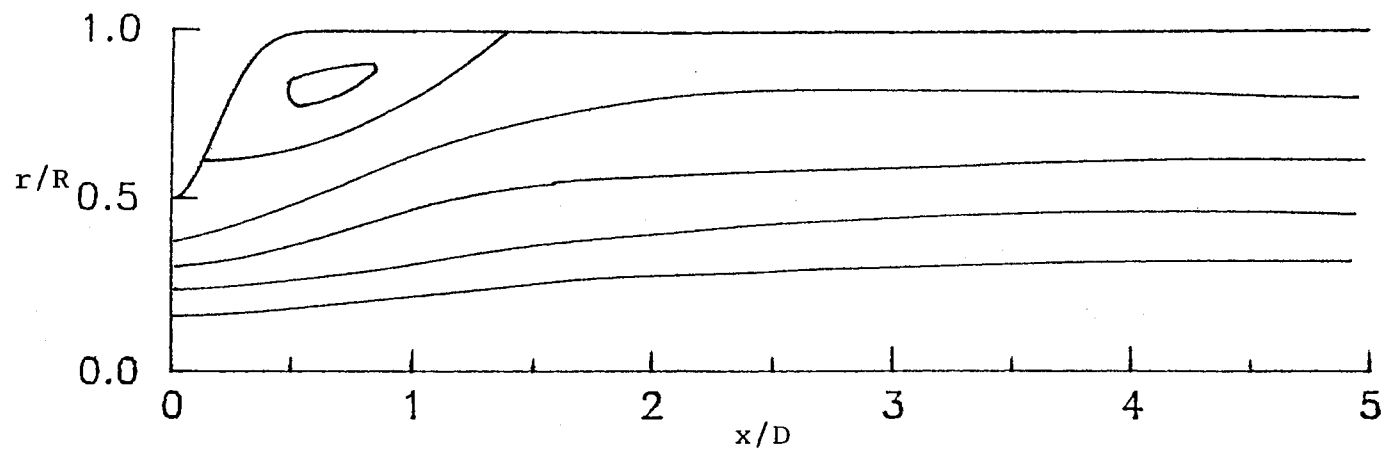


Figure 18. Predicted Streamline Pattern of Case 1

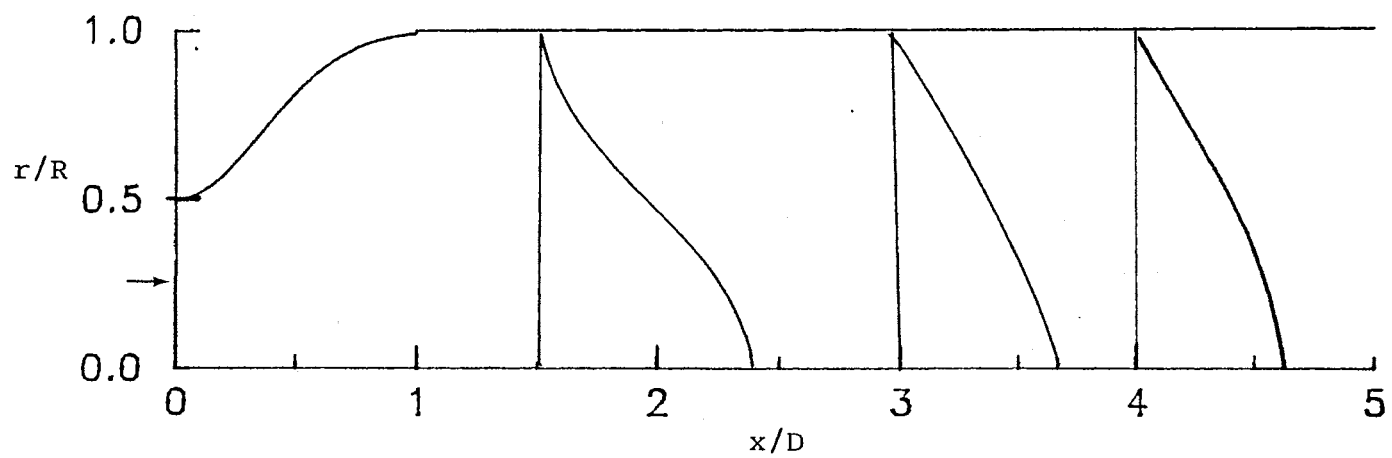


Figure 19. Predicted Mean Axial Velocity Profiles of Case 1

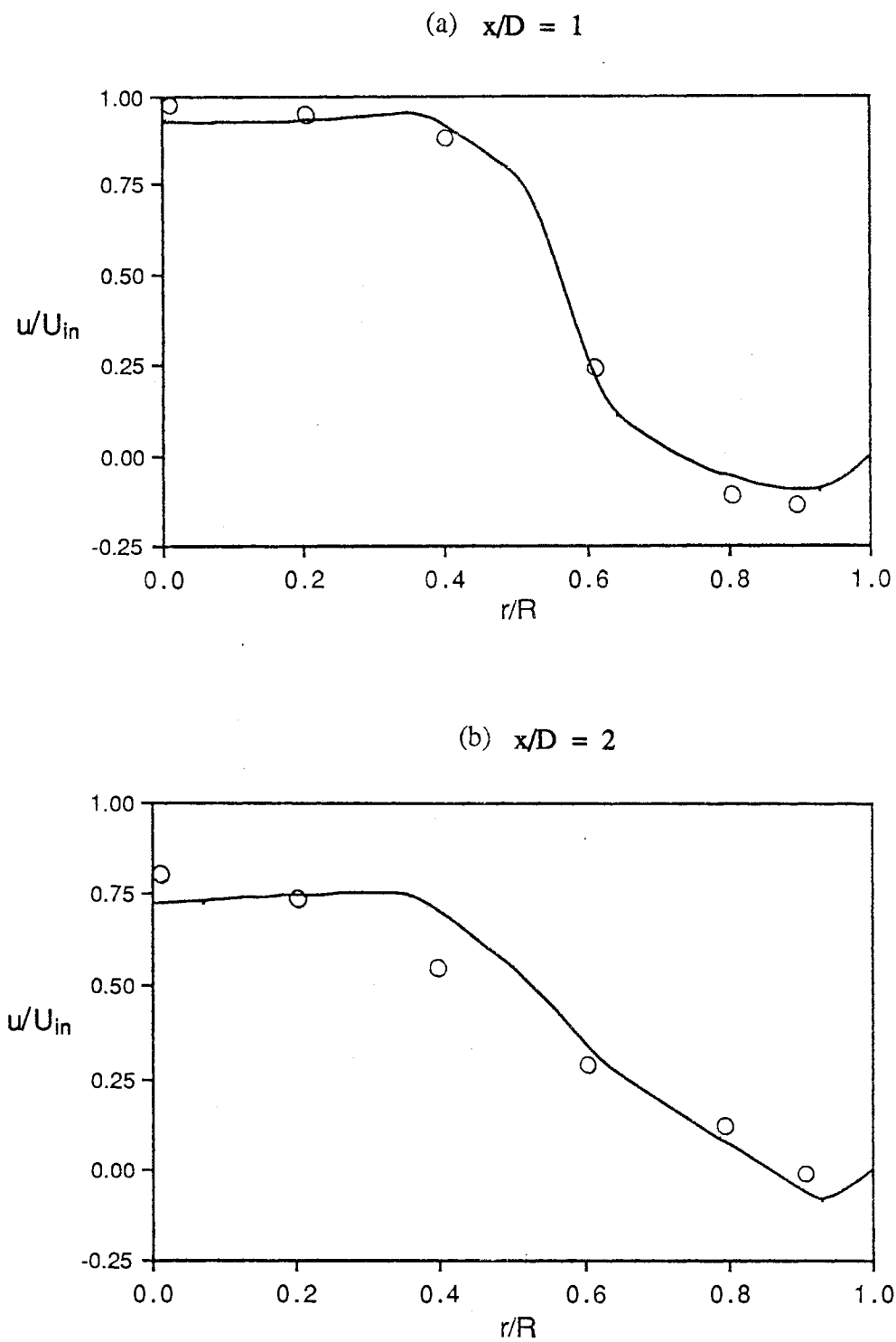


Figure 20. Mean Axial Velocity Profiles of Case 2
[O ; Experiment Ref. (124)]

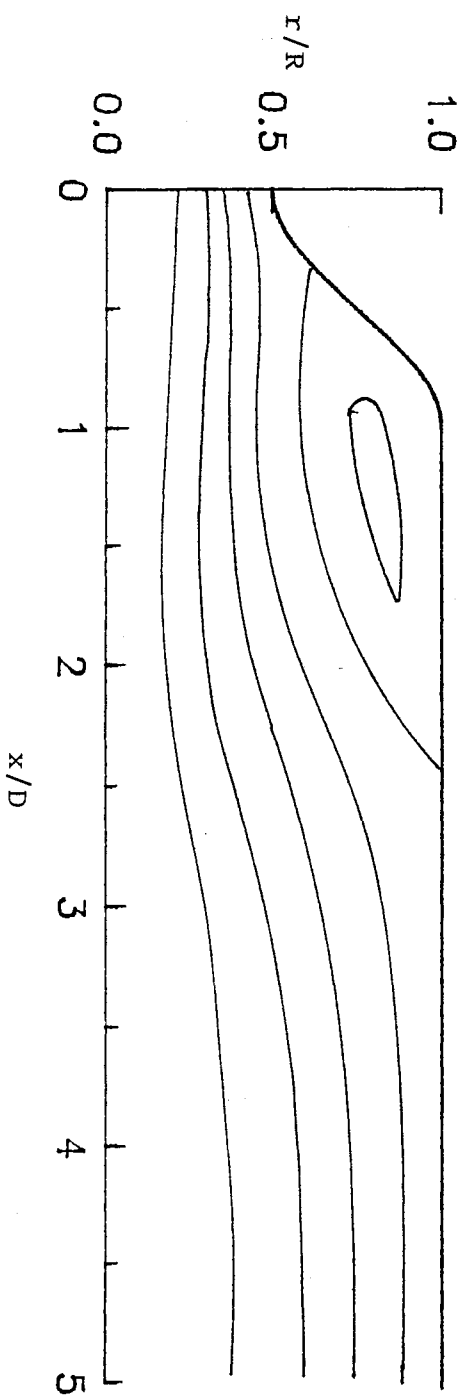


Figure 21. Predicted Streamline Pattern of Case 2

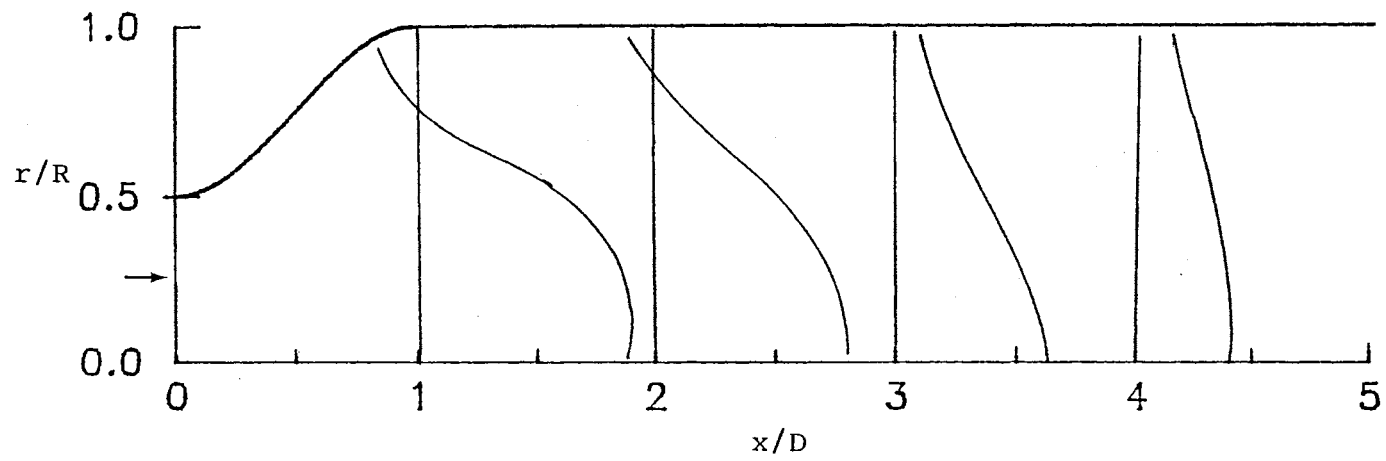


Figure 22. Predicted Mean Axial Velocity Profiles of Case 2

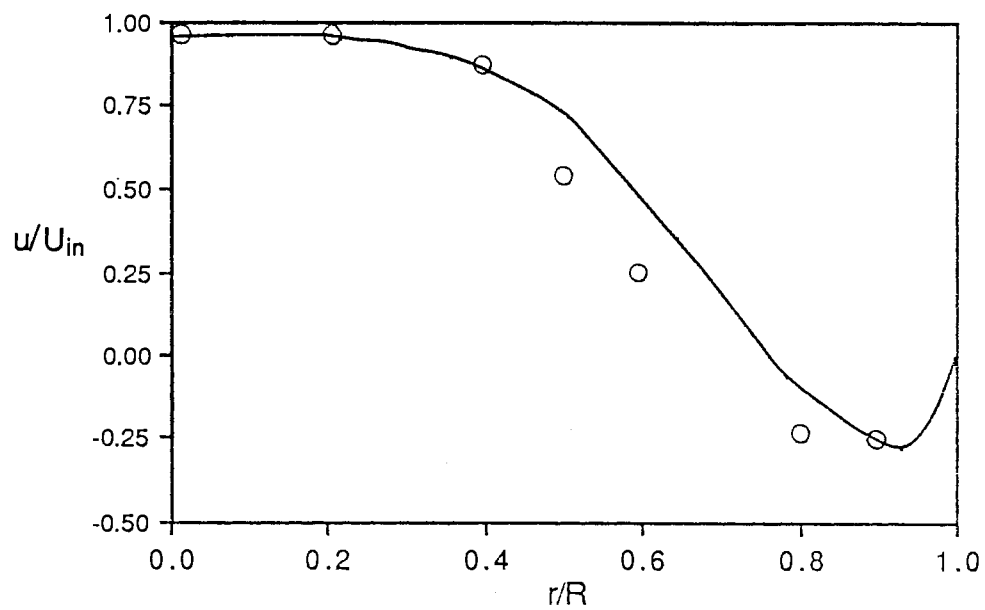
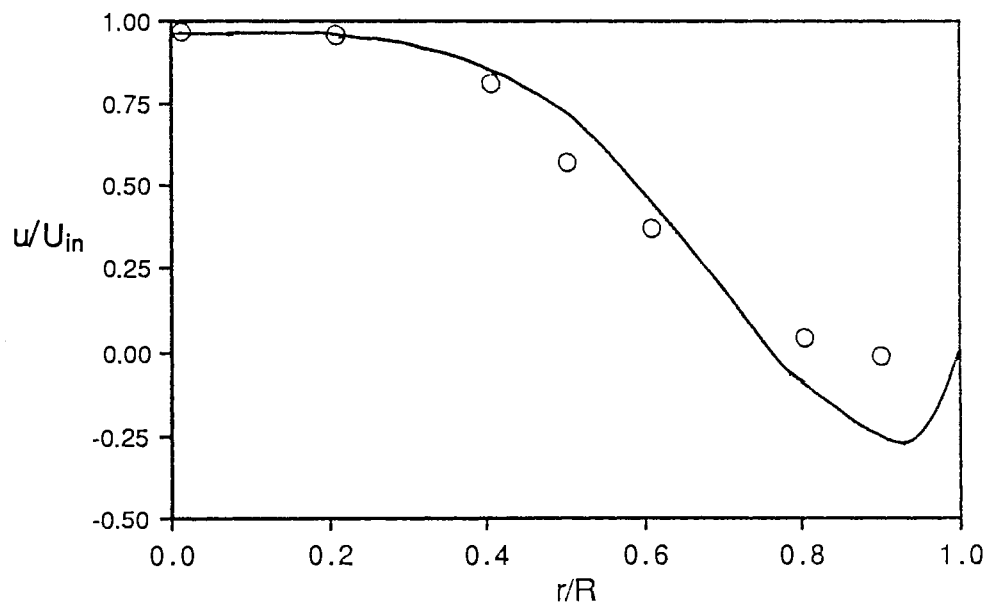
(a) $x/D = 0.5$ (b) $x/D = 1$ 

Figure 23. Mean Axial Velocity Profiles of Case 3 (without Swirl)
[\circ ; Experiment Ref. (34)]

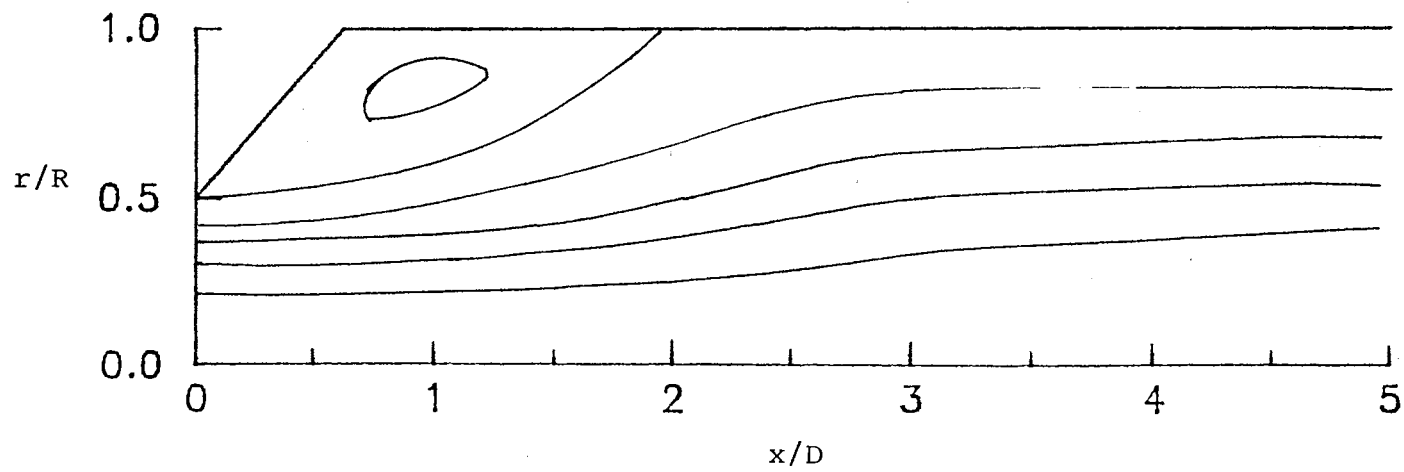


Figure 24. Predicted Streamline Pattern of Case 3

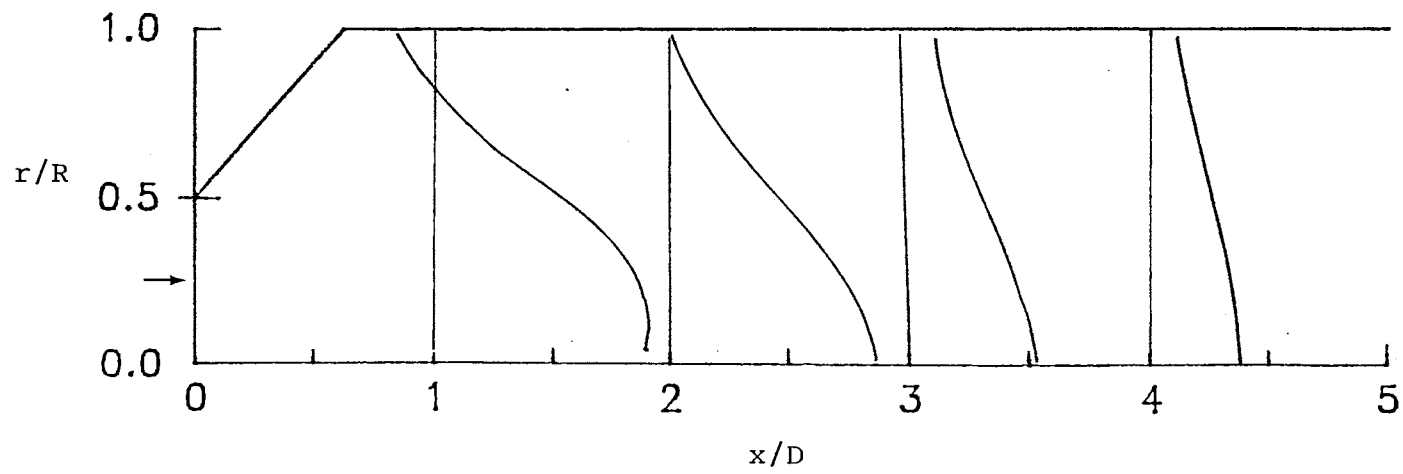


Figure 25. Predicted Mean Axial Velocity Profiles of Case 3

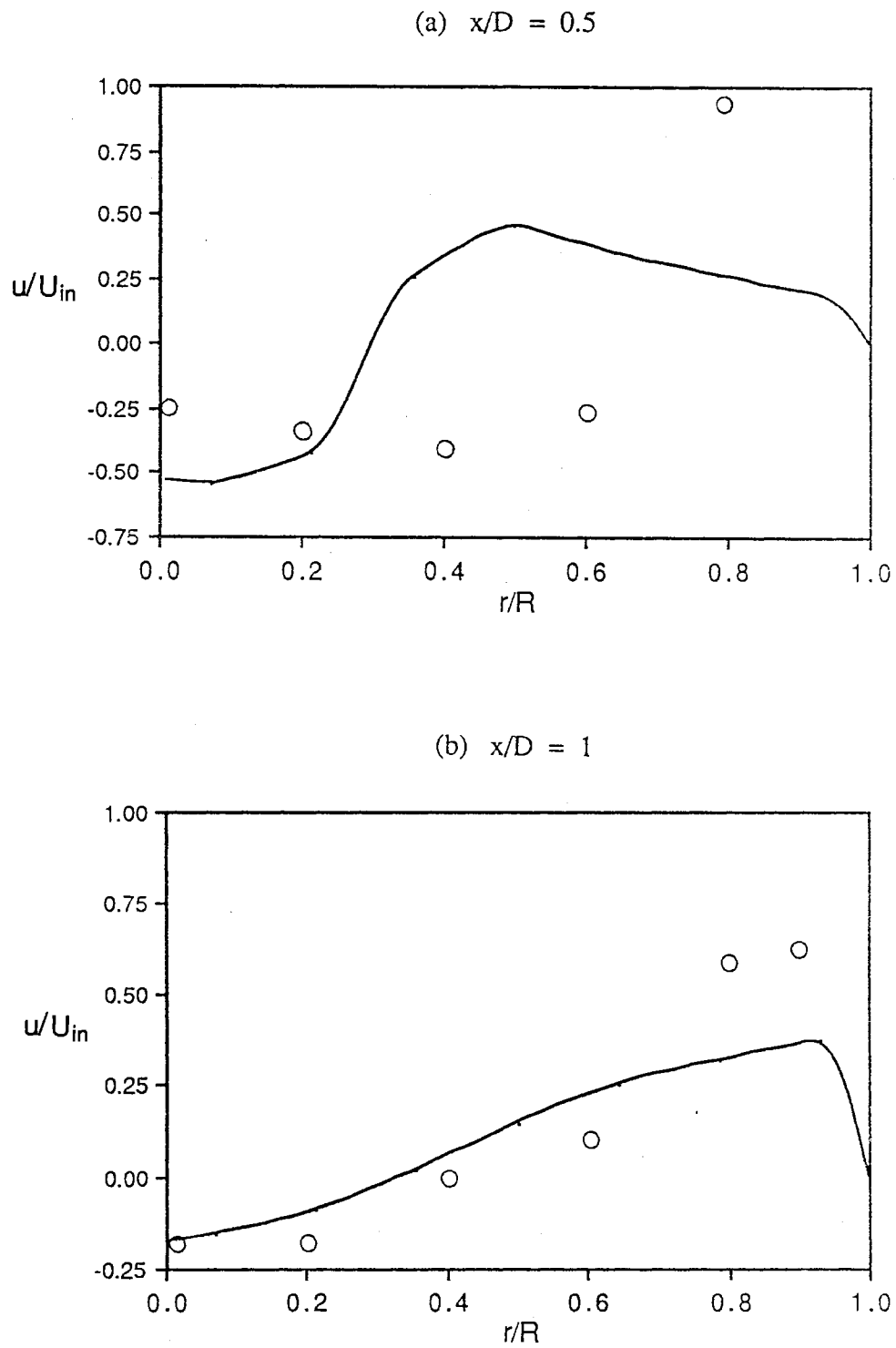


Figure 26. Mean Axial Velocity Profiles of Case 3 (Swirl No. 0.67)
[O ; Experiment Ref. (34)]

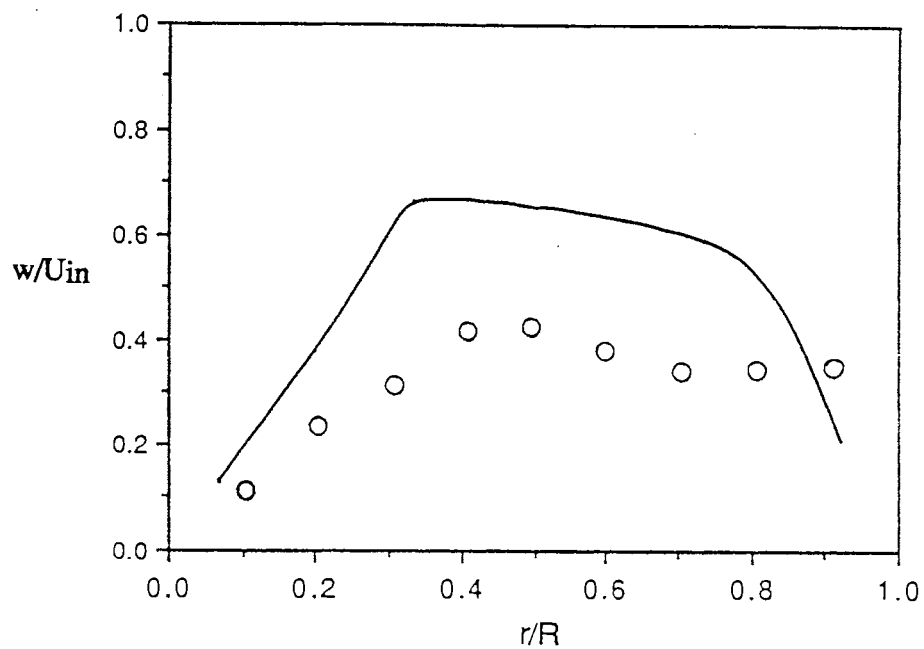
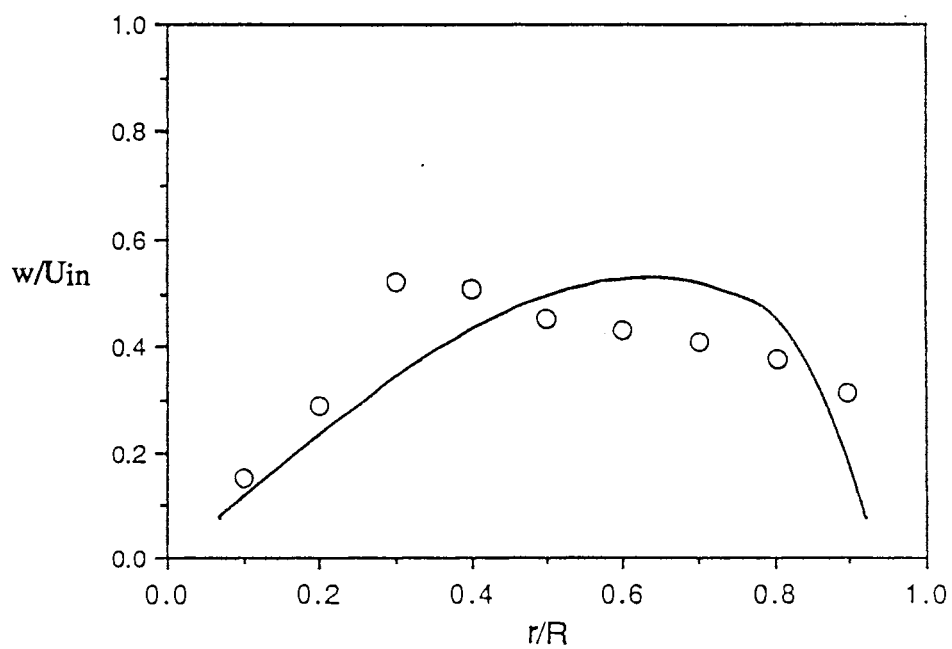
(a) $x/D = 0.5$ (b) $x/D = 1$ 

Figure 27. Mean Swirl Velocity Profiles of Case 3 (Swirl No. 0.67)
[O ; Experiment Ref. (34)]

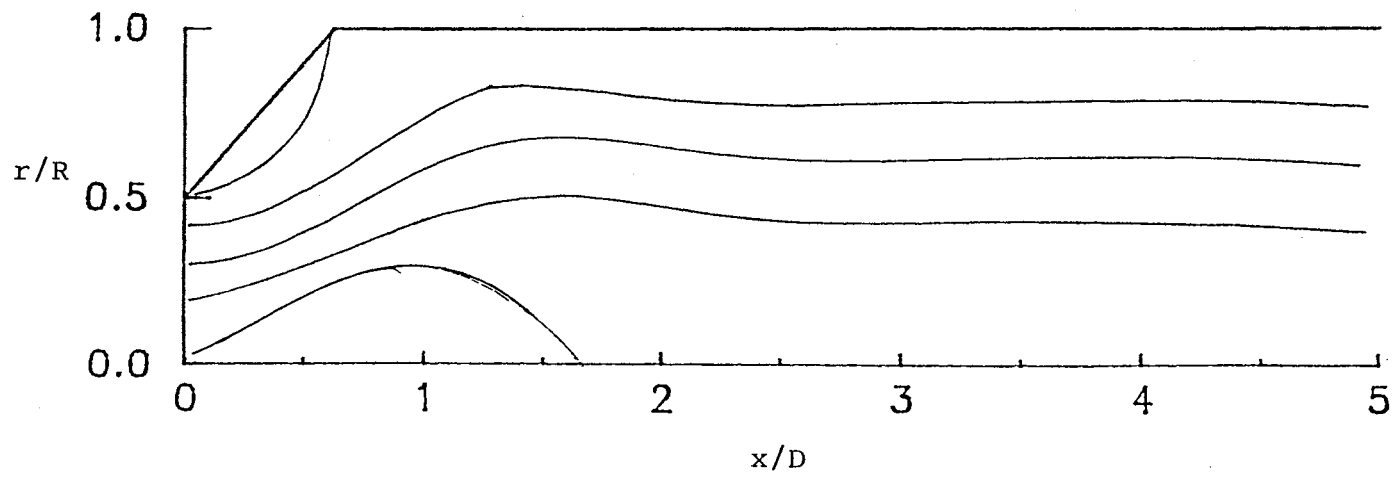


Figure 28. Predicted Streamline Pattern of Case 3

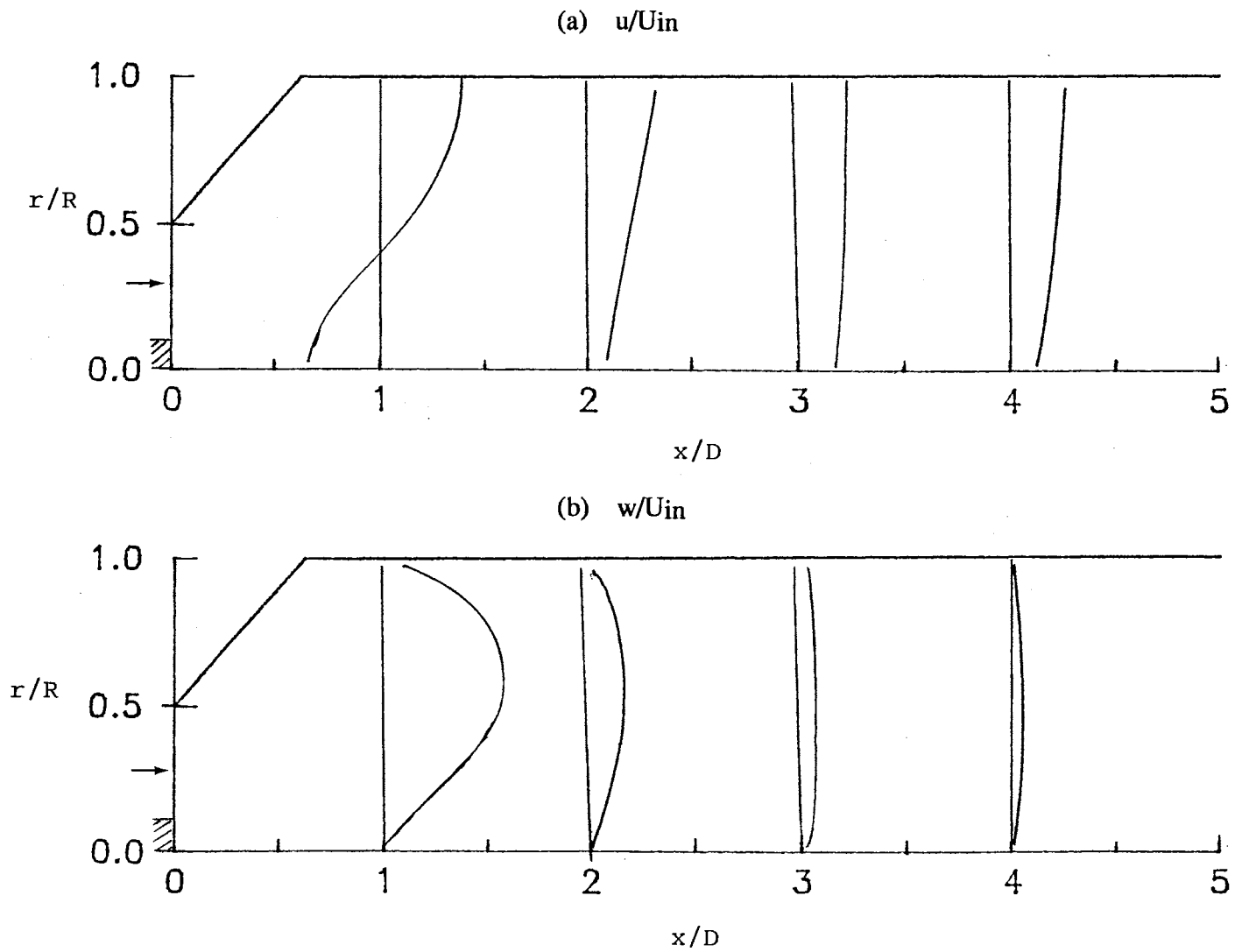


Figure 29. Predicted Mean Axial and Swirl Velocity Profiles of Case 3

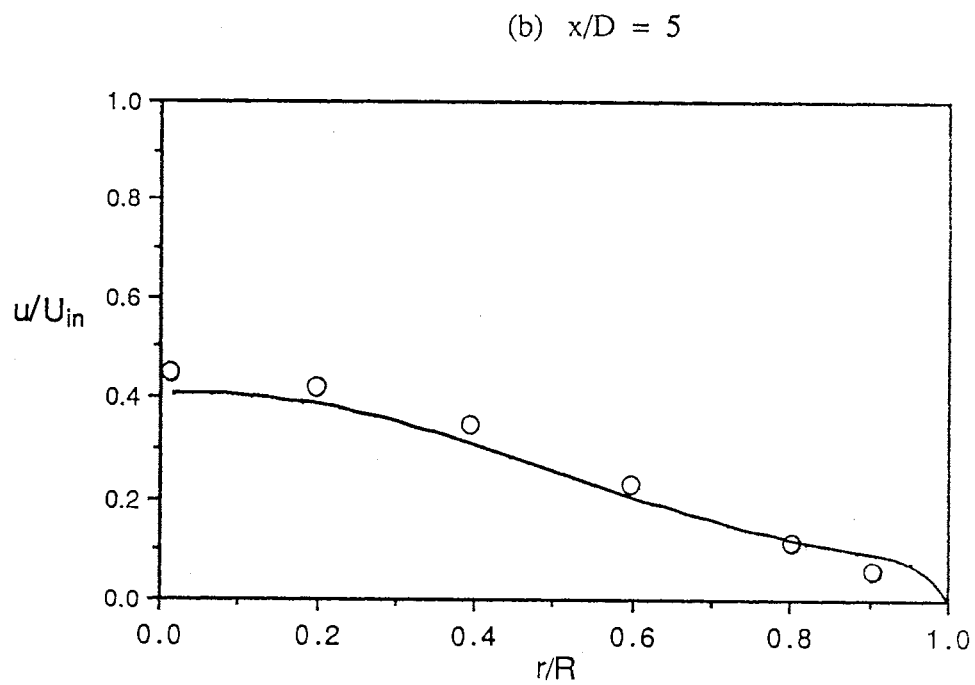
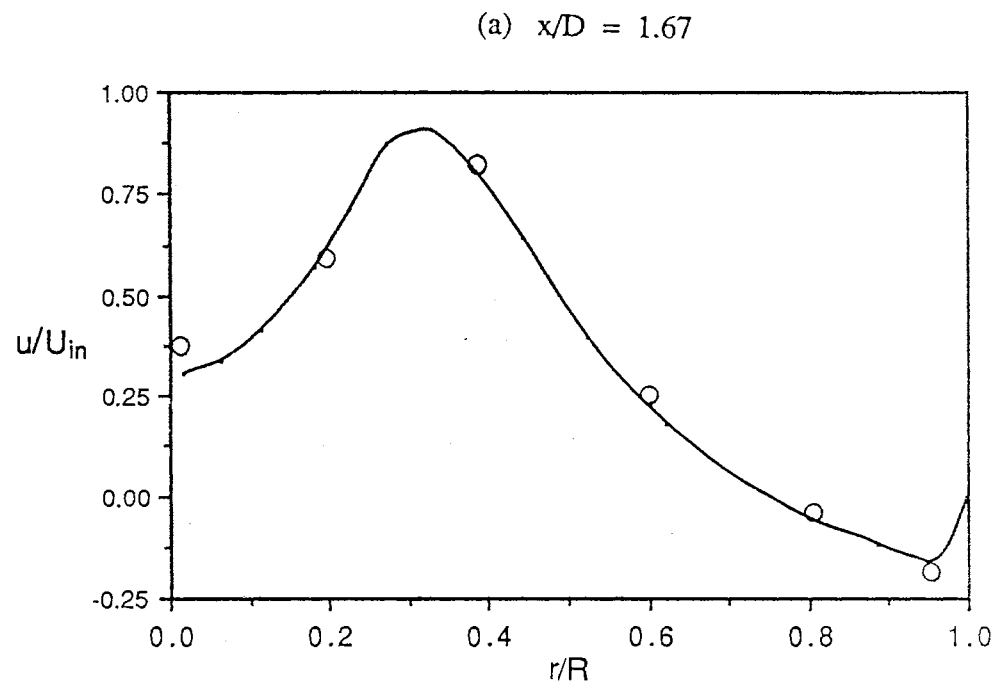


Figure 30. Mean Axial Velocity Profiles of Case 4
[O ; Experiment Ref. (127)]

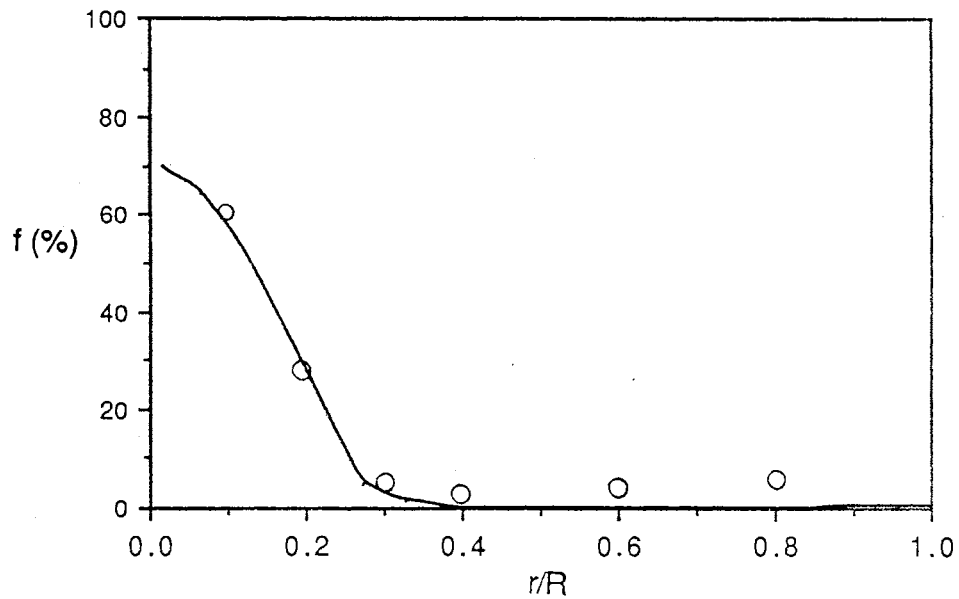
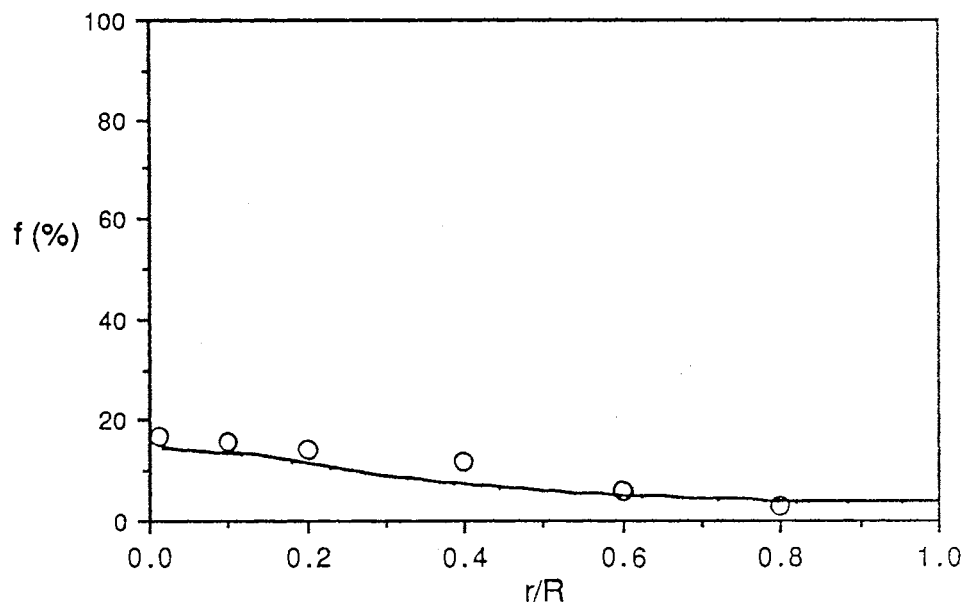
(a) $x/D = 1.67$ (b) $x/D = 5$ 

Figure 31. Inner Jet Mean Concentration Profiles of Case 4
[O ; Experiment Ref. (127)]

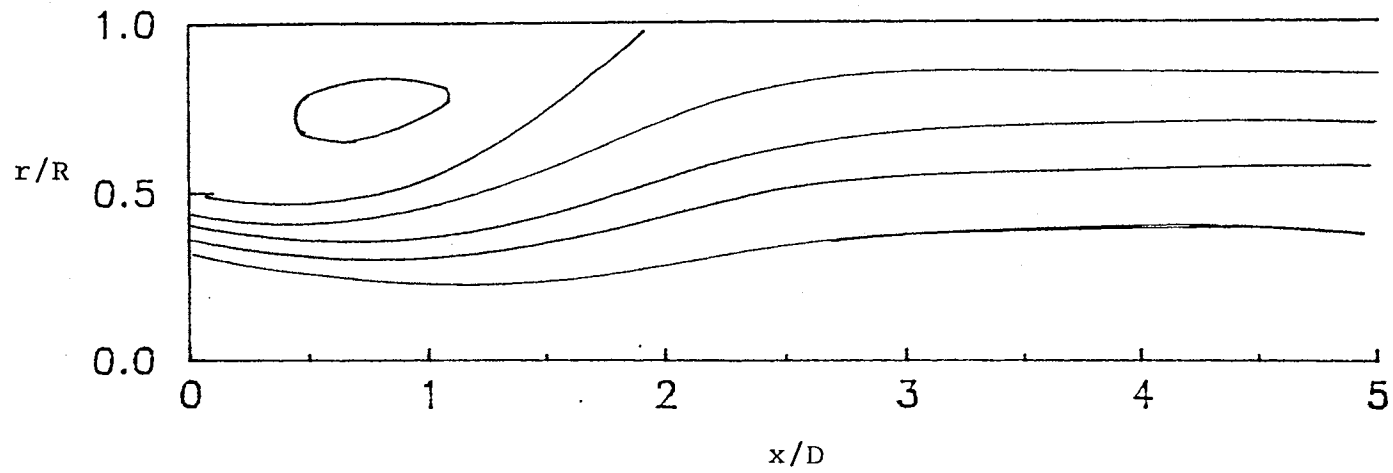


Figure 32. Predicted Streamline Pattern of Case 4

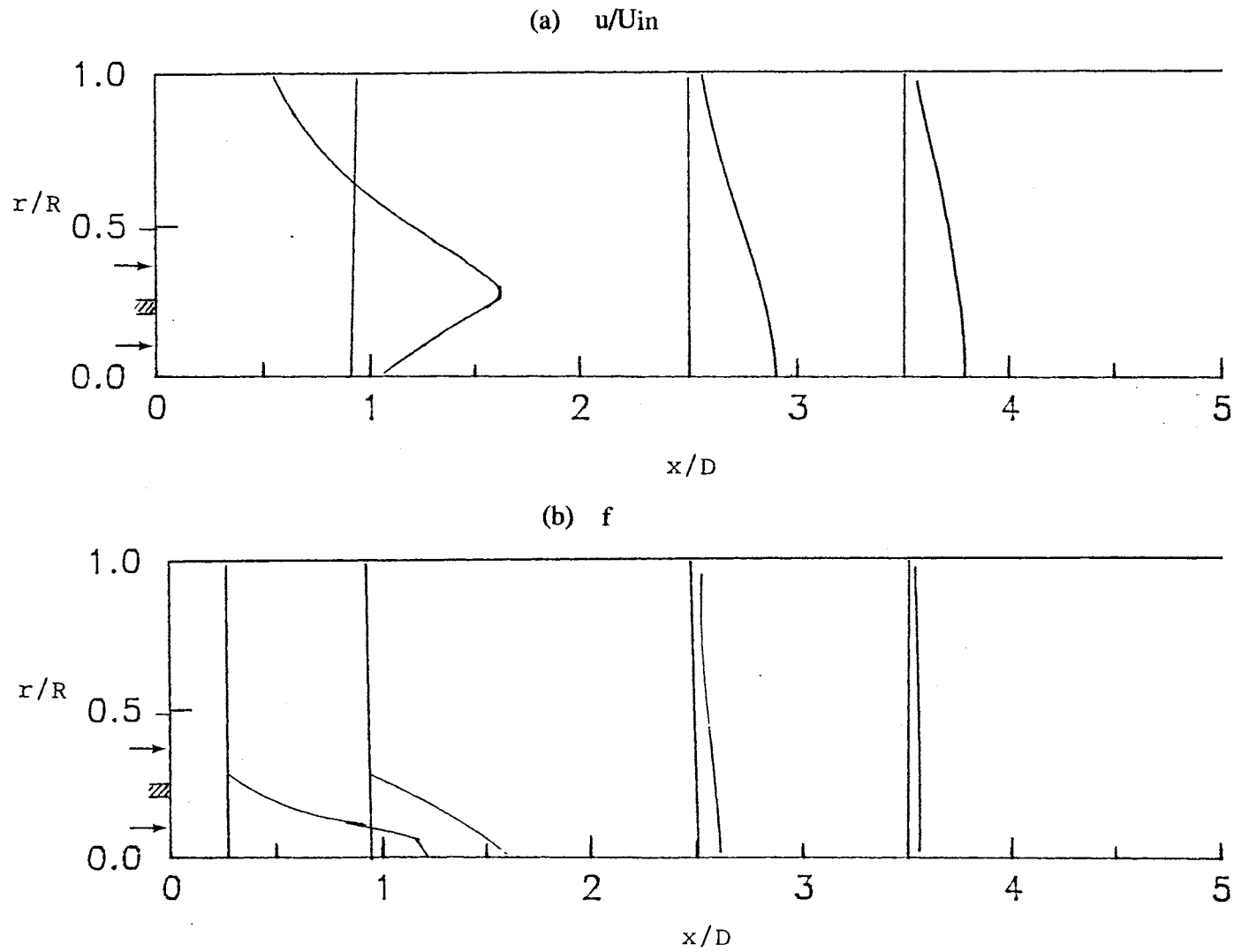


Figure 33. Predicted Mean Axial Velocity and Concentration Profiles of Case 4

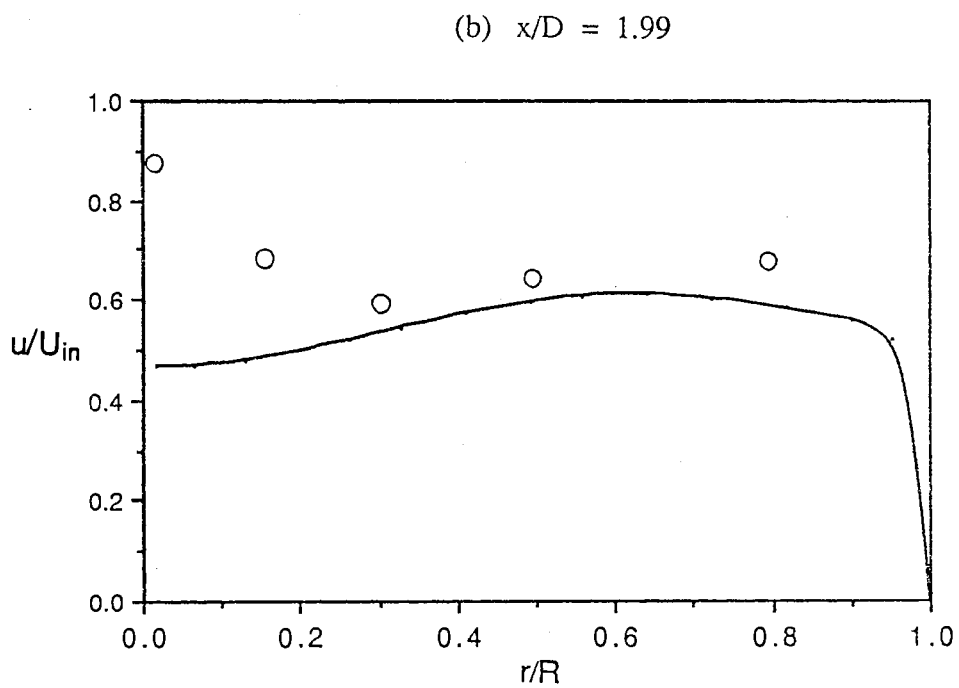
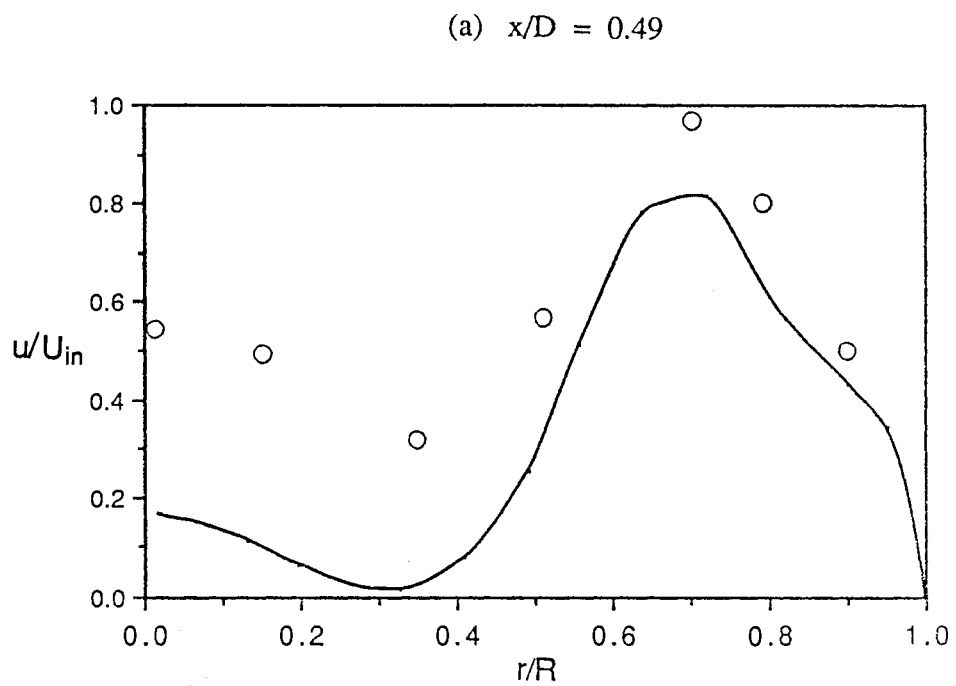


Figure 34. Mean Axial Velocity Profiles of Case 5
[O ; Experiment Ref. (12)]

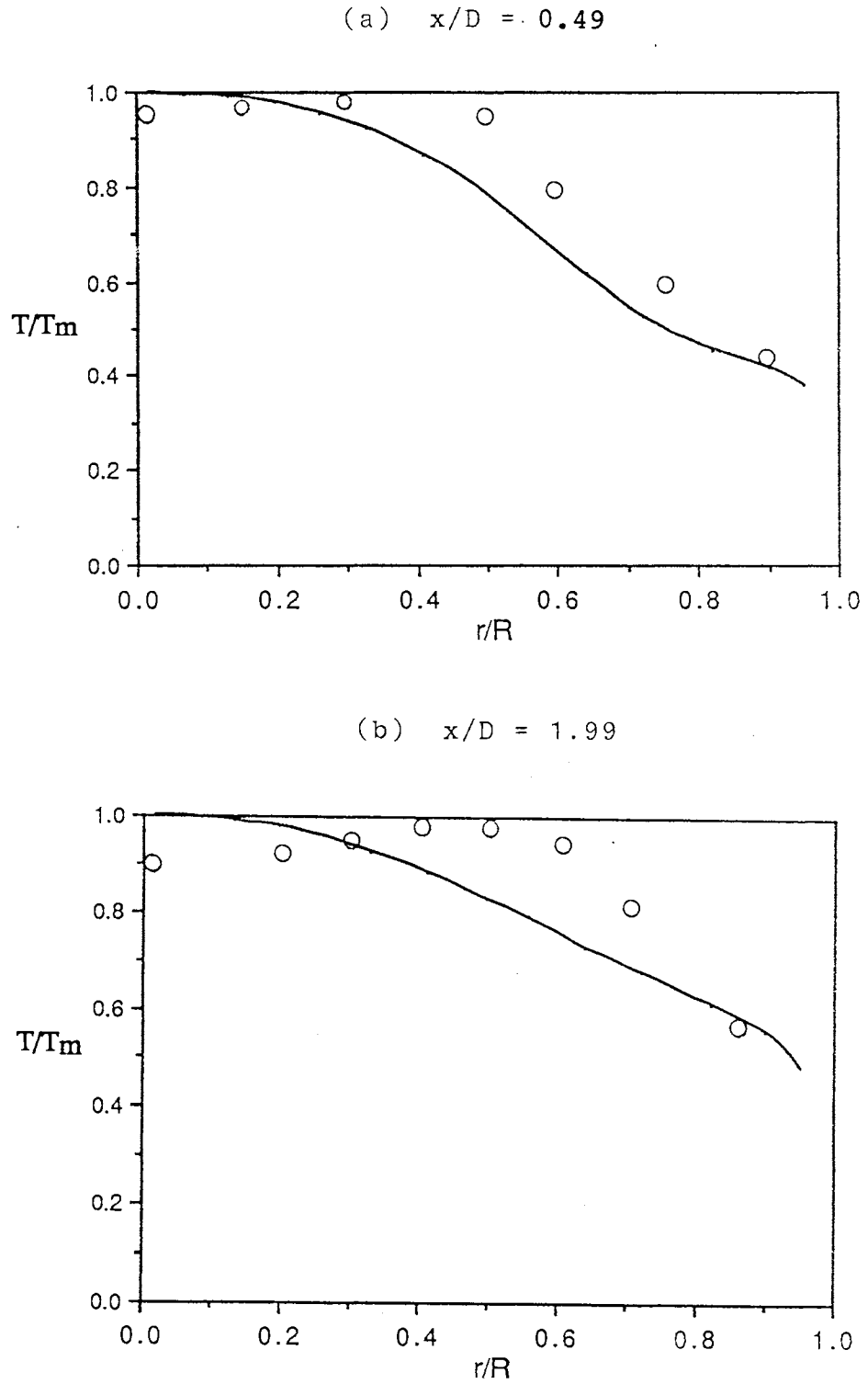


Figure 35. Mean Temperature Profiles of Case 5
[O ; Experiment Ref. (12)]

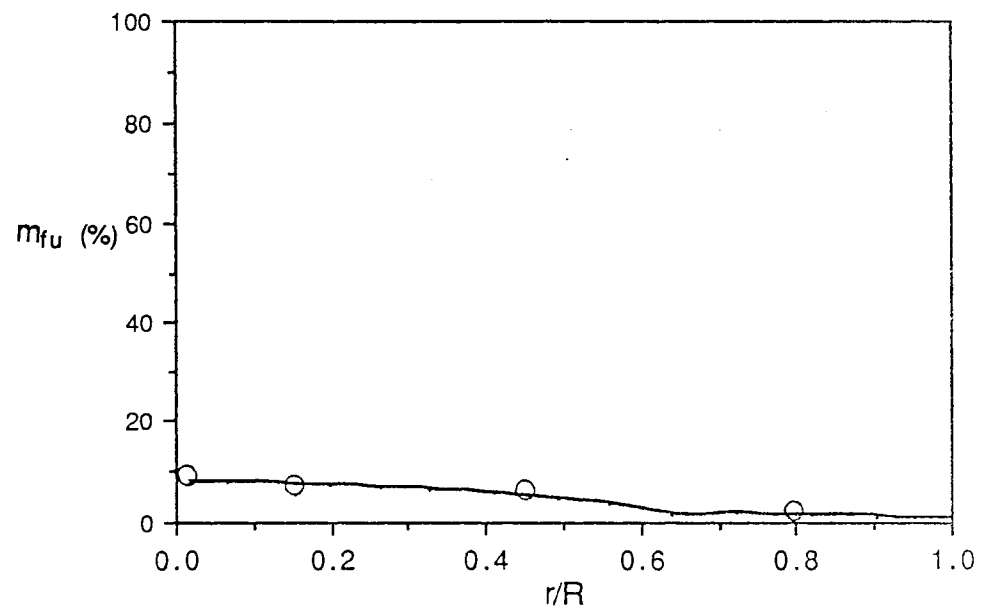
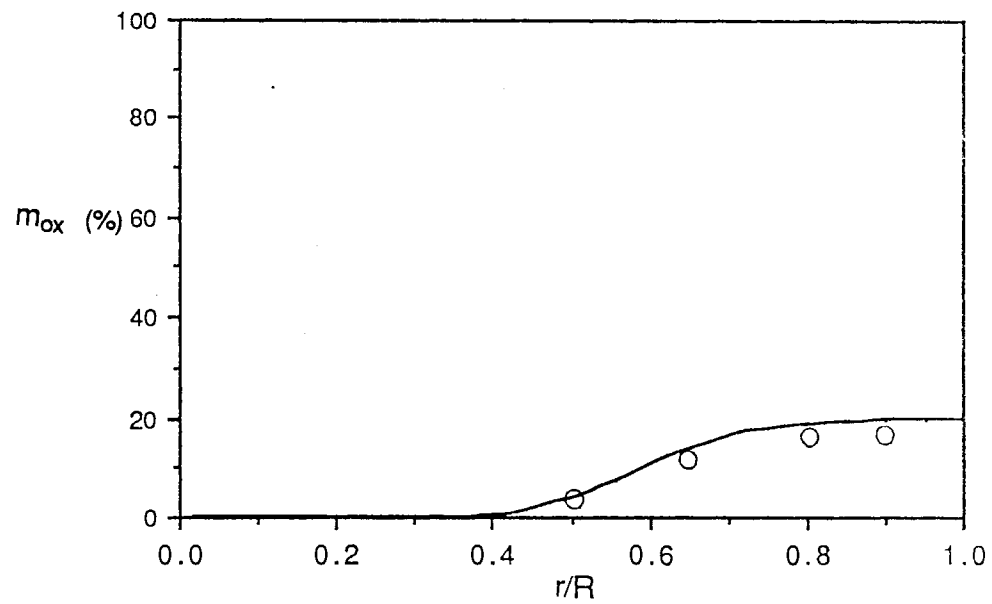
(a) $x/D = 1.47$ (b) $x/D = 1.47$ 

Figure 36. Mean Concentration Profiles of Case 5
[○ ; Experiment Ref. (12)]

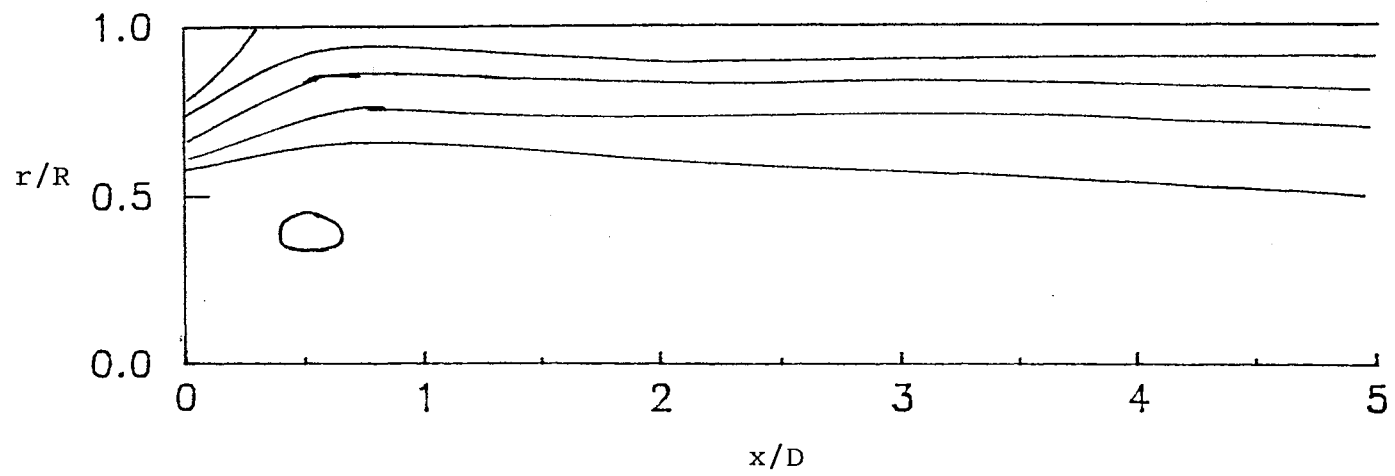


Figure 37. Predicted Streamline Pattern of Case 5

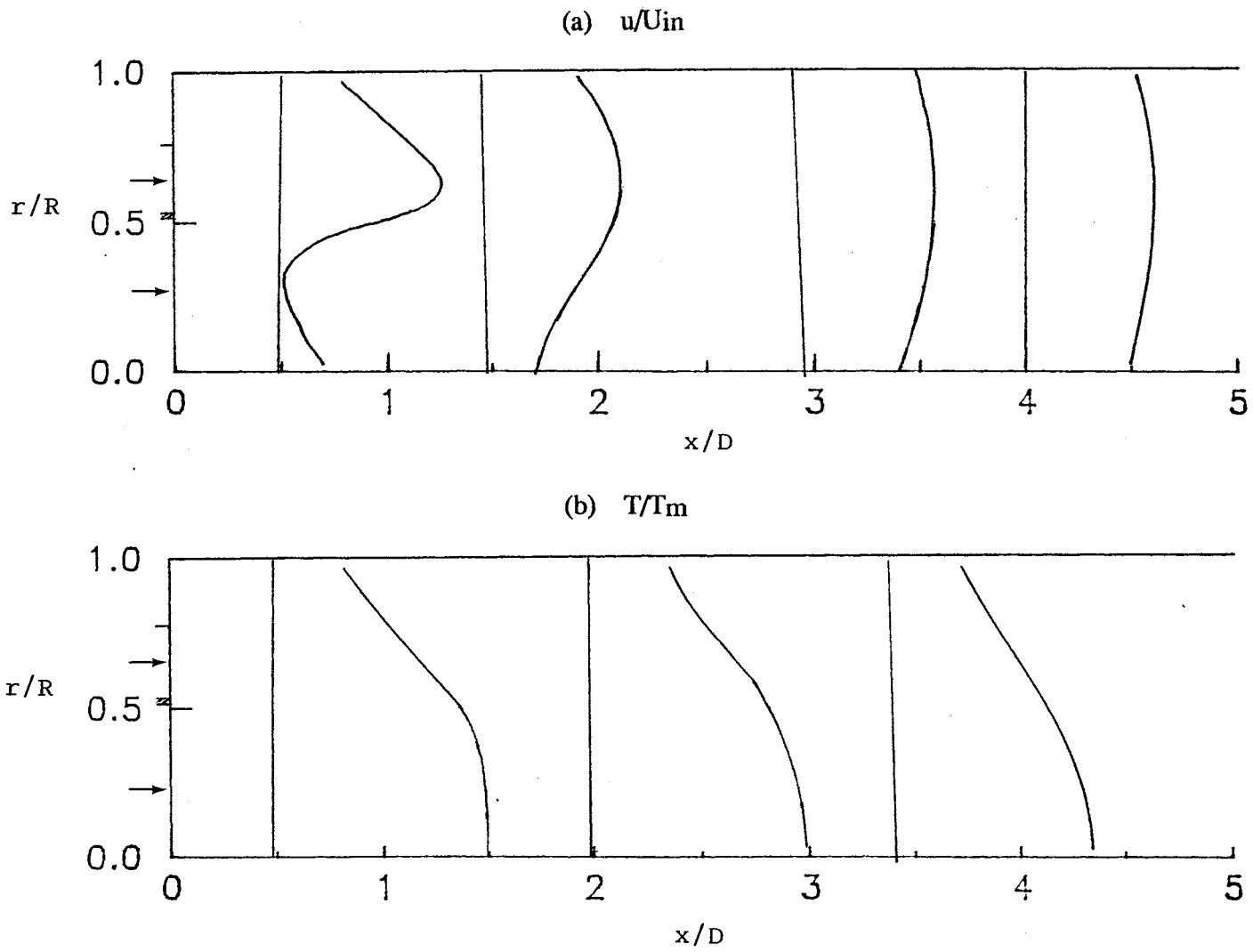


Figure 38. Predicted Mean Flowfield Property Profiles of Case 5

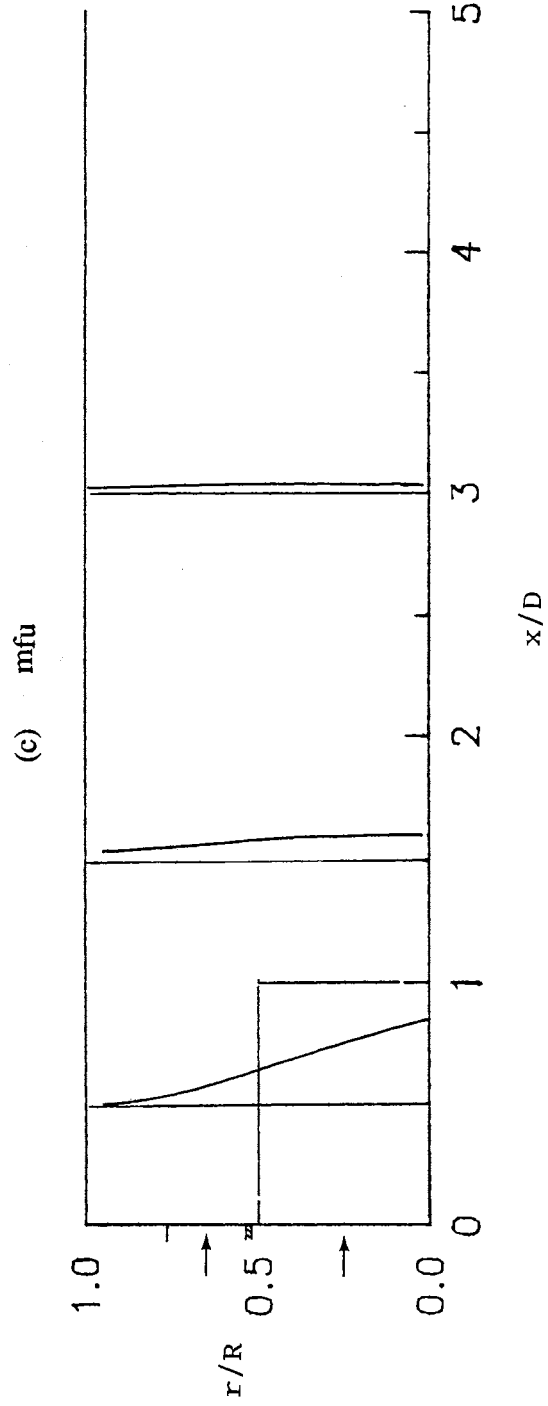


Figure 38. (Continued)

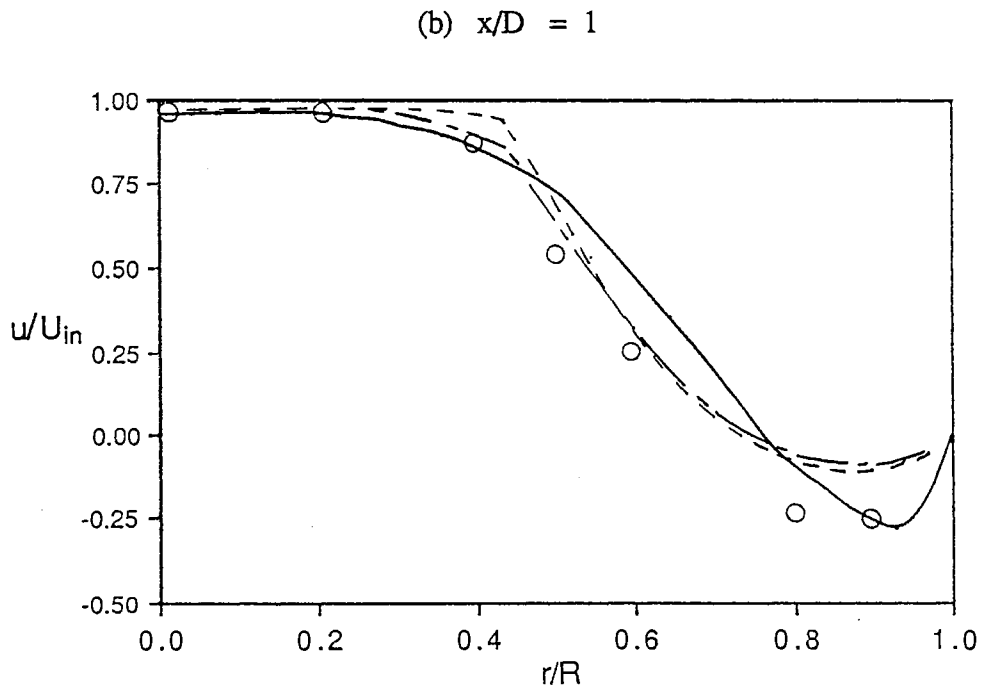
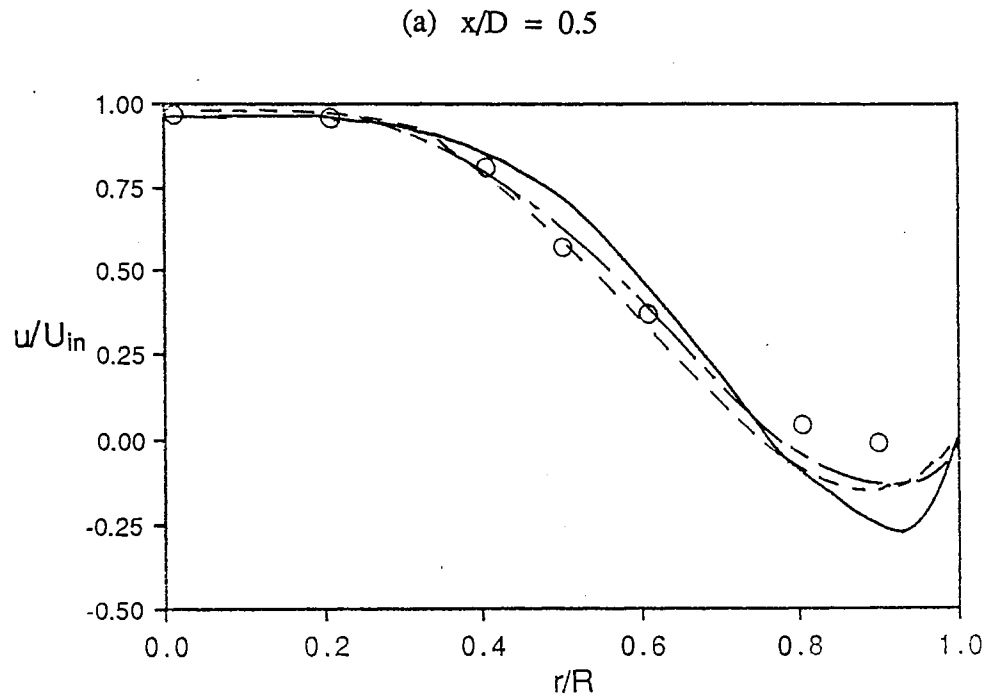


Figure 39. Mean Axial Velocity Profiles of Case 3(a) (without Swirl)
 [\circ ; Experiment Ref. (34), — ; New Code,
 - - - ; Coarse Grid STARPIC, - · - · ; Fine Grid STARPIC]

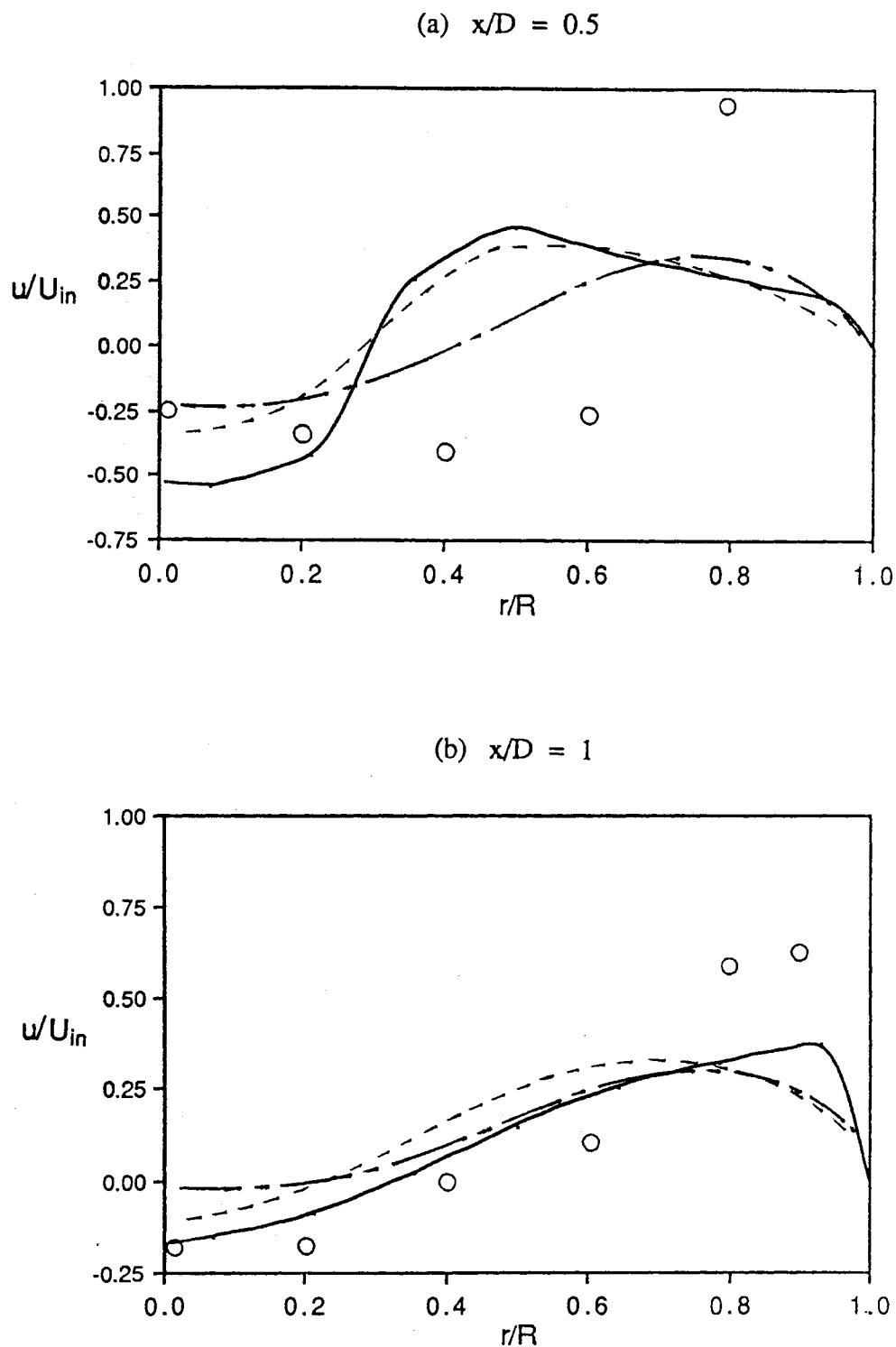


Figure 40. Mean Axial Velocity Profiles of Case 3(b) (Swirl No. 0.67)
 [\circ ; Experiment Ref. (34), — ; New Code,
 - - - ; Coarse Grid STARPIC, - · - ; Fine Grid STARPIC]

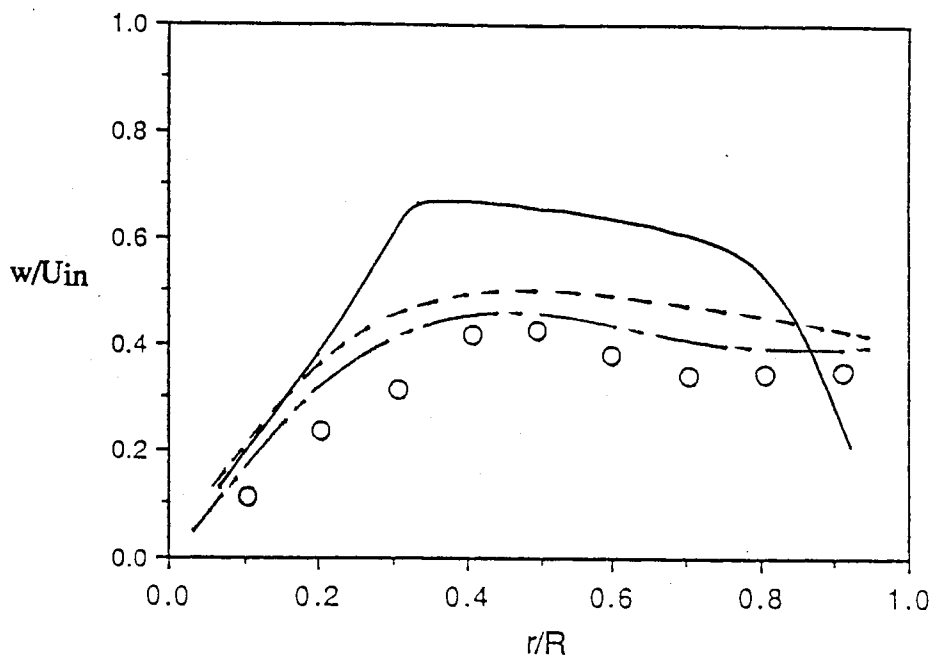
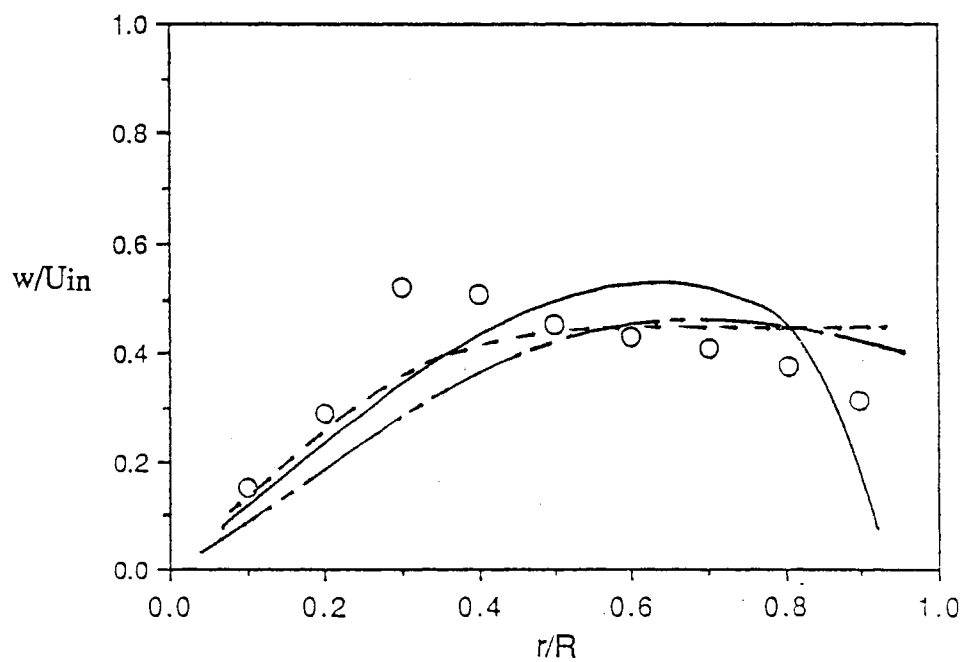
(a) $x/D = 0.5$ (b) $x/D = 1$ 

Figure 41. Mean Swirl Velocity Profiles of Case 3(b) (Swirl No. 0.67)
 [\circ ; Experiment Ref. (34), — ; New Code,
 - - - ; Coarse Grid STARPIC, - · - · ; Fine Grid STARPIC]

APPENDIX C
TYPICAL OUTPUTS

***** U VELOCITY *****

I =	1	2	3	4	5	6	7	8	9	10	11	12
X =	0.00000	0.00000	0.02000	0.04000	0.06000	0.08000	0.10000	0.12000	0.14000	0.16000	0.18500	0.22000

J	Y	1	2	3	4	5	6	7	8	9	10	11	12
9	0.15000	0.00E+00	0.00E+00	0.00E+00	0.00E+00	0.00E+00	0.00E+00	0.00E+00	0.00E+00	0.00E+00	0.00E+00	0.00E+00	0.00E+00
8	0.13000	2.00E+01	2.00E+01	1.45E+01	9.49E+00	5.23E+00	0.00E+00	0.00E+00	-2.77E+00	-4.25E+00	-4.81E+00	-3.53E+00	5.01E-01
7	0.11000	2.00E+01	2.00E+01	2.12E+01	2.24E+01	2.16E+01	2.22E+01	2.39E+01	2.18E+01	2.02E+01	1.82E+01	1.49E+01	1.37E+01
6	0.09000	0.00E+00	0.00E+00	7.75E+00	1.46E+01	2.07E+01	2.54E+01	2.77E+01	2.85E+01	2.77E+01	2.51E+01	2.07E+01	1.96E+01
5	0.07000	2.86E+00	2.86E+00	5.27E+00	1.08E+01	1.79E+01	2.36E+01	2.66E+01	2.83E+01	2.40E+01	2.10E+01	2.09E+01	2.08E+01
4	0.05000	2.86E+00	2.86E+00	4.08E+00	6.84E+00	1.43E+01	2.30E+01	2.25E+01	2.17E+01	2.05E+01	1.99E+01	2.01E+01	1.97E+01
3	0.03000	2.86E+00	2.86E+00	4.85E+00	7.69E+00	1.09E+01	1.32E+01	1.42E+01	1.48E+01	1.48E+01	1.44E+01	1.40E+01	1.40E+01
2	0.01000	2.86E+00	2.86E+00	5.60E+00	8.07E+00	1.13E+01	1.32E+01	1.41E+01	1.46E+01	1.45E+01	1.40E+01	1.34E+01	1.35E+01
1	-0.01000	2.86E+00	2.86E+00	5.60E+00	8.22E+00	1.15E+01	1.30E+01	1.33E+01	1.35E+01	1.37E+01	1.45E+01	1.51E+01	1.54E+01

I =	13	14	15	16	17	18	19	20	21	22	23
X =	0.26000	0.30000	0.34000	0.38000	0.42000	0.46000	0.50000	0.54500	0.59500	0.64500	0.70000

J	Y	13	14	15	16	17	18	19	20	21	22	23
9	0.15000	0.00E+00	0.00E+00	0.00E+00	0.00E+00	0.00E+00	0.00E+00	0.00E+00	0.00E+00	0.00E+00	0.00E+00	0.00E+00
8	0.13000	6.84E+00	1.44E+01	2.30E+01	2.99E+01	3.35E+01	3.48E+01	3.53E+01	3.54E+01	3.55E+01	3.55E+01	3.52E+01
7	0.11000	1.66E+01	2.24E+01	3.15E+01	4.02E+01	4.49E+01	4.49E+01	4.45E+01	4.39E+01	4.32E+01	4.26E+01	4.26E+01
6	0.09000	2.09E+01	2.40E+01	3.16E+01	4.65E+01	5.09E+01	5.05E+01	4.95E+01	4.86E+01	4.78E+01	4.71E+01	4.74E+01
5	0.07000	2.14E+01	2.33E+01	2.85E+01	4.08E+01	5.70E+01	5.45E+01	5.36E+01	5.30E+01	5.26E+01	5.21E+01	5.29E+01
4	0.05000	1.99E+01	1.98E+01	2.18E+01	3.29E+01	5.20E+01	5.63E+01	5.53E+01	5.55E+01	5.62E+01	5.68E+01	5.85E+01
3	0.03000	1.49E+01	1.60E+01	1.96E+01	2.87E+01	4.55E+01	6.09E+01	5.62E+01	5.61E+01	5.74E+01	5.86E+01	6.09E+01
2	0.01000	1.56E+01	1.01E+01	1.15E+01	2.12E+01	4.55E+01	6.08E+01	5.71E+01	5.61E+01	5.70E+01	5.81E+01	6.03E+01
1	-0.01000	1.55E+01	5.83E+00	9.41E+00	2.52E+01	5.43E+01	5.84E+01	5.62E+01	5.54E+01	5.64E+01	5.78E+01	6.03E+01

***** V VELOCITY *****

I =	1	2	3	4	5	6	7	8	9	10	11	12
X =	-0.01000	0.01000	0.03000	0.05000	0.07000	0.09000	0.11000	0.13000	0.15000	0.17000	0.20000	0.24000

J	Y	1	2	3	4	5	6	7	8	9	10	11	12
9	0.14000	0.00E+00	0.00E+00	0.00E+00	0.00E+00	0.00E+00	-5.00E+00	0.00E+00	0.00E+00	0.00E+00	0.00E+00	0.00E+00	0.00E+00
8	0.12000	0.00E+00	1.55E+00	9.01E-01	6.82E-01	-5.62E+00	-1.20E+01	-5.23E+00	-3.43E+00	-1.83E+00	1.51E-01	2.64E+00	3.91E+00
7	0.10000	0.00E+00	-3.71E+00	-4.90E+00	-4.81E+00	-7.74E+00	-1.06E+01	-8.65E+00	-6.92E+00	-5.28E+00	-2.83E+00	1.44E+00	3.49E+00
6	0.08000	0.00E+00	-1.85E+00	-6.83E+00	-8.41E+00	-9.96E+00	-1.07E+01	-9.93E+00	-8.61E+00	-4.57E+00	8.50E-01	2.77E+00	1.94E+00
5	0.06000	0.00E+00	-5.25E+00	-6.83E+00	-7.37E+00	-8.77E+00	-9.12E+00	-6.09E+00	-1.31E+00	1.50E+00	2.38E+00	2.66E+00	1.44E+00
4	0.04000	0.00E+00	-2.43E+00	-4.69E+00	-5.98E+00	-5.08E+00	-1.51E+00	3.49E-01	1.30E+00	1.69E+00	1.89E+00	2.49E+00	2.20E+00
3	0.02000	0.00E+00	-1.95E+00	-2.61E+00	-2.03E+00	-1.13E+00	-7.05E-02	6.80E-01	1.19E+00	1.48E+00	1.63E+00	1.58E+00	8.52E-01
2	0.00000	0.00E+00	0.00E+00	0.00E+00	0.00E+00	0.00E+00	0.00E+00	0.00E+00	0.00E+00	0.00E+00	0.00E+00	0.00E+00	0.00E+00
1	0.00000	0.00E+00	0.00E+00	0.00E+00	0.00E+00	0.00E+00	0.00E+00	0.00E+00	0.00E+00	0.00E+00	0.00E+00	0.00E+00	0.00E+00

I =	13	14	15	16	17	18	19	20	21	22	23
X =	0.28000	0.32000	0.36000	0.40000	0.44000	0.48000	0.52000	0.57000	0.62000	0.67000	0.73000

J	Y	13	14	15	16	17	18	19	20	21	22	23
9	0.14000	0.00E+00	0.00E+00	0.00E+00	0.00E+00	0.00E+00	0.00E+00	0.00E+00	0.00E+00	0.00E+00	0.00E+00	0.00E+00
8	0.12000	4.86E+00	6.32E+00	5.78E+00	3.33E+00	1.42E+00	3.77E-01	-1.76E-01	-4.33E-01	-5.39E-01	-6.02E-01	0.00E+00
7	0.10000	4.22E+00	7.73E+00	1.30E+01	7.62E+00	2.70E+00	3.89E-01	-6.77E-01	-1.05E+00	-1.10E+00	-1.14E+00	0.00E+00
6	0.08000	1.23E+00	1.56E+00	5.92E+00	1.23E+01	3.78E+00	1.77E-01	-1.23E+00	-1.57E+00	-1.51E+00	-1.43E+00	0.00E+00
5	0.06000	-5.31E-01	-9.13E-01	-4.37E-01	1.67E+00	4.61E+00	3.89E-01	-1.54E+00	-1.97E+00	-1.88E+00	-1.58E+00	0.00E+00
4	0.04000	-8.86E-01	-3.01E+00	-2.24E+00	3.75E+00	1.01E+01	1.27E+00	-1.24E+00	-1.73E+00	-1.71E+00	-1.30E+00	0.00E+00
3	0.02000	-6.05E-01	-1.08E+00	-4.42E-01	-6.05E-02	-2.83E+00	9.54E-02	-5.57E-01	-9.21E-01	-9.52E-01	-6.90E-01	0.00E+00
2	0.00000	0.00E+00	0.00E+00	0.00E+00	0.00E+00	0.00E+00	0.00E+00	0.00E+00	0.00E+00	0.00E+00	0.00E+00	0.00E+00
1	0.00000	0.00E+00	0.00E+00	0.00E+00	0.00E+00	0.00E+00	0.00E+00	0.00E+00	0.00E+00	0.00E+00	0.00E+00	0.00E+00

W VELOCITY												
I =	1	2	3	4	5	6	7	8	9	10	11	12
X =	-0.01000	0.01000	0.03000	0.05000	0.07000	0.09000	0.11000	0.13000	0.15000	0.17000	0.20000	0.24000
J	Y											
9	0.15000	0.00E+00	0.00E+00	0.00E+00	0.00E+00	0.00E+00	0.00E+00	0.00E+00	0.00E+00	0.00E+00	0.00E+00	0.00E+00
8	0.13000	1.14E+01	1.16E+01	4.31E+00	8.16E-01	8.98E-01	3.41E+00	4.86E+00	5.80E+00	5.66E+00	5.64E+00	5.80E+00
7	0.11000	9.67E+00	1.05E+01	1.10E+01	9.05E+00	5.82E+00	5.27E+00	5.37E+00	5.57E+00	5.65E+00	5.70E+00	6.13E+00
6	0.09000	0.00E+00	1.03E+01	1.16E+01	1.19E+01	1.07E+01	9.85E+00	9.34E+00	9.06E+00	8.88E+00	8.85E+00	9.01E+00
5	0.07000	0.00E+00	2.99E+00	1.04E+01	1.23E+01	1.27E+01	1.27E+01	1.25E+01	1.22E+01	1.20E+01	1.17E+01	1.12E+01
4	0.05000	0.00E+00	1.75E+00	7.87E+00	1.12E+01	1.26E+01	1.33E+01	1.35E+01	1.32E+01	1.26E+01	1.18E+01	1.05E+01
3	0.03000	0.00E+00	6.53E-01	5.51E+00	9.30E+00	1.13E+01	1.14E+01	1.07E+01	9.62E+00	8.59E+00	7.54E+00	6.37E+00
2	0.01000	0.00E+00	2.22E-01	1.72E+00	2.90E+00	3.53E+00	3.53E+00	3.29E+00	2.99E+00	2.71E+00	2.44E+00	2.12E+00
1	-0.01000	0.00E+00	0.00E+00	0.00E+00	0.00E+00	0.00E+00	0.00E+00	0.00E+00	0.00E+00	0.00E+00	0.00E+00	0.00E+00
I =	13	14	15	16	17	18	19	20	21	22	23	
X =	0.28000	0.32000	0.36000	0.40000	0.44000	0.48000	0.52000	0.57000	0.62000	0.67000	0.73000	
J	Y											
9	0.15000	0.00E+00	0.00E+00	0.00E+00	0.00E+00	0.00E+00	0.00E+00	0.00E+00	0.00E+00	0.00E+00	0.00E+00	0.00E+00
8	0.13000	6.34E+00	6.36E+00	6.33E+00	6.31E+00	6.31E+00	6.35E+00	6.41E+00	6.50E+00	6.60E+00	6.73E+00	6.73E+00
7	0.11000	7.06E+00	7.13E+00	7.01E+00	6.90E+00	6.83E+00	6.83E+00	6.86E+00	6.92E+00	7.00E+00	7.09E+00	7.09E+00
6	0.09000	8.62E+00	8.31E+00	8.04E+00	7.69E+00	7.43E+00	7.27E+00	7.17E+00	7.12E+00	7.10E+00	7.11E+00	7.11E+00
5	0.07000	1.07E+01	1.03E+01	9.64E+00	8.89E+00	8.30E+00	7.99E+00	7.78E+00	7.62E+00	7.48E+00	7.36E+00	7.36E+00
4	0.05000	1.01E+01	1.07E+01	1.05E+01	9.39E+00	8.37E+00	8.14E+00	8.08E+00	7.98E+00	7.83E+00	7.63E+00	7.63E+00
3	0.03000	6.61E+00	8.67E+00	9.03E+00	8.24E+00	7.63E+00	7.19E+00	7.15E+00	7.07E+00	6.90E+00	6.90E+00	6.90E+00
2	0.01000	2.25E+00	2.78E+00	2.68E+00	2.45E+00	2.30E+00	2.23E+00	2.21E+00	2.19E+00	2.16E+00	2.12E+00	2.12E+00
1	-0.01000	0.00E+00	0.00E+00	0.00E+00	0.00E+00	0.00E+00	0.00E+00	0.00E+00	0.00E+00	0.00E+00	0.00E+00	0.00E+00
STAGNATION ENTHALPY												
I =	1	2	3	4	5	6	7	8	9	10	11	12
X =	-0.01000	0.01000	0.03000	0.05000	0.07000	0.09000	0.11000	0.13000	0.15000	0.17000	0.20000	0.24000
J	Y											
9	0.15000	0.00E+00	0.00E+00	0.00E+00	0.00E+00	0.00E+00	3.30E+05	0.00E+00	0.00E+00	0.00E+00	0.00E+00	0.00E+00
8	0.13000	3.30E+05	4.35E+05	5.67E+05	7.23E+05	1.03E+06	1.25E+06	1.01E+06	8.14E+05	8.93E+05	9.54E+05	1.03E+06
7	0.11000	3.30E+05	3.73E+05	5.46E+05	7.48E+05	1.03E+06	1.10E+06	1.08E+06	1.05E+06	1.04E+06	1.05E+06	1.11E+06
6	0.09000	3.30E+05	3.46E+05	4.57E+05	6.14E+05	8.66E+05	9.24E+05	9.57E+05	9.73E+05	9.82E+05	1.04E+06	1.36E+06
5	0.07000	4.73E+07	1.71E+07	4.17E+06	2.20E+06	1.85E+06	1.57E+06	1.41E+06	1.32E+06	1.50E+06	2.03E+06	2.95E+06
4	0.05000	4.73E+07	3.67E+07	2.10E+07	1.37E+07	1.00E+07	6.93E+06	5.84E+06	6.66E+06	8.05E+06	9.77E+06	1.24E+07
3	0.03000	4.73E+07	4.69E+07	3.54E+07	2.87E+07	2.61E+07	2.52E+07	2.60E+07	2.71E+07	2.81E+07	2.91E+07	3.01E+07
2	0.01000	4.73E+07	4.87E+07	4.25E+07	3.91E+07	3.77E+07	3.79E+07	3.83E+07	3.86E+07	3.90E+07	3.93E+07	3.95E+07
1	-0.01000	4.73E+07	4.87E+07	4.25E+07	3.91E+07	3.77E+07	3.79E+07	3.83E+07	3.86E+07	3.90E+07	3.93E+07	3.95E+07
I =	13	14	15	16	17	18	19	20	21	22	23	
X =	0.28000	0.32000	0.36000	0.40000	0.44000	0.48000	0.52000	0.57000	0.62000	0.67000	0.73000	
J	Y											
9	0.15000	0.00E+00	0.00E+00	0.00E+00	0.00E+00	0.00E+00	0.00E+00	0.00E+00	0.00E+00	0.00E+00	0.00E+00	0.00E+00
8	0.13000	1.34E+06	1.52E+06	1.69E+06	1.79E+06	1.84E+06	1.88E+06	1.93E+06	1.99E+06	2.05E+06	2.12E+06	2.12E+06
7	0.11000	1.52E+06	1.88E+06	2.36E+06	2.74E+06	2.97E+06	3.13E+06	3.26E+06	3.38E+06	3.49E+06	3.60E+06	3.60E+06
6	0.09000	1.81E+06	2.17E+06	2.95E+06	3.87E+06	4.43E+06	4.77E+06	5.01E+06	5.22E+06	5.41E+06	5.60E+06	5.60E+06
5	0.07000	3.42E+06	3.51E+06	4.09E+06	5.28E+06	6.78E+06	7.39E+06	7.70E+06	7.92E+06	8.17E+06	8.42E+06	8.42E+06
4	0.05000	1.33E+07	1.22E+07	1.19E+07	1.35E+07	1.49E+07	1.47E+07	1.41E+07	1.36E+07	1.32E+07	1.30E+07	1.30E+07
3	0.03000	2.85E+07	2.35E+07	2.21E+07	2.24E+07	2.28E+07	2.32E+07	2.30E+07	2.25E+07	2.22E+07	2.19E+07	2.19E+07
2	0.01000	3.75E+07	3.24E+07	3.12E+07	3.11E+07	3.04E+07	3.08E+07	3.09E+07	3.07E+07	3.05E+07	3.04E+07	3.04E+07
1	-0.01000	3.75E+07	3.24E+07	3.12E+07	3.11E+07	3.04E+07	3.08E+07	3.09E+07	3.07E+07	3.05E+07	3.04E+07	3.04E+07

 MASS FRACTION OF FUEL

I =	1	2	3	4	5	6	7	8	9	10	11	12
X =	-0.01000	0.01000	0.03000	0.05000	0.07000	0.09000	0.11000	0.13000	0.15000	0.17000	0.20000	0.24000
J	Y											
9	0.15000	0.00E+00	0.00E+00	0.00E+00	0.00E+00	0.00E+00	0.00E+00	0.00E+00	0.00E+00	0.00E+00	0.00E+00	0.00E+00
8	0.13000	0.00E+00	0.00E+00	5.90E-07	0.00E+00	2.29E-03	4.81E-03	5.09E-03	3.91E-03	3.91E-03	4.53E-03	6.72E-03
7	0.11000	0.00E+00	0.00E+00	9.11E-06	0.00E+00	1.00E-04	1.69E-03	2.46E-03	2.71E-03	2.81E-03	3.41E-03	7.68E-03
6	0.09000	0.00E+00	0.00E+00	2.12E-05	0.00E+00	0.00E+00	4.03E-04	8.02E-04	1.05E-03	1.56E-03	5.73E-03	1.93E-02
5	0.07000	1.00E+00	2.87E-01	5.70E-02	2.44E-02	1.65E-02	1.22E-02	1.03E-02	1.04E-02	1.71E-02	3.38E-02	6.00E-02
4	0.05000	1.00E+00	8.09E-01	4.60E-01	2.65E-01	1.64E-01	9.88E-02	8.69E-02	1.10E-01	1.38E-01	1.60E-01	2.09E-01
3	0.03000	1.00E+00	1.00E+00	8.11E-01	6.71E-01	6.18E-01	6.12E-01	6.36E-01	6.52E-01	6.62E-01	6.68E-01	6.73E-01
2	0.01000	1.00E+00	1.00E+00	9.49E-01	9.01E-01	8.81E-01	8.81E-01	8.75E-01	8.66E-01	8.56E-01	8.47E-01	8.37E-01
1	-0.01000	1.00E+00	1.02E+00	9.49E-01	9.01E-01	8.81E-01	8.81E-01	8.75E-01	8.66E-01	8.56E-01	8.47E-01	8.37E-01

I =	13	14	15	16	17	18	19	20	21	22	23
X =	0.28000	0.32000	0.36000	0.40000	0.44000	0.48000	0.52000	0.57000	0.62000	0.67000	0.73000
J	Y										
9	0.15000	0.00E+00	0.00E+00	0.00E+00	0.00E+00	0.00E+00	0.00E+00	0.00E+00	0.00E+00	0.00E+00	0.00E+00
8	0.13000	9.92E-03	9.31E-03	8.54E-03	8.35E-03	8.87E-03	9.73E-03	1.05E-02	1.11E-02	1.15E-02	1.15E-02
7	0.11000	2.00E-02	2.10E-02	1.85E-02	1.48E-02	1.28E-02	1.26E-02	1.31E-02	1.36E-02	1.39E-02	1.39E-02
6	0.09000	4.32E-02	4.89E-02	4.78E-02	3.93E-02	2.89E-02	2.28E-02	2.05E-02	2.00E-02	2.01E-02	1.99E-02
5	0.07000	9.72E-02	1.07E-01	1.10E-01	1.01E-01	8.22E-02	6.04E-02	4.70E-02	4.10E-02	3.88E-02	3.75E-02
4	0.05000	2.13E-01	2.06E-01	2.15E-01	2.50E-01	2.39E-01	2.06E-01	1.76E-01	1.54E-01	1.38E-01	1.25E-01
3	0.03000	6.11E-01	5.02E-01	4.99E-01	4.96E-01	4.62E-01	4.14E-01	3.58E-01	3.10E-01	2.70E-01	2.36E-01
2	0.01000	7.59E-01	6.83E-01	6.69E-01	6.47E-01	5.98E-01	5.44E-01	4.79E-01	4.15E-01	3.58E-01	3.08E-01
1	-0.01000	7.59E-01	6.83E-01	6.69E-01	6.47E-01	5.98E-01	5.44E-01	4.79E-01	4.15E-01	3.58E-01	3.08E-01

 TEMPERATURE

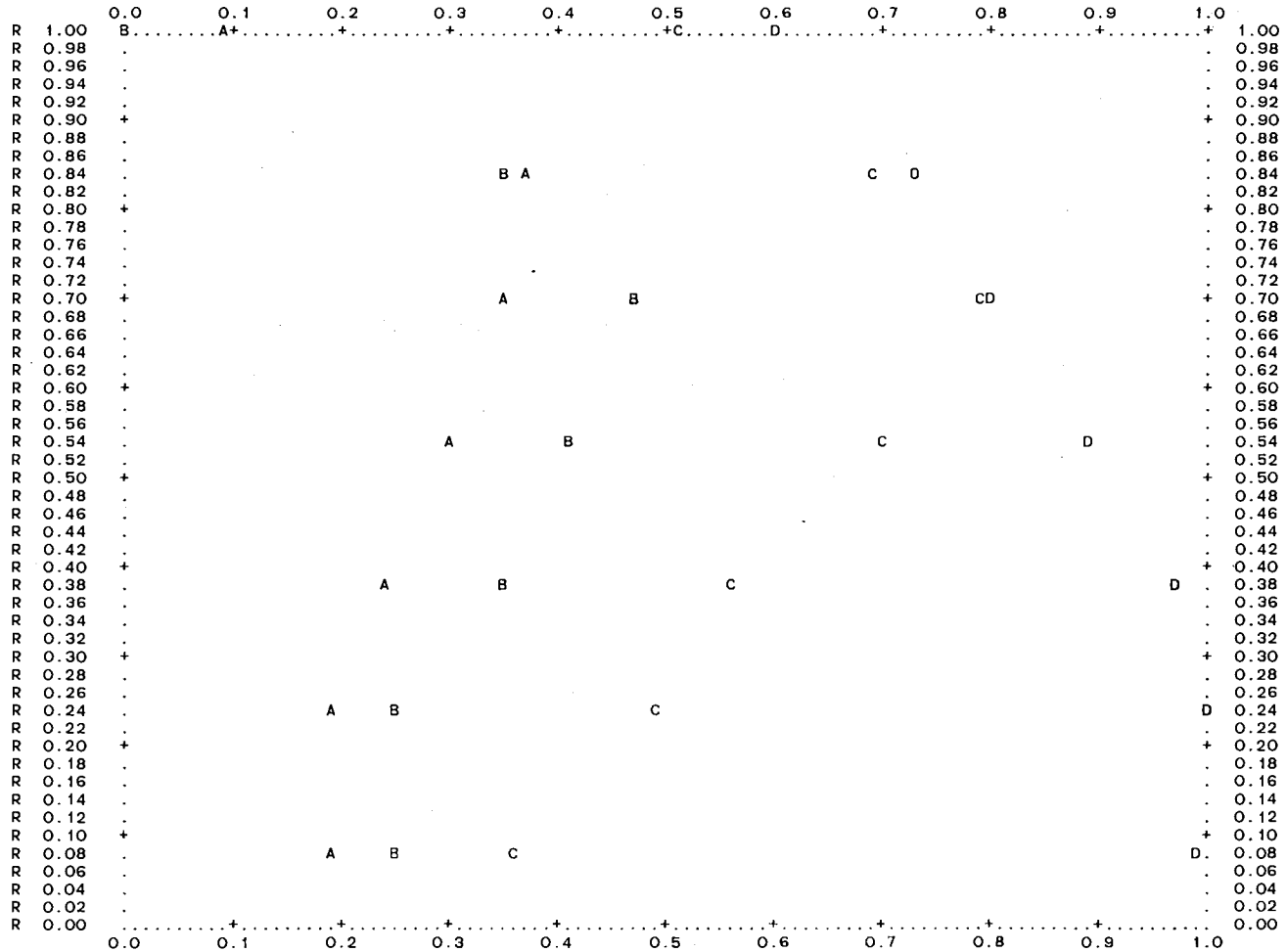
I =	1	2	3	4	5	6	7	8	9	10	11	12
X =	-0.01000	0.01000	0.03000	0.05000	0.07000	0.09000	0.11000	0.13000	0.15000	0.17000	0.20000	0.24000
J	Y											
9	0.15000	0.00E+00	0.00E+00	0.00E+00	0.00E+00	0.00E+00	3.00E+02	0.00E+00	0.00E+00	0.00E+00	0.00E+00	0.00E+00
8	0.13000	3.00E+02	3.96E+02	5.15E+02	6.57E+02	8.38E+02	9.29E+02	7.02E+02	5.73E+02	6.45E+02	6.74E+02	6.45E+02
7	0.11000	3.00E+02	3.39E+02	4.96E+02	6.80E+02	9.29E+02	9.25E+02	8.80E+02	8.37E+02	8.27E+02	8.07E+02	6.81E+02
6	0.09000	3.00E+02	3.14E+02	4.14E+02	5.58E+02	7.88E+02	8.23E+02	8.36E+02	8.40E+02	8.26E+02	6.97E+02	4.14E+02
5	0.07000	3.00E+02	2.50E+03	1.36E+03	9.59E+02	9.81E+02	9.04E+02	8.44E+02	7.59E+02	6.31E+02	4.01E+02	3.00E+02
4	0.05000	3.00E+02	3.00E+02	3.00E+02	1.10E+03	2.09E+03	2.08E+03	1.60E+03	1.37E+03	1.42E+03	2.06E+03	2.39E+03
3	0.03000	3.00E+02	3.00E+02	3.00E+02	3.00E+02	3.00E+02	3.00E+02	3.00E+02	3.00E+02	3.00E+02	3.00E+02	3.00E+02
2	0.01000	3.00E+02	1.55E+03	3.00E+02	3.00E+02	3.00E+02	3.00E+02	3.00E+02	3.00E+02	3.00E+02	3.00E+02	3.00E+02
1	-0.01000	3.00E+02	0.00E+00	0.00E+00	0.00E+00	0.00E+00	0.00E+00	0.00E+00	0.00E+00	0.00E+00	0.00E+00	0.00E+00

I =	13	14	15	16	17	18	19	20	21	22	23
X =	0.28000	0.32000	0.36000	0.40000	0.44000	0.48000	0.52000	0.57000	0.62000	0.67000	0.73000
J	Y										
9	0.15000	0.00E+00	0.00E+00	0.00E+00	0.00E+00	0.00E+00	0.00E+00	0.00E+00	0.00E+00	0.00E+00	0.00E+00
8	0.13000	7.92E+02	9.83E+02	1.17E+03	1.27E+03	1.29E+03	1.30E+03	1.31E+03	1.34E+03	1.38E+03	1.44E+03
7	0.11000	5.29E+02	8.09E+02	1.35E+03	1.85E+03	2.15E+03	2.31E+03	2.41E+03	2.49E+03	2.50E+03	2.50E+03
6	0.09000	3.00E+02	3.00E+02	6.39E+02	1.84E+03	2.50E+03	2.50E+03	2.50E+03	2.50E+03	2.50E+03	2.50E+03
5	0.07000	3.00E+02	3.00E+02	3.00E+02	4.87E+02	2.50E+03	2.50E+03	2.50E+03	2.50E+03	2.50E+03	2.50E+03
4	0.05000	2.50E+03	2.29E+03	1.69E+03	1.62E+03	2.50E+03	2.50E+03	2.50E+03	2.50E+03	2.50E+03	2.50E+03
3	0.03000	3.00E+02	3.00E+02	3.00E+02	3.00E+02	9.95E+02	2.50E+03	2.50E+03	2.50E+03	2.50E+03	2.50E+03
2	0.01000	1.65E+03	3.00E+02	3.00E+02	6.42E+02	2.11E+03	2.50E+03	2.50E+03	2.50E+03	2.50E+03	2.50E+03
1	-0.01000	0.00E+00	0.00E+00	0.00E+00	0.00E+00	0.00E+00	0.00E+00	0.00E+00	0.00E+00	0.00E+00	0.00E+00

DIMENSIONLESS STREAM FUNCTION												
I =	1	2	3	4	5	6	7	8	9	10	11	12
X =	0.00000	0.00000	0.02000	0.04000	0.06000	0.08000	0.10000	0.12000	0.14000	0.16000	0.18500	0.22000
J	Y											
9	0.15000	0.00E+00	1.00E+00	1.00E+00	1.00E+00	1.00E+00	1.00E+00	1.00E+00	1.00E+00	1.00E+00	1.00E+00	1.00E+00
8	0.13000	0.00E+00	6.63E-01	7.35E-01	7.84E-01	8.15E-01	8.57E-01	9.70E-01	1.01E+00	1.03E+00	1.05E+00	1.10E+00
7	0.11000	0.00E+00	2.40E-01	3.94E-01	5.30E-01	6.37E-01	7.31E-01	8.31E-01	9.00E-01	9.44E-01	9.84E-01	1.04E+00
6	0.09000	0.00E+00	3.92E-02	1.30E-01	2.50E-01	3.71E-01	4.67E-01	5.46E-01	6.19E-01	6.73E-01	7.24E-01	7.65E-01
5	0.07000	0.00E+00	3.28E-02	5.68E-02	1.16E-01	1.86E-01	2.48E-01	2.99E-01	3.49E-01	3.82E-01	4.03E-01	3.98E-01
4	0.05000	0.00E+00	1.85E-02	3.63E-02	7.02E-02	1.06E-01	1.36E-01	1.56E-01	1.72E-01	1.76E-01	1.68E-01	1.50E-01
3	0.03000	0.00E+00	6.24E-03	1.34E-02	3.10E-02	5.14E-02	6.60E-02	7.04E-02	7.09E-02	6.86E-02	6.43E-02	5.73E-02
2	0.01000	0.00E+00	9.48E-04	2.21E-03	6.07E-03	9.92E-03	1.23E-02	1.28E-02	1.24E-02	1.15E-02	1.01E-02	8.13E-03
1	-0.01000	0.00E+00	0.00E+00	0.00E+00	0.00E+00	0.00E+00	0.00E+00	0.00E+00	0.00E+00	0.00E+00	0.00E+00	0.00E+00
I =	13	14	15	16	17	18	19	20	21	22	23	
X =	0.26000	0.30000	0.34000	0.38000	0.42000	0.46000	0.50000	0.54500	0.59500	0.64500	0.70000	
J	Y											
9	0.15000	1.00E+00	1.00E+00	1.00E+00	1.00E+00	1.00E+00	1.00E+00	1.00E+00	1.00E+00	1.00E+00	1.00E+00	1.00E+00
8	0.13000	1.20E+00	1.23E+00	1.22E+00	1.16E+00	1.02E+00	8.79E-01	8.52E-01	8.39E-01	8.28E-01	8.19E-01	8.23E-01
7	0.11000	1.04E+00	1.02E+00	9.72E-01	8.86E-01	7.33E-01	5.92E-01	5.68E-01	5.63E-01	5.61E-01	5.60E-01	5.69E-01
6	0.09000	7.26E-01	7.11E-01	6.95E-01	6.54E-01	5.28E-01	3.96E-01	3.78E-01	3.78E-01	3.81E-01	3.84E-01	3.94E-01
5	0.07000	3.40E-01	3.43E-01	3.62E-01	3.78E-01	3.27E-01	2.40E-01	2.25E-01	2.28E-01	2.33E-01	2.38E-01	2.46E-01
4	0.05000	1.16E-01	1.28E-01	1.51E-01	1.77E-01	1.73E-01	1.25E-01	1.12E-01	1.14E-01	1.18E-01	1.23E-01	1.28E-01
3	0.03000	3.99E-02	4.64E-02	6.30E-02	7.78E-02	7.22E-02	4.81E-02	4.09E-02	4.19E-02	4.39E-02	4.60E-02	4.83E-02
2	0.01000	3.49E-03	4.92E-03	8.04E-03	9.55E-03	9.07E-03	8.37E-03	7.97E-03	8.10E-03	8.50E-03	8.93E-03	9.40E-03
1	-0.01000	0.00E+00	0.00E+00	0.00E+00	0.00E+00	0.00E+00	0.00E+00	0.00E+00	0.00E+00	0.00E+00	0.00E+00	0.00E+00

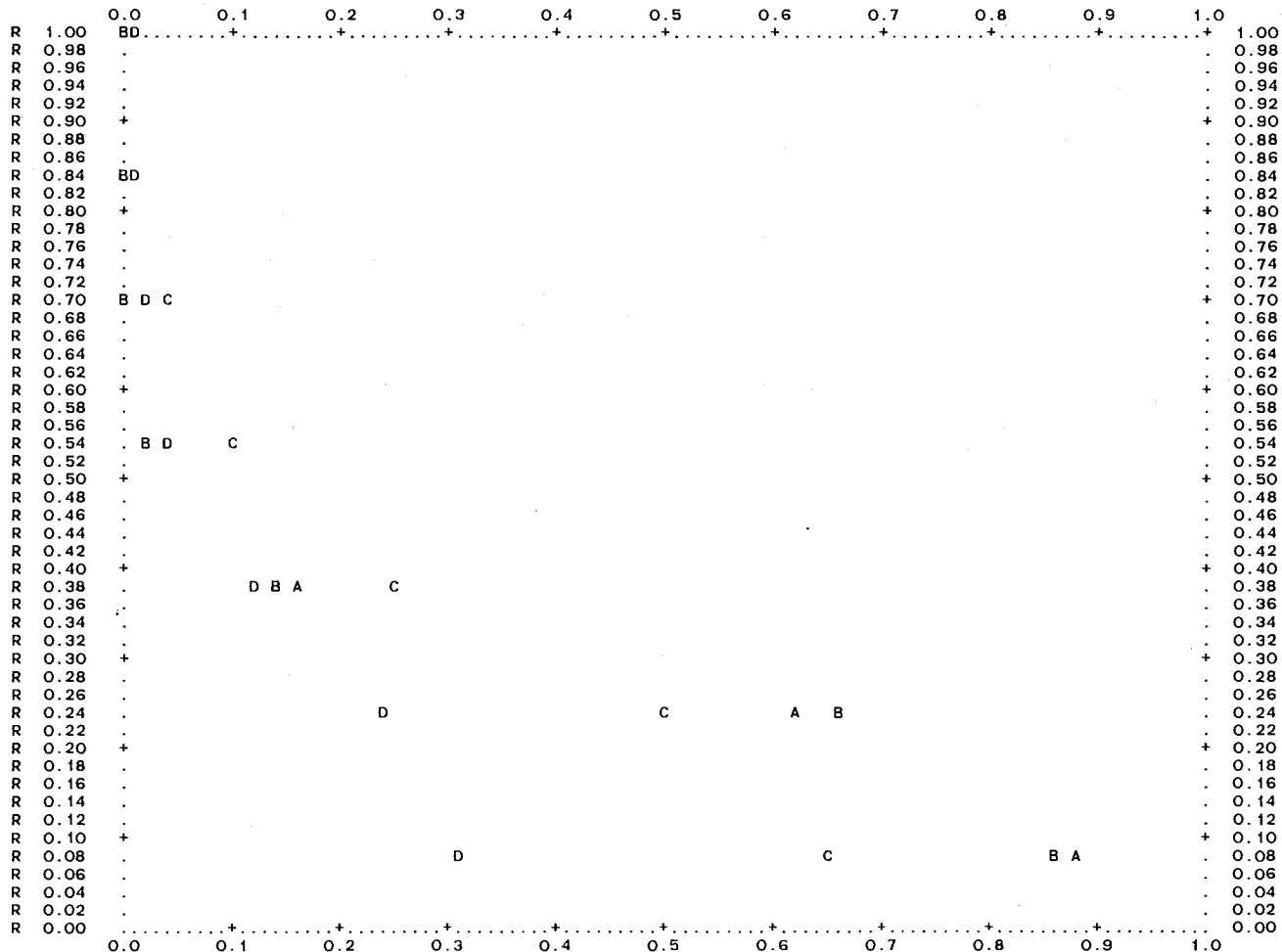
NORMALIZED U VELOCITY : ANNULAR WIDTH=0.787 IN - SEC VOL FLOW RATE= 350.0 SCFM - INJECTION ANGLE= 0.0 DEG
 ===== PRIM SWIRL ANGLE= 0.0 DEG - SEC SWIRL ANGLE= 0.0 DEG - PRIM CONTRACTION ANGLE= 0.0 DEG

I VALUES FOR PROFILE PLDTTNG = 5 9 16 22
 SYMBOLS A B C D
 MAXIMUM VALUES 2.161E+01 2.774E+01 4.650E+01 5.862E+01



MASS FRACTION OF SEC : ANNULAR WIDTH=0.787 IN - SEC VOL FLDW RATE=350.0 SCFM - INJECTION ANGLE= 0.0 DEG
 ----- PRIM SWIRL ANGLE= 0.0 DEG - SEC SWIRL ANGLE= 0.0 DEG - PRIM CONTRACTION ANGLE= 0.0 DEG

I VALUES FDR PROFILE PLOTTING = 5 9 16 22
 SYMBOLS A B C D
 MAXIMUM VALUES 8.806E-01 8.563E-01 6.472E-01 3.084E-01



X-AXIS IS XI
 Y-AXES ARE 00 02 04 06 08 10
 SYMBOL 0 2 4 6 8 1
 MAXIMUM VALUES 0.100E-29 0.294E+00 0.332E+00 0.404E+00 0.459E+00 0.500E+00

RADIAL POSITION R/D

	0.0	0.1	0.2	0.3	0.4	0.5	0.6	0.7	0.8	0.9	1.0
X 0.00	0	.	.	2	4	6	1	.	.	.	0.00
X 0.02	0	.	.	2	4	6	1	.	.	.	0.02
X 0.04	0.04
X 0.06	0	.	.	2	4	6	1	.	.	.	0.06
X 0.08	0	.	.	2	4	6	8	1	.	.	0.08
X 0.10	+	0.10
X 0.12	0	.	2	4	6	8	1	.	.	.	0.12
X 0.14	0	.	2	4	6	8	1	.	.	.	0.14
X 0.16	0.16
X 0.18	0	.	2	4	6	8	1	.	.	.	0.18
X 0.20	0	.	2	4	6	8	1	.	.	+	0.20
X 0.22	0	.	2	4	6	8	1	.	.	.	0.22
X 0.24	0.24
X 0.26	0	.	2	4	6	8	1	.	.	.	0.26
X 0.28	0.28
X 0.30	+	0.30
X 0.32	0	.	2	4	6	8	1	.	.	.	0.32
X 0.34	0.34
X 0.36	0.36
X 0.38	0	.	2	4	6	8	1	.	.	.	0.38
X 0.40	+	+	0.40
X 0.42	0	.	2	4	6	8	1	.	.	.	0.42
X 0.44	0.44
X 0.46	0.46
X 0.48	0	.	2	4	6	8	1	.	.	.	0.48
X 0.50	+	+	0.50
X 0.52	0.52
X 0.54	0	.	2	4	6	8	1	.	.	.	0.54
X 0.56	0.56
X 0.58	0.58
X 0.60	0	.	2	4	6	8	1	.	.	+	0.60
X 0.62	0.62
X 0.64	0.64
X 0.66	0	.	2	4	6	8	1	.	.	.	0.66
X 0.68	0.68
X 0.70	+	+	0.70
X 0.72	0	.	2	4	6	8	1	.	.	.	0.72
X 0.74	0.74
X 0.76	0.76
X 0.78	0	.	2	4	6	8	1	.	.	.	0.78
X 0.80	+	+	0.80
X 0.82	0.82
X 0.84	0.84
X 0.86	0	.	2	4	6	8	1	.	.	.	0.86
X 0.88	0.88
X 0.90	+	+	0.90
X 0.92	0	.	2	4	6	8	1	.	.	.	0.92
X 0.94	0.94
X 0.96	0.96
X 0.98	0.98
X 1.00	0	.	2	4	6	8	1	.	.	+	1.00

VITA

Seongdo Ha

Candidate for the Degree of

Doctor of Philosophy

Thesis: PREDICTION OF TURBULENT SWIRLING REACTING FLOW WITH
NONORTHOGONAL GRID SYSTEM

Major Field: Mechanical Engineering

Biographical :

Personal Data: Born in Jinyang, Korea, 1950, the son of Mr. S. Ha and Mrs. H. Song.

Education: Graduated from Jinjoo High School, Jinjoo, Korea, in February, 1970; received the Bachelor of Science Degree in Mechanical Engineering from Yonsei University Seoul, Korea, in February, 1977; received the Master of Science in Engineering degree from the University of Texas at Austin, Texas, in December, 1983; completed requirements for the Doctor of Philosophy degree at Oklahoma State University in July, 1989.

Professional Experience: Deputy Assistant Director, Ministry of Science and Technology, Seoul, Korea, 1977-1980; Teaching Assistant, Department of Mechanical Engineering, University of Texas at Austin, 1982-1983; Teaching Assistant, School of Mechanical and Aerospace Engineering, Oklahoma State University, January, 1986, to May, 1989

Professional Societies: American Institute of Aeronautics and Astronautics